ENVIRONMENTAL MANAGEMENT AND POTENTIAL USE OF HEAVY OIL FLY ASH

by

©**Abdullah Mofarrah, B.Sc. (Eng.), M.Eng.**

A thesis submitted to the school of Graduate Studies
in partial fulfillment of the requirements for the degree of

Doctor of Philosophy

Faculty of Engineering and Applied Science
Memorial University of Newfoundland

May 2014

St. John's Newfoundland and Labrador

Abstract

Heavy oil fly ash (HOFA) is a by-product generated in power plants by the burning of heavy fuel oil. The main constituent of HOFA is unburned carbon; it also contains other elements such as arsenic (As), cadmium (Cd), cobalt (Co), chromium (Cr), mercury (Hg), nickel (Ni), lead (Pb), copper (Cu), zinc (Zn), selenium (Se), calcium (Ca), magnesium (Mg), sodium (Na), silicon (Si), aluminium (Al), iron (Fe), and vanadium (V) in different forms of oxides or sulfates. Due to insufficient knowledge of the physical and chemical properties and related applications of this by-product, it is usually disposed off into landfills.

In order to explore the beneficial utilization of HOFA, this research study analyzes the physical, chemical, and morphological characteristics of HOFA. It also includes an in-depth investigation on its reuse as (i) a natural absorbent such as activated carbon (AC), (ii) fill material for construction use, and (iii) a colour ingredient in ornamental concrete.

Chemical and physical activation techniques were used to produce fly ash activated carbon (FAC). Before activation, the minerals and other metals present in the HOFA were removed by standard leaching procedures. The performances of the produced FAC were tested for the removal of selected pollutants such as dyes, naphthalene, and metals from aqueous solutions. The results from the laboratory batch experiments indicated that the developed FAC has the potential to remove organic and inorganic (e.g., 85% to 90%) pollutants from wastewater.

Soil stabilizer or fill material for construction use was prepared by mixing HOFA with Portland cement at different ratios. The leaching behaviour of the trace elements and compounds within HOFA and fill materials was studied by standard laboratory batch and column leaching tests. The results of the study showed that the toxic elements in HOFA are

easily leachable and can be toxic to the environment. However, the addition of 40% Portland cement with HOFA significantly decreased the leaching concentration of most elements below the permissible level.

To explore the possible use of HOFA as a black pigment or admixture in ornamental concrete, it was mixed with cement mortar at different percentages. The standard compressive strength test with 50 mm cement mortar cubes showed that the addition of 2% to 5% HOFA in cement mortar does not affect its compressive strength. The leaching behaviour of trace elements within HOFA mixed concrete material was also investigated through laboratory batch leaching experiments. The findings confirmed that HOFA can be used as a black pigment in ornamental concrete, which is environmentally safe, and provides a good balance between colour and concrete quality.

In the final phase of this research, a human health risk assessment methodology was developed in order to assess the potential health risk to people living in the area surrounding the HOFA dumping site. This study also explores environmental concerns and the importance of HOFA management practices.

Acknowledgements

I want to take this opportunity to express my deepest gratitude to my supervisor, Dr. Tahir Husain, for his insightful guidance, encouragement, and support throughout the course of this research. I am thankful to Dr. Bing Chen and Dr. Christina Bottaro, members of my supervisory committee, for their help and valuable suggestions on this research.

I acknowledge the Faculty of Engineering and Applied Science, Memorial University of Newfoundland (MUN), and the Natural Sciences and Engineering Research Council Collaborative Research and Development (NSERC/CRD) for their financial support.

I would like to thank all of my friends at MUN for providing a pleasant working environment. Special thanks to Ms. Pam King for her help during laboratory work in the Earth Sciences Department of Memorial University.

I am very grateful to my family, especially my wife, Afsana Khandokar, and my children, Mardiah Farzeen and Ribi Mofarrah, for their sacrifices and support.

Finally, the useful results of this research are dedicated to all people who are struggling for clean and peaceful environment.

Table of Contents

List of Tables

List of Figures

List of Abbreviations

AC	Activated Carbon
ANC	Acid Neutralization Capacity
ASTM	American Society for Testing and Materials
BDDT	Brunauer-Deming-Deming-Teller
BET	Brunauer Emmett Teller
CAC	Commercial Activated Carbon
CDF	Cumulative Distribution Function
CID	Chronic Daily Intake
cm	Centimeter
CR	Cumulative Cancer Risk
DR	Dubinin-Radushkevich
EDS	Energy Dispersive Spectrometer
ELT	Equilibrium Leach Test
ESP	Electrostatic Precipitator
FA	Fly Ash
FAC	Fly Ash Activated Carbon
g	Gram
GAC	Granular Activated Carbon
HFO	Heavy Fuel Oil
HI	Hazard Index
HOFA	Heavy Fuel Oil Fly Ash
HQ	Hazard Quotient
hr	Hour
ICP-MS	Inductively Coupled Plasma-Mass Spectrometry
IN	Iodine number
IUPAC	International Union of Pure and Applied Chemistry
kg	Kilogram
L	Liter
m	Meter

MBN	Methylene blue number
MCS	Monte Carlo Simulation
mg	Milligram
ml	Milliliter
MLC	Maximum Leachate Concentration
mm	Millimeter
mph	Mile per Hour
PAC	Powdered Activated Carbon
PHL	Preliminary Hazard List
PRA	Probabilistic Risk Assessment
RfD	Reference Dose
rpm	Revolutions per Minute
sec	Second
SEM	Scanning Electron Microscope
SF	Slope Factor
STP	Standard Temperature and Pressure
TCLP	Toxicity Characteristic Leaching Procedure
TPV	Total Pore Volume
USA	United State of America
USEPA	United States Environmental Protection Agency
µm	Micrometer
XRD	X-ray diffraction

Chapter 1

Introduction and Overview

1.1 Background

During combustion, oil drops are heated and burned with oxygen. At the same time, impurities such as sulphur, vanadium, and nickel within the fuel oil are transformed and react with gaseous hydrocarbons to form particulate matter, which is known as ash (Wayne et al., 2009). The ash accumulated on boilerplates is called bottom ash, and ash with the exhaust collected by dust collector devices is called fly ash (Sakai and Sugiyama, 1970). The burning of a kiloliter of heavy fuel oil (HFO) yields about 3 kilograms (kg) of ash (Tsai and Tsai, 1997), and most of this ash (approximately 90%) is passed through a flue gas steam, which is collected by air pollution control devices such as electrostatic precipitators (ESP) or cyclones (Hsieh and Tsai, 2003). The fly ash generated by the burning of HFO is generally termed heavy fuel oil fly ash (HOFA). On average, 50-60 tonnes of HOFA are generated per day from a mid-range (i.e., 2300 MW power generating capacity) power plant (Hsieh and Tsai, 2003; Wayne et al., 2009).

HOFA, which is composed of low density fine particles, has the potential to disperse into the air during handling and transportation. Due to their light density, these particles can travel a long distance before settling on land, water, or vegetation. The dispersion of HOFA may result in the contamination of soil, water, and air. Inhalation of HOFA particles may pose potential health impacts, since they contain high levels of heavy metals. HOFA is an

environmental concern. Indeed, due to poor management and uncontrolled disposal it may pose an environmental and public health hazard (Mohapatra and Rao, 2001; Choi et al., 2002; Fernandez et al., 2003). An HOFA dumping area is a potential source of airborne particles; leach from an HOFA dumping site may contaminate a nearby water body, soil, and groundwater and have a negative impact on the environment (Fernandez et al., 2003; Mofarrah and Husain, 2013).

People exposed to HOFA may suffer from coughing, bronchial irritation, gastrointestinal diseases, and conjunctivitis (Zhang et al., 1995; Jiang et al., 2000; Lozano and Juan, 2001; Navarro et al., 2007;). Improper handling and disposal of HOFA may cause negative health effects on workers and the surrounding exposed population (e.g., lung irritation injury) (Andrew et al., 2002).

Considering the long-term impact of HOFA on the environment, it is important to find a sustainable eco-friendly economical method for the proper management of HOFA. The recycling of HOFA by producing new products or reusing it as a product for use in pollution control technology has substantial economical and environmental benefits.

1.2 Scope of this study

Yearly a million tonnes of HOFA are generated worldwide but only a small portion is reused for productive purposes (Mõtlep et al., 2010). Generally, HOFA is dumped into landfills or waste containment facilities (Baek et al., 2007). This dumping of HOFA could be a potential source for soil, groundwater, and surface water contamination. Although in different parts of the world vanadium and nickel are recovered from HOFA, the major part of this waste (about 90-95%) is dumped into landfills (Akita et al., 1995; Miura et al., 2001; Guibal et al., 2003), which need to be managed. The cost associated with the management of this vast quantity of

HOFA is high, and an increasing trend is expected due to the stringent environmental regulations being enforced worldwide.

A potential economic incentive exists for developing innovative and environmentally safe applications of this waste. This study explores the potential uses of HOFA as a natural adsorbent in removing organic and inorganic compounds from wastewater. The research also indentified that HOFA blended with cement can be used as soil stabilization material in an environmentally safe manner. This research contributes to minimizing the scientific gap regarding HOFA management and attempts to develop a good approach to its reuse as a value-added commercial product.

1.3 Research objectives

A significant amount of research has been conducted on the reuse of coal fly ash but very little research has been done on the beneficial utilization of HOFA. Due to the different chemical compositions of coal and HFO, the characteristics of the two types of fly ash that result also differ. Fly ash from HFO burning has a higher percentage of unburned carbon, less silica, and a higher level of vanadium, nickel, and magnesium than coal fly ash. Considering the above research scope, this study aims to develop environmentally friendly management options of HOFA. The main objectives of this research are to

a. Analyze the physical and chemical characteristics of HOFA.
b. Evaluate the human health risk associated with HOFA dumping (i.e., current management practices).
c. Conduct different leaching tests to evaluate the environmental impacts associated with HOFA.

d. Evaluate potential uses of HOFA as construction material such as a soil stabilizer and a colour ingredient in ornamental concrete.
e. Extract clean carbon from HOFA and prepare fly ash activated carbon (FAC).
f. Investigate the efficiency of the produced FAC to adsorb selected pollutants from wastewater.
g. Evaluate the regeneration efficiency of used FAC.
h. Model the FAC adsorption characteristics of selected pollutants in wastewater.

1.4 Originality and contributions

Through the development of HOFA management strategies, this research focused on the conversion of HOFA into environmentally friendly products such as AC, a soil stabilizer, and a colour ingredient in ornamental concrete. The author's contributions and originality of this study can be summarized as follows:

- Analyzed physical and chemical characteristics of different types of HOFA.
- Extracted clean carbon from HOFA and prepared fly ash activated carbon (FAC).
- Studied the FAC adsorption characteristics of pollutants such as Cr (IV), naphthalene, and MB from aqueous solution.
- Conducted leaching tests to evaluate the environmental impact of HOFA.
- Evaluated the potential application of HOFA in construction material such as a soil stabilizer and a colour ingredient in ornamental concrete.
- Developed a health risk assessment methodology to assess the human health risk posed by HOFA dumping.

This research also contributed to the scientific platform through different publications. The list of publications from this study, including a paper under review or in preparation, are as follows:

- **Mofarrah, A.**, Husain, T., (2013). Evaluation of Environmental Pollution and Possible Management Options of Heavy Oil Fly Ash. Journal of Material Cycles and Waste Management, vol. 15 (1), pp. 73-81.
- **Mofarrah, A**., Husain, T., (2013). Use of Heavy Oil Fly Ash as a Color Ingredient in Cement Mortar. International Journal of Concrete Structures and Materials, vol. 7 (2), pp. 111-117.
- **Mofarrah, A**., Husain, T., Bottaro, C., (2013). Characterization of Activated Carbon Obtained from Saudi Arabian Fly Ash, International Journal of Environmental Science and Technology (IJEST), Volume 11, Issue 1, pp 159-168.
- **Mofarrah, A.**, Husain, T., Ekram, Y. D., (2012). Investigation of the Potential Use of Heavy Oil Fly Ash as Stabilized Fill Material for Construction. Journal of Materials in Civil Engineering, vol. 24 (6), pp. 684-690.
- **Mofarrah, A.**, Husain, T., Ekram, Y. D., (2012). Communicating human health risks associated with airborne particulate released from fly ash dumping site: Probabilistic Approach, book chapter Academy Publish.
- **Mofarrah, A.**, Husain, T., Ekram, Y. D, (2012). Production of activated carbon from Saudi Arabian fly ash to develop pollution mitigation technology. First International Conference on Environmental Challenges in Arid Regions, 2012, Jeddah, paper No. 0747.

- **Mofarrah, A**., Husain, T., Chen, B., (2013). Optimizing Cr (VI) adsorption on activated carbon produced from heavy oil fly ash. Journal of Material Cycles and Waste Management, DOI: 10.1007/s10163-013-0197-7.

1.5 Overview of the thesis

The organization of the thesis follows the guidelines approved by the Faculty of Engineering and Applied Science of Memorial University of Newfoundland. This study is organized into eight chapters. Chapter 1 presents a statement of problems, the scope of the study, and the objectives of this research. The background of HOFA, its available management options, and related literature are presented in Chapter 2. The experimental setup and characteristics analysis of HOFA are presented in Chapter 3. The methodology used to assess the human health risk associated with the dumping of HOFA in landfills is presented in Chapter 4. The potential application of HOFA as a construction material and different leaching tests are described in Chapter 5. Chapter 6 describes the production and characterization of fly ash activated carbon (FAC). Adsorption experiments and related modeling are presented in Chapter 7. This study concludes in Chapter 8 with recommendations for future work. Figure 1-1 schematically shows how various chapters are organized in this thesis.

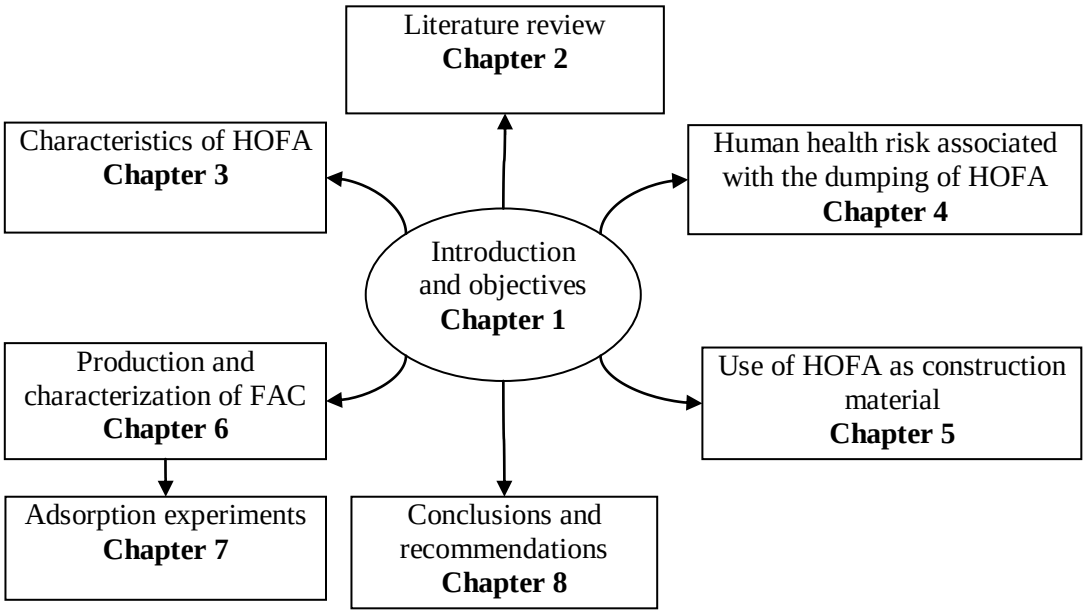

Figure1-1 Structure of the thesis

Chapter 2

Literature Review

2.1 Introduction

Heavy fuel oil (HFO) plays an important role in power generation in many parts of the world. Due to its availability in local market and relatively low cost, major power generation facilities in several countries, including Spain, Italy, Taiwan, and Saudi Arabia, use HFO. Saudi Arabia uses about 320 million barrels of HFO and crude oil annually for its power generation (Breakbulk Online News, 2010-07-20), which produces about one-quarter million tonnes of HOFA, most of which is dumped into landfills.

Although Canada has reduced its use of HFO for power generation, in some parts of Canada a mixture of HFO and petroleum coke is used to generate electricity. According to statistics, Newfoundland and Labrador uses 3.4%, Nova Scotia and Prince Edward Island use 15.8%, and New Brunswick uses 36.1% HFO or a mixture of HFO and petroleum coke for power generation (Paul and Caouette, 2007). This indicates that a large amount of HOFA is being generated by provincial power industries.

In Italy, approximately 14 million tonnes of HFO is used for power generation, and its annual production of HOFA is about 27,600 tonnes (Rapporto Ambientale, 2000). According to Hsieh and Tsai (2003), Taiwan consumes 15 million kiloliters of fuel oil per year, which produces about 45,000 tonnes of HOFA. The improper disposal of HOFA can cause the air quality deterioration and impact surface water and groundwater. The volume of fly ash waste generated by power plants, as well as the cost of disposal of this waste, are continually

increasing, and this challenges environmental engineers to develop improved cost-effective and environmentally sound management plans.

Table 2-1 Typical chemical composition of HOFA

(Gupta and Krishnamurthy, 1992; Kwon, et al., 2005)

Parameters	**Fly Ash**	**Unit**
Arsenic (As)	2.84	mg/kg
Barium (Ba)	4.23	mg/kg
Cadmium (Cd)	ND	mg/kg
Cobalt (Co)	0.042	mg/kg
Chromium (Cr)	2.25	mg/kg
Copper (Cu)	16.36	mg/kg
Iron (Fe)	1368	mg/kg
Mercury (Hg)	ND	mg/kg
Manganese (Mn)	29.6	mg/kg
Molybdenum (Mo)	0.153	mg/kg
Nickel (Ni)	135.6	mg/kg
Lead (Pb)	4.355	mg/kg
Selenium (Se)	228.6	mg/kg
Tin (Sn)	ND	mg/kg
Vanadium (V)	1508	mg/kg
Zinc (Zn)	8.36	mg/kg
Unburned Ash %	3.14	%
Carbon %	50-90	%

Until 2014, the most of the research related to HOFA management has been confined to its characterization and to the recovery of valuable materials like vanadium and nickel from this by product (Akita et al., 1995; Miura et al., 2001; Vitolo et al., 2001; Guibal et al., 2003; Baek et al., 2007). A large volume of residue is left after metal extraction, which is currently considered waste residue for landfill disposal. HOFA characteristics depend on the type of fuel and the method of combustion. Chemical analysis shows that HOFA is composed

mainly of carbon (e.g., 70~80%), sulphur, and residue ash (Tsai and Tsai, 1997; Kwon et al., 2005). It also contains inorganic substances such as silicon dioxide (SiO_2), iron (III) oxide (Fe_2O_3), and aluminum oxide (Al_2O_3) (Kwon et al., 2005); valuable metallic compounds such as 20-30% vanadium and 0.8-6% nickel (Zhang et al., 1995; Lozano and Juan, 2001); and heavy metals such as arsenic (As), cadmium (Cd), mercury (Hg), and copper (Cu) which exist in crude petroleum (Hwang et al., 1996). The typical chemical composition of HOFA as found in the literature is shown in Table 2-1.

The moisture content, density, and porosity of HOFA as found in the literature are listed in Table 2-2. The bulk density of HOFA varies from 0.20 to 1.50 g/cm^3, and its true density and porosity are reported as 2.15 g/cm^3 and 10.31% respectively (Kwon et al., 2005).

Table 2-2 Physical properties of heavy HOFA

(Gupta and Krishnamurthy, 1992; Kwon et al., 2005)

Sample	**Moisture content (%)**	**Bulk density (g/cm^3)**	**True density (g/cm^3)**	**Porosity (%)**
HOFA	11.54	0.52	2.15	10.31

The particle size of HOFA ranges from 10 to 120 (μm). The particles of HOFA contain small pores of a few μm in size which may have formed during the combustion process (Kwon et al., 2005). The colour of HOFA is close to carbon black (Kwon et al., 2005); however, the colour of HOFA mainly depends on the burning process and the characteristics of the HFO.

2.2 Activated carbon

Activated carbon (AC) is a family of carbonaceous material which has been processed to make it highly porous (Ahmadpour and Do, 1996; Rodriguez-Reinoso, 1997). Because of its

extensive surface area and high adsorption capacity, AC is widely used as an adsorbent to control pollution in many industries (Mohan and Pittman, 2006). Usually two broad types of AC, such as (i) Granular activated carbon (GAC), and (ii) Powdered activated carbon (PAC), are used in industrial applications. According to the American Water Works Association Standard (AWWA, 1997), carbon having particle size 0.297 mm or larger is defined as GAC; on the other hand, a carbon particle finer than 0.297 mm is termed as PAC.

The pore size of AC ranges from 1 nm to 1000 nm, and its surface area from 500 m^2/g to 1500 m^2/g (Cooney, 1999). The large surface area (e.g., 300-2500 m^2/g) of AC allows it to absorb more substances from the liquid and gas phases (Snell et al., 1974). Generally AC is free from all non-carbon impurities (Lua and Guo, 2000), but, depending on the nature of the raw material and the activation process, it may contain a trace amount of mineral matter (e.g., ash content) (Mattson, 1971; Menendez and Martin, 2006).

Porosity is a favourable characteristic of AC: high porosity provides more surface area, which leads to a greater adsorption capacity. The porosity of AC depends mainly on the nature of the raw material and the activation process (Diaz-Teran et al., 2001). According to the International Union of Pure and Applied Chemistry (IUPAC) definitions, the pore size of AC can be classified into three major groups: (i) micropores (< 2 nm), (ii) mesopores (2-50 nm), and (iii) macropores (>50 nm) (Sing et al., 1985; Menendez and Martin, 2006). The main part of the internal surface and the total pore volume of AC are composed of micropores and mesopores (Menendez and Martin, 2006). In the adsorption process, macropores act as an entrance gateway through which the adsorptive molecules travel to the mesopores, from where the smaller molecules enter micropore regions. Mesopore regions are

suitable only for trapping large molecular species such as colour molecules (Mattson, 1971; Menendez and Martin, 2006).

2.3 Production of activated carbon

Materials with a high carbon and low inorganic content such as wood, lignite, peat, and coal are generally used as raw materials for AC production (Lua and Guo, 2001). Industrial and agricultural waste or by-products such as macadamia nutshell, paper mill sludge, peach stone, fly ash etc. can also be used to produce AC (Ahmadpour and Do, 1997; Hsieh and Tsai, 2003; Menendez and Martin, 2006). The production of AC involves various cleaning and pyrolysis steps. Some impurities in the raw material are removed by systematic leaching and washing processes. Sometimes chemical agents are used in this process. The removal of volatile components from the raw materials and the development of AC are followed by different pyrolysis processes. Pyrolysis can be followed by chemical or physical activation (Menendez and Martin, 2006).

In chemical activation, the raw material is treated with an applicable amount of the chemical agent. Common chemical agents such as alkali, salt of alkaline-earth, and some acids (e.g., KOH, K_2CO_3, NaOH, Na_2CO_3, $AlCl_3$, $ZnCl_2$, $MgCl_2$, HCl, H_3PO_4, and H_2SO_4) are well documented in the literature (Smisek and Cerny, 1970; Ahmadpour and Do, 1996; Caramuscio et al., 2003; Menendez and Martin, 2006). Calcium hydroxide, calcium chloride, manganese chloride, and sodium hydroxide are also used as common dehydrating agents (Bansal and Goyal, 2005). In this process, the raw material is mixed with a chemical solution to form a plastic mass, which is burnt at a low temperature (i.e., generally 90-100°C) for several hours (depending on the raw material) to allow for chemical decomposition. The mass is then carbonized at a high temperature, generally above 600°C (Bansal and Goyal,

2005). After carbonization, the activated product is thoroughly washed with water to eliminate any excess chemical. Finally, the product is dried at a low temperature (e.g., 90-100°C) to obtain AC (Rodriguez-Reinoso, 1997). In chemical activation, the mixing ratio of the chemical agent and raw material depends on the characteristics of the raw material and the activation process, usually a 1:4 ratio is used (Rodriguez-Reinoso, 1997). The chemical dose, temperature, and reaction time are the main factors that control the properties of the final product (Bansal and Goyal, 2005). The physical activation process usually involves two steps: first, the raw material is burnt for an extended period at a low temperature (e.g., 400-700°C) under an inert environment to form charcoal (Cuhadaroglu and Uygun, 2008; Lowell 2004). This process, called carbonization, eliminates the volatile and liquid components from the raw material and produces a solid carbon-rich residue. The burning period could range from 1 hr to 48 hrs, depending on the property of the raw material (Rodriguez-Reinoso, 1997).

In the activation process, char from carbonization is burnt at temperatures ranging from 400°C to 1000°C by an oxidizing agent such as steam or carbon dioxide (CO_2) for a limited period of time (Jankowaka et al., 1991; Lua and Guo, 2000; Lillo-Rodenas et al., 2007). Nitrogen (N_2) is generally used as an inert gas to carry the oxidizing agent to the system (Lillo-Rodenas et al., 2005). Different types of furnaces such as vertical multi-hearth furnaces, tube furnaces, and fluidized bed reactors have been used to produce AC. Various activation methods have been developed (Mor et al., 2007; Okiemmen et al., 2007; Sari et al., 2007; Gupta and Ali, 2004; Mohan et al., 2005), but these procedures all follow the same basic principle: carbonization and activation with an oxidizing agent (Menendez and Martin, 2006). The interlinking of the steps involved in producing AC is shown in Figure 2-1.

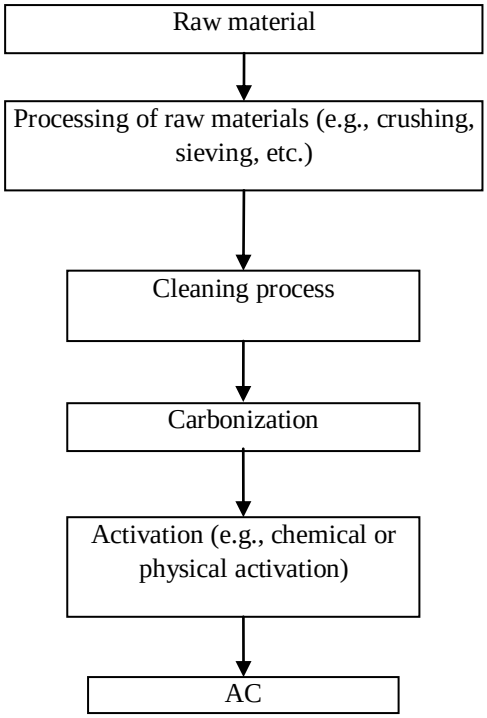

Figure 2-1 Graphical representation of activation methods

2.4 Application of AC

AC has proven applications in environmental purification. It has been broadly applied to the removal of different pollutants from industrial processes (Gupta and Ali, 2004; Mohan et al., 2005; Gode and Pehlivan, 2006). However, the use of commercial activated carbon (CAC) for the treatment of industrial pollutants involves a high cost, which has led researchers to develop alternative cost-effective adsorbents. In many areas around the world, high carbon content materials such as agricultural wastes and industrial by-products are locally available in large quantities; these can be utilized as low-cost adsorbents. Researchers have focused on seeking a low-cost adsorbent from industrial and/or agricultural by-products (Ahmed and Dhedan, 2012; Gode and Pehlivan, 2006). The conversion of agricultural by-products or industrial wastes into adsorbents for pollution control would reduce its disposal cost and provide an alternative to CAC (Kurniawan et al., 2006). Based on a recent review by Mohan

and Pittman (2006), these low-cost adsorbents can be divided into three categories: (1) biomass, (2) agricultural and industrial wastes, and (3) nano-sized particles. Among other industrial wastes, carbon rich fly ash has been extensively studied by researchers for their removal of pollutants from the air and aqueous solutions (Akgerman and Zardkoohi, 1996; Banerjee et al., 2004; Ahmaruzzaman and Sharma, 2005; Sarkar and Acharya, 2006). Bayat (2002) used Turkish fly ash to remove Cr (VI) ions from wastewater. Gupta and Ali (2004) used bagasse fly ash to remove lead and chromium from wastewater. Mukherjee et al. (2007) studied the adsorption of phenol onto AC derived from bagasse fly ash as well. Rachakornkij et al. (2004) studied the adsorption of dyes from aqueous solutions by bagasse fly ash. These studies show that fly ash from different sources has the potential to be used for the sorption of both inorganic and organic pollutants. Most of these studies use fly ash from coal combustion or agricultural wastes. On the other hand, the burning of HFO in power generation industries produces thousands of tonnes of HOFA with a very high carbon content; this HOFA has potential reuse scope. Studies have been conducted to recover vanadium and nickel from HOFA (Akita et al., 1995; Tsai and Tsai, 1998; Vitolo et al., 2001; Miura et al., 2001; Guibal et al., 2003), but, after recovering the metals, the major part of the fly ash is dumped into landfills (Akita et al., 1995). Until now, few studies have been conducted on HOFA as a possible absorbent source. Caramuscio et al. (2003) prepared AC from HOFA and found that the surface area was 156 m^2/g. Davini (2002) prepared AC from HOFA with a surface area greater than 1000 m^2/g, and used it for flue gas treatment. Using chemical activation process, Yaumi et al. (2013) prepared AC from oil fly ash with a maximum Brunauer Emmett Teller (BET) surface area of 318 m^2/g. This study used produced AC to capture carbon dioxide gas from industrial system. A survey of the literature

confirms that HOFA could be a potential source of adsorbent, but this has not been fully explored. All the possibilities mentioned in the literature prompts the proposed research with HOFA for detailed investigation and to produce high quality adsorbent or to explore other reuse options.

2.5 Regeneration of spent activated carbon

When the adsorption capacity of AC is reached in saturation, it must be regenerated or discarded (Hiltz, 1988). Reactivation involves the modification of AC. In this process the contaminants are desorbed and burnt at a temperature generally above 800^{o}C in a furnace (e.g., rotary kiln) (Zanitsch, 1997). Carbon reactivation is feasible for the large scale production (Schuliger, 1988).

The regeneration of AC usually involves removing the adsorbed contaminants without destroying the structure of the AC. In a common regeneration process steam is passed through the spent AC bed to restored its capacity (Hiltz, 1988; Junjie et al., 1999; ADG, 2001). Sometimes a hot inert gas such as nitrogen is used to remove the contaminants from the saturated AC bed (ADG, 2001). The application of steam or gas flow could be either counter-current or co-current to the original waste stream's flow. Regeneration processes usually run on-site inside an adsorption vessel. The main advantages of on-site regeneration include a greater saving of AC, which is destroyed during off-site reactivation (ADG, 2001).

Chapter 3

Characterization of Heavy Fuel Oil Fly Ash

3.1 Sample collection

Depending on the properties of HFO and burning process, the chemical compositions of HOFA vary considerably, but all HOFA includes substantial amounts of unburned carbon and minor percentage of other elements including heavy metal. To understand the properties of HOFA, characterization is necessity. For this study fly ash samples were collected from two sources: the first (FA-SA) was collected from a power plant in Saudi Arabia; the second (FA-NB) was collected from a power plant in New Brunswick, Canada. The FA samples were collected directly from an electrostatic precipitator (ESP). The FA-SA sample was produced by the burning of HFO with high sulphur content (about 2-3%); the FA-NB sample was produced from a mixture of petroleum coke and 2% HFO.

Dry samples were collected from the ESP and stored in an airtight container. Two layers of packing were used during transportation of the samples. The sample was stored in a polyethylene bag to prevent moisture adsorption, then the bag containing the sample was placed in an airtight plastic box and transferred to the laboratory. In the laboratory, the samples were always kept in a dry place in the manner in which they were received.

3.2 Sample analysis

Visually the two FA samples appeared different in colour: the FA-NB sample can be represented as a true black; the FA-SA sample looked a dark greenish grey. Both samples are lightweight and consist of airborne particulates. The physical properties of HOFA, such as

bulk density, specific gravity, and moisture content, were analyzed by following the standard testing method described in the following sections.

3.2.1 Bulk density

The bulk density of FA was determined using the method suggested by Ahmedna et al. (1997), which consists of placing a known weight of FA in a 25 ml cylinder to a specified volume, tapping the cylinder for at least 1-2 minutes, and measuring the volume of FA. The bulk density can be determined as

$$\rho = \frac{W_s}{V_s} \tag{3-1}$$

where, ρ is the bulk density (g/cm^3), *Ws* is the weight of the FA sample g, and *Vs* is the volume of the packed sample (cm^3). The bulk densities of the FAs are reported in Table 3-1.

3.2.2 Specific gravity

The specific gravity (G_S) of FA was determined by standard test procedures (ASTM D854-00). The main steps involved in this testing can be summarized as follows: (i) weigh an empty clean and dry pycnometer, W_P, (ii) place about 10 g of oven-dried FA in the pycnometer and record the weight of the pycnometer containing the dry FA, W_{Pf}, (iii) add distilled water to fill about one-half to three-quarters of the pycnometer and soak the sample for 10 minutes to remove the entrapped air, and apply a partial vacuum to the contents for 10 minutes, (iv) carefully remove the vacuum from the pycnometer, (v) fill the pycnometer with distilled water (to the mark), clean the exterior surface of the pycnometer with a dirt-free dry cloth/tissue, and determine the weight of the pycnometer and its contents, W_B, (vii) empty the pycnometer, clean it, and fill with distilled water (to the mark); clean the exterior surface of

the pycnometer with a clean, dry cloth/tissue, and determine the weight of the pycnometer with the distilled water, *Wpw*, and (viii) the specific gravity of the FA can be calculated as follows:

$$G_s = \frac{W_o}{W_o + (Wpw - W_B)} \qquad (3\text{-}2)$$

where, W_o is the mass of dry FA (*Wpf* -*Wp*) in g. G_s of FA is reported in Table 3-1.

3.2.3 Moisture content

Approximately 10 g (weighed to an accuracy of 0.1 mg) of FA was placed on a flat aluminum tray and heated in a well-ventilated oven at 105±5°C for 12 hrs. After cooling in a desiccator, the sample was reweighed. The moisture content of FA was determined as follows (Wesche et al., 1989):

$$m_c = \frac{m1 - m2}{m2} \times 100(\%\quad by\quad mass) \qquad (3\text{-}3)$$

where, *ml* is the original mass of wet FA in g, *m2* is the final mass of dried FA in g, m_c is the moisture content %. The moisture content of the FA is reported in Table 3-1.

3.2.4 Loss on ignition

Approximately 1 g (weighed to an accuracy of 0.1 mg) of FA was placed on a flat aluminum tray and heated in a well-ventilated oven at 975±25°C for 1 hr. After cooling in a desiccator, the sample was reweighed. The following equation was used to calculate the loss of ignition of FA samples (Wesche et al., 1989):

$$L_i = \frac{w1 - w2}{w2} \times 100 \quad (\%\quad by\quad mass) \qquad (3\text{-}4)$$

where, *wl* is the original mass of wet FA in g, *w2* is the final mass of dried FA in g. *Li* is the loss on ignition %. Li of FA is reported in Table 3-1.

Table 3-1 Physical properties of HOFA

Parameters	FA-SA	FA-NB
Colour (Visual observation)	Grey	Black
Bulk density (g/cm^3)	0.255	0.250
Specific gravity (G_S)	1.44	1.39
Moisture content	9.62%	12.79%
Li	25%	32%
Ash content	14.5%	16.32%
pH	8.90	8.70
Iodine number	2.95	5.25

3.2.5 Ash content

The ash content was determined by the standard method (D2866-94) suggested by ASTM (2000). In this case, 0.5 g of FA was dried at 105°C for 24 hrs and placed in a weighed ceramic crucible. The sample was heated in an electrical furnace at 650°C for 3 hrs. The crucible was cooled in a desiccator and weighed. The percentage of ash was calculated as follows:

$$\text{Ash}(\%) = \frac{W_{si} - W_{sf}}{W_i} \times 100 \qquad (3\text{-}5)$$

where, W_{Si} is the weight of the crucible containing the FA in g, W_{Sf} is the weight of the crucible in g, and W_i is the weight of the original FA used in g. The ash content of the FA is reported in Table 3-1.

3.2.6 Iodine number

Iodine number (IN) can be defined as the milligrams of iodine adsorbed by 1.0 g of FA. The ASTM standard method (D4607-94) was used to determine the iodine number. In this case, 10.0 ml of 0.1 N iodine solution in a conical flask was titrated with a 0.1 N sodium thiosulfate solution in the presence of 2 drops of 1% by wt starch solution until the solution became colourless. Then 0.05 g of FA was added to a flask containing 15 ml of a 0.1 N iodine solution and the mixture shaken for 4 min and then filtered. Ten milliliters of filtrate were titrated with a standard sodium thiosulfate solution using 2 drops of starch solution as the indicator. The iodine number was calculated by the equation suggested by ASTM 1112-01 (2006) as follows:

$$IN = \frac{(V_b - V_s).N.126.9(15/10)}{M} \qquad (3\text{-}6)$$

where, V_b and V_s (ml) are, respectively, volume of sodium thiosulfate solution required for blank and FA sample titrations, N (mol/L) is the normality of the sodium thiosulfate solution, 126.9 is the atomic weight of iodine, and M (g) is the mass of FA used. The iodine number of the FA is reported in Table 3-1.

3.2.7 pH determination

The pH of FA was measured according to the procedure outlined by Belen et al. (2009). In this case, 4.0 g of FA was weighed into a 250 ml beaker and 100 ml of distilled water added to it. The beaker was covered with a cap and the mixture boiled for 5 minutes. The supernatant liquid was poured off while it was at a temperature above 60°C. The decanted portion was cooled to the ambient temperature and its pH measured by a VWR scientific pH meter model 3000. The pH of the FA is reported in Table 3-1.

3.2.8 Trace elements

A quantitative chemical analysis was performed to determine the concentration of major elements in the FA samples. Microwave-assisted acid digestion followed by an inductively coupled plasma-mass atomic spectrometry (ICP-MS) examination was used to determine the trace element concentrations. A standard method (e.g., EPA 6020-B) was used to analyze the samples. An energy dispersive spectrometer (EDS) was used to analyze the carbon and sulphur in the FA samples. The concentration of selected trace elements found in HOFA is listed in Table 3-2.

Table 3-2 Chemical composition of HOFA

Elements (ppm = mg/kg)	**FA- SA**	**FA -NB**
Arsenic (As)	2.239	68.281
Bromide (Br)	370.9	124.5
Cadmium (Cd)	3.275	1.588
Cobalt (Co)	*3.28*	247.79
Chromium (Cr)	4.056	107.60
Copper (Cu)	170.40	120.30
Iron (Fe)	981.0	22633.0
Mercury (Hg)	0.245	*Not detectable*
Manganese (Mn)	20.675	135.385
Molybdenum (Mo)	26.047	398.387
Nickel (Ni)	1762.22	11852.93
Lead (Pb)	10.995	116.095
Selenium (Se)	11.592	13.186
Tin (Sn)	17.274	9.556
Vanadium (V)	2957.701	34487.12
Zinc (Zn)	130.84	592.131

The elemental analysis shows that HOFA is composed mainly of carbon. However, other elements which are significantly elevated in HOFA include V, Ni, As, Cr, Cd, Cu, Fe, Zn, and Pb. Chemical analysis confirmed FA-SA and FA-NB contained 85.56% and 51.86%

carbon respectively. The sulphur (S) content of FA-SA measured 6.24%. The chemical composition of HOFA mainly depends on HFO characteristics and the burning environment. However, for reuse purposes a lower impurity is favourable. From a comparative analysis of the two FA samples, FA-SA was found to have a higher percentage of carbon and relatively low impurities, which is a favourable characteristic for its reuse as an adsorbent. High-carbon-content materials have significant economic advantages for reuse as adsorbents (Melih et al., 2011).

3.2.9 X-ray diffraction analysis

To study their crystallographic structure and mineral composition, the FA samples were analyzed using a powder X-ray diffraction (XRD) technique. A Rigaku Americas Corporation Ultima IV X-ray diffractometer operated at 40 kV and 44 mA was used for these measurements. The detector was scanned over a range of 2Θ angles from 5^{o} to 75^{o}, at a step size of 0.02^{o} and a dwell time of 2 s per step. The resulting powder diffraction patterns were analyzed utilizing the JADE version 9 software developed by Materials Data Inc. (MDI).

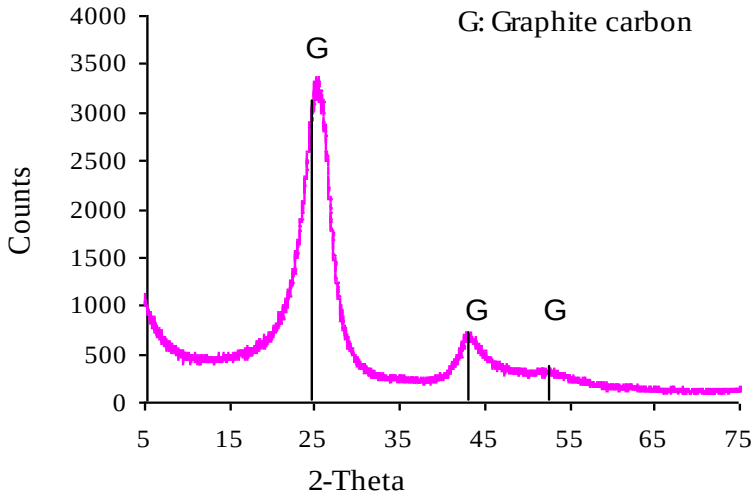

Figure 3-1 X-ray diffraction analysis of FA-SA

Although both FA samples exhibited an unstructured nature in the X-ray, some distinct mineral and compound peaks (i.e., quartz, vanadium oxide) were observed for the FA- NB. In this case, some peaks were attributed to carbon in its graphite state. The XRD structure of sample FA-NB is shown in Figure 3-2. An XRD study of sample FA-SA (Figure 3-1) exhibits high peaks of carbon in its graphite state, metallic sulfate and minerals were found to be very low compared to the carbon element.

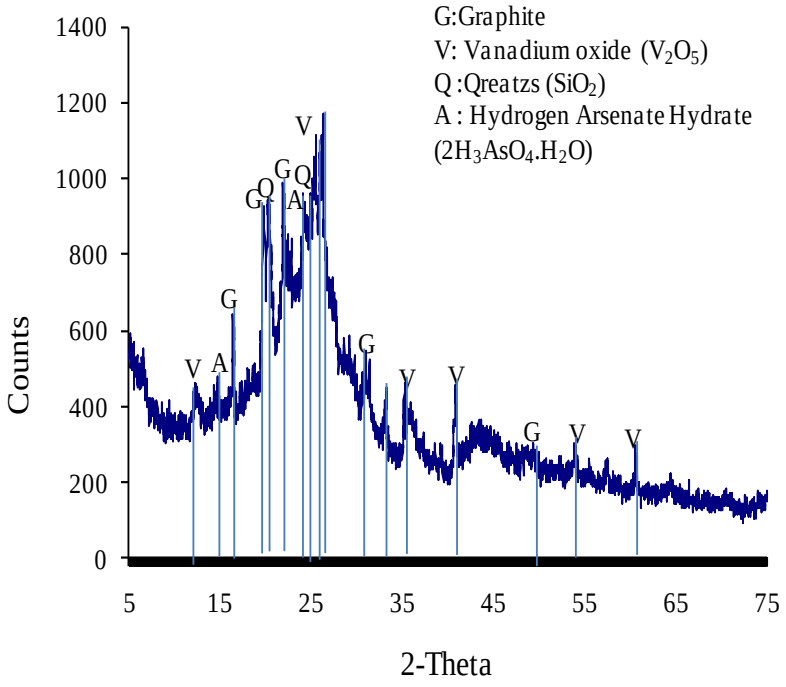

Figure 3-2 X-ray diffraction analysis of FA- NB

3.2.10 Scanning electron microscopy analysis

In the scanning electron microscopy (SEM) investigations, a Quartz PIC image measurement system observed the microstructure of the FA samples. Each sample was mounted in an epoxy resin and the surface ground flat by 600 grit abrasive paper. The sample was polished to achieve a smooth surface. The polished sample was placed in a vacuum and etched with

argon (Ar) gas for 20 min. The microstructures of FA were examined with SEM and photographs taken.

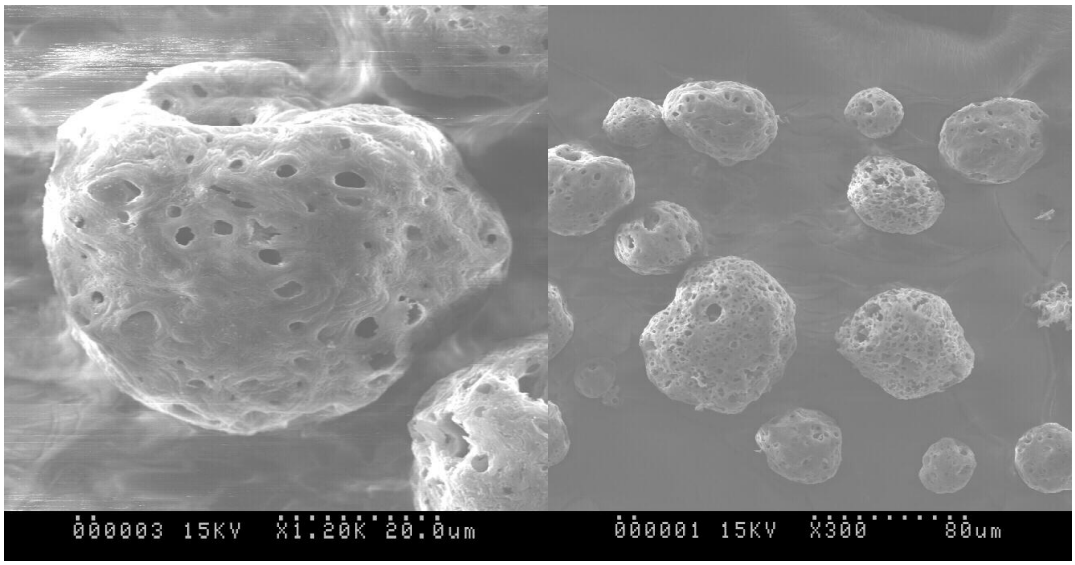

(a) SEM micrographs of FA-SA

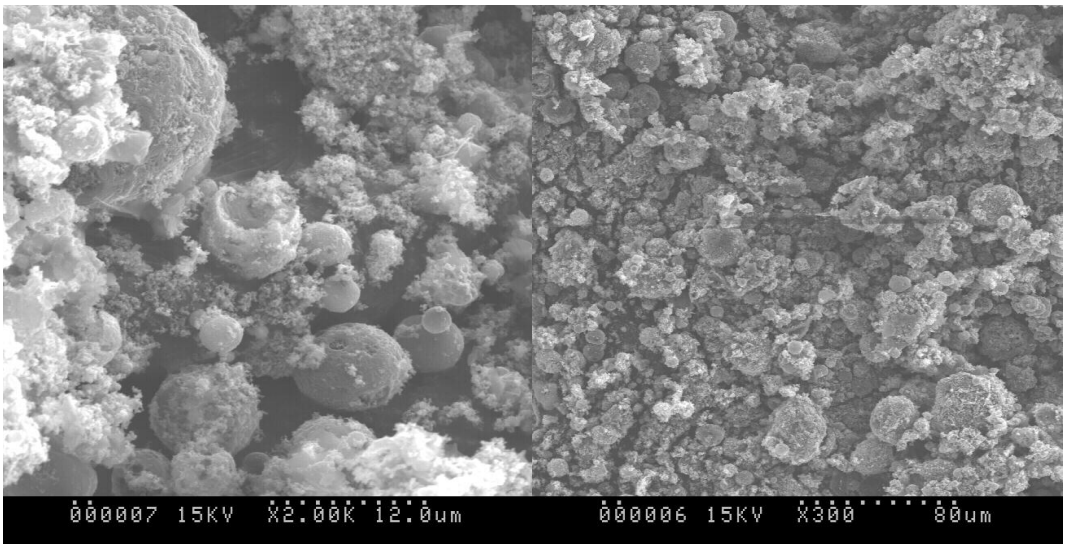

(b) SEM micrographs of FA- NB

Figure 3-3 SEM analysis of FA

The SEM micrographs (Figure 3-3) show that FA particles can be compared with spherical shapes ranging from a few to several micrometers in size. The particles are highly porous in

nature especially for the FA-SA sample (Figure 3-3a). These pores are individual and randomly located on the particle surface. Pores on the particles are generally formed by the explosion of gas inside the particle during the burning and particle formation phase (Wayne et al., 2009).

3.2.11 Particle size determination

With a spatula a small amount of FA sample was placed in a laboratory centrifuge tube. The tube was then filled with approximately 40 ml of 0.05% $NaPO_3$ solution. After hand shaking, it was placed in a tray in a Branson Ultrasonic Bath Model 5510 for overnight. Finally, the particle size of the FA sample was measured by a HORBIA PARTICA laser scattering particle size analyzer model LA-950 using a wet dispersion method in a $NaPO_3$ solution.

This analysis confirmed that the mean diameter of FA samples FA-NB and FA-SA is 8.56 and 53.50 µm with a standard deviation of 5.21 and 32.90 µm respectively as shown in Figure 3-4. According to Itskos et al. (2009), the chemical and physical properties, and subsequently the potential industrial utilization of FA, greatly depend on particle size distribution. Particle size is an important property of FA: smaller particles provide a greater surface area. Particle size affects the mobilization of any trace element through FA.

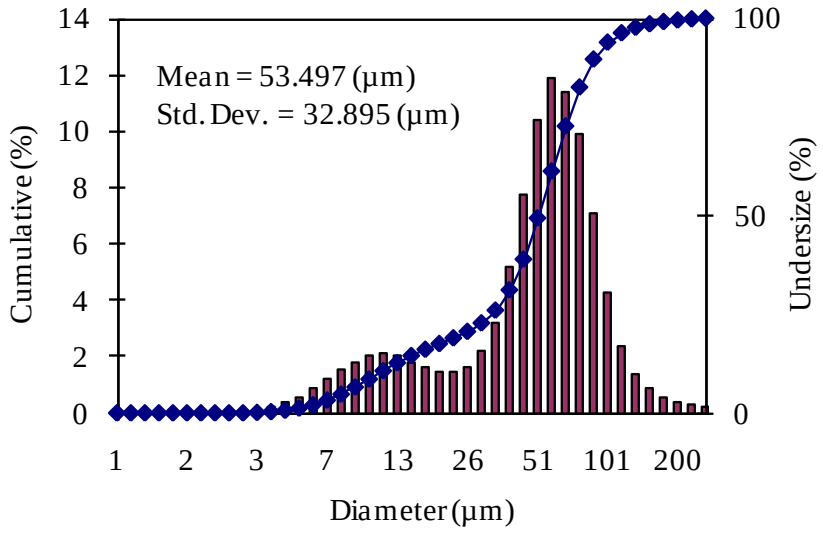

(a) Particle size distribution of FA-SA

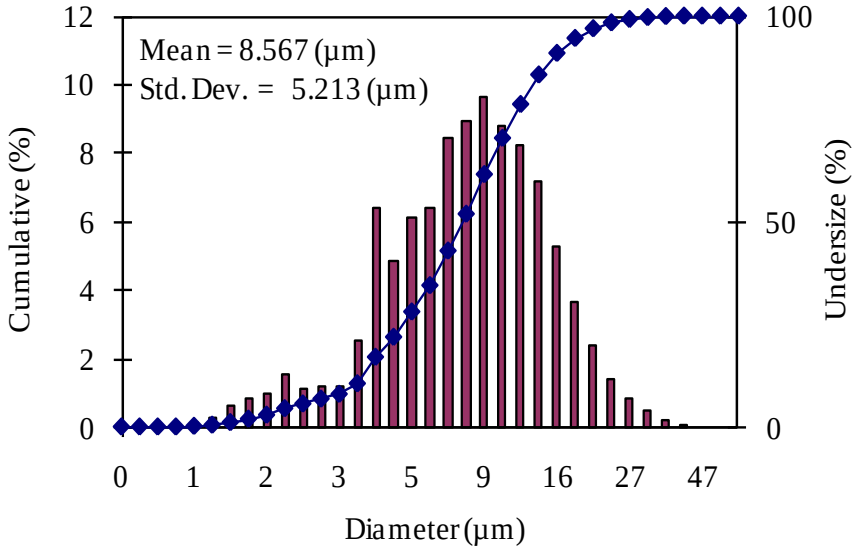

(b) Particle size distribution of FA-NB

Figure 3-4 Particle size distribution of FA

3.2.12 Surface area and pore volume analysis

The BET surface area and porosity of the FA samples were measured by N_2 adsorption at 77K using an automated adsorption apparatus BEL SOPR-MAX, BEL Japan Inc. The

surface area (m^2/g) was measured by an isotherm from the (BET) equation (Equations 3-7 to 3-11), using a relative pressure range of 0.05-0.35, considering the area of the N_2 molecule as 0.162 nm^2 at 77K (Rodriguez-Reinoso, 1997). The total pore volume, V_T, was obtained from the N_2 adsorption isotherm at $p/p_0 = 0.99$.

$$\frac{1}{v\left(\frac{P_o}{P}-1\right)} = \frac{1}{v_m c} + \left(\frac{c-1}{v_m c}\right)\left(\frac{p}{p_o}\right) \tag{3-7}$$

$$v_m = \frac{1}{S+I} \tag{3-8}$$

$$c = 1 + \frac{S}{I} \tag{3-9}$$

$$SA_{BET} = \frac{(v_m N A_{(N)})}{v} \tag{3-10}$$

$$S_{BET} = \frac{SA_{BET}}{a} \tag{3-11}$$

where, v is the volume of adsorbed N_2 molecule at standard temperature and pressure (STP), P and P_0 are equilibrium and saturation pressures of adsorbate, v_m is the volume of gas (STP) required to form one monolayer, c is the BET constant related to energy of adsorption, N is the Avogadro's number (6.02E+23), $A_{(N)}$ is the cross-section of N_2 (0.162 nm^2), SA_{BET} is the total BET surface area (m^2), S_{BET} is the specific BET surface area (m^2/g), and a = mass of adsorbent (g). The BET surface area was calculated by plotting $1 / v\,[(P_0 / P) - 1]$ on the y-axis and P/P_0 on the x-axis in the range of $0.05 < P/P_0 < 0.35$. The slope (S) and the y-intercept (I) of the plot were used to calculate v_m and the BET constant c.

Figure 3-5 shows the N_2-77K adsorption isotherms for raw HOFA samples. According to the Brunauer-Deming-Deming-Teller (BDDT) classification, these isotherms can be classified between Type II and Type III. The isotherm concave to the p/p_o axis typical represent microporous materials. However, the study isotherms do not reach the plateau at higher relative pressure, indicating the presence of meso and macro-porosity, which can be considered Type II isotherm. The surface areas of the FA were estimated by the BET equation and reported in Table 3-3. As can be seen (Table 3-3), the maximum surface area and micropore structures of FA- NB are higher than for FA- SA.

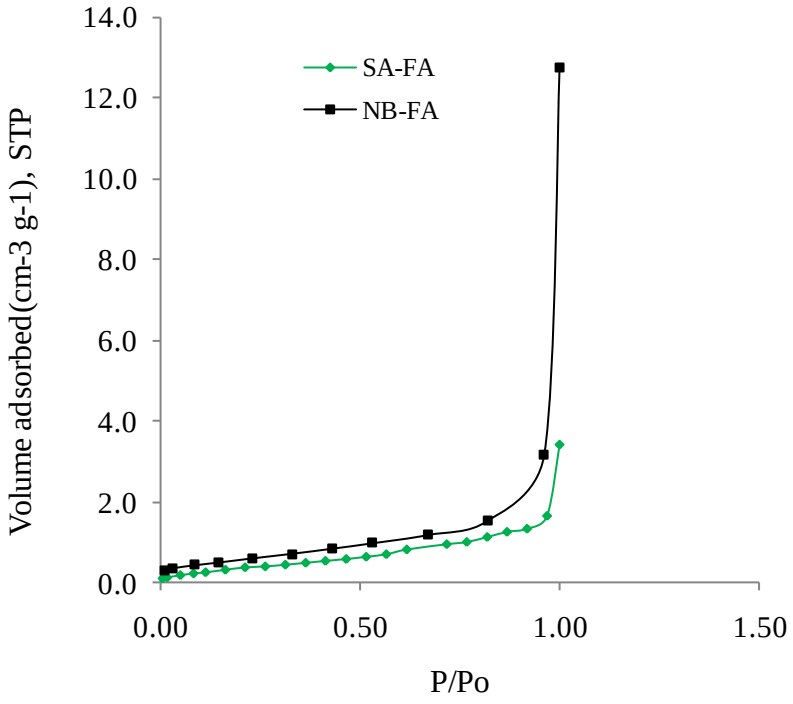

Figure 3-5 N_2-77K adsorption isotherms for prepared FAC and raw HOFA

Although there are many available methods by which to calculate pore size (Gregg and Sing, 1982; Sing et al., 1985; Rouquerol et al., 1999), the Dubinin-Radushkevich (DR) equation is

the most acceptable way of deriving the total micropore volume from any isotherm (Gregg and Sing, 1982). For this study, the DR theory (Equation 3-12) was applied to N_2 isotherms to obtain the micropore volume of the FA samples.

$$v = v_o \exp\left[-\left(\frac{BT}{\beta}\right)^2 \ln^2\left(\frac{p_0}{p}\right)\right] \qquad (3\text{-}12)$$

where, v is the pore volume that has been filled at p/p_o (cm^3/g), v_o is the micropore volume of monolayer (cm^3/g), B is a constant related to the Gaussian pore distribution (K^{-2}), T is the temperature at which the isotherm has been taken (K), β is a constant, depends on the adsorbate, p_o/p is the inverse of the relative pressure at which the isotherm developed. For a given isotherm, a plot $[\log_{10}(po/pi)]^2$ versus log (v) yields a straight line (at least some part of the plot). Finally, the total pore volume can be estimated at a partial pressure of 0.99 p/p_0 (STP) using a conversion factor of 0.001547 (Kruk and Jaroniec, 2001). Stepwise procedures for the DR method can be described as follows:

(i) Review the adsorption data, (ii) calculate $\log_{10}$, (v) and $[\log_{10}(po/p)]^2$, (iii) plot $\log_{10}$, (v) versus $[\log_{10}(po/p)]^2$, (iv) select the appropriate linear region of the curve, (v) calculate the slope and the intercept of the linear model by least squares, (iv) check the goodness of fit, (vi) calculate the monolayer capacity, *v*o, using the intercept of the linear model on the y-axis, i.e., $\log_{10}$ (*v*o), (vii) calculate the total micropore volume by multiplying *v*o by the density conversion factor (values of density conversion factor for nitrogen is 0.001547 cm^3 liquid/cm^3 STP). For example, the y-intercept of the raw FA- SA sample is 0.1.25 (Figure 3-6); the micropore volume (V_{mc}) of FA- SA can be estimated as:

$$V_{mc} = 10^{0.125} \times 0.001547 = 0.00116 \quad (cm^3/g) \qquad (3\text{-}13)$$

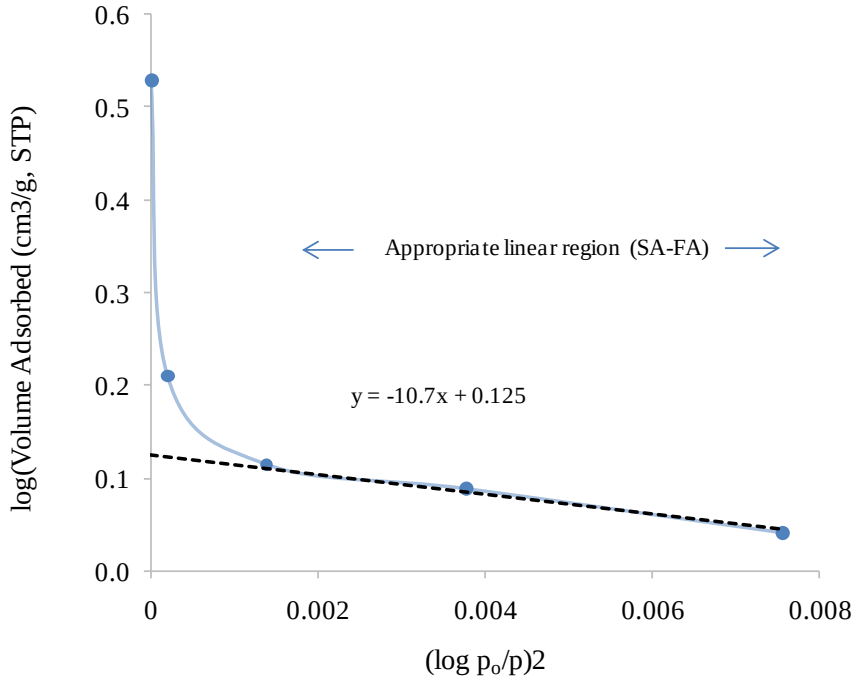

Figure 3-6 DR plot for micropore volume estimation (FA-SA)

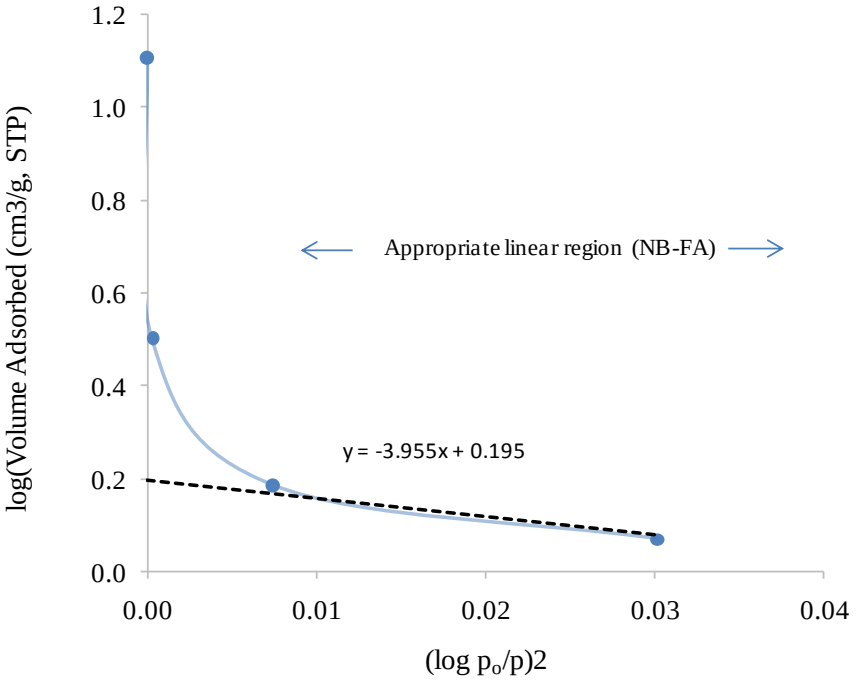

Figure 3-7 DR plot for micropore volume estimation (FA-NB)

Table 3-3 Textural properties of HOFA

Parameters	**FA-SA**	**FA-NB**
[a]BET Surface area (m^2/g)	1.4496	2.1815
[b]Total pore volume v_T (cm^3/g)	0.004416	0.01574
[c]Micropore volume v_{mc} (cm^3/g)	0.00116	0.0024
[d]Mesopore volume (cm^3/g)	0.00325	0.0133
Mean pore diameter (nm)	12.185	28.861

[a] Specific surface area (m^2/g): BET equation (P/P0 = 0.05~0.35)
b Total pore volume v_T (cm^3/g): v (P/P0=0.99) × 0.001547
c Micropore volume (cm^3/g): DR equation, v_o × 0.001547
d Mesopore volume (cm^3/g): v_T - v_{mc}

3.3 Batch leaching test

A batch leaching test (BLT) was conducted to investigate the leaching behaviour and mobility of trace elements in FA. The management of FA often requires this information in order to interpret the leachability of metals in the environment (Scott et al., 1990). Many leaching test protocols, such as the toxicity characteristic leaching procedure (TCLP), equilibrium leach test (ELT), and acid neutralization capacity (ANC), have been cited in the literature (USEPA, 1989; ECAEC, 1986). These tests were developed to simulate the leaching processes of waste materials in landfills or other disposal facilities in order to evaluate their possible risk to humans and/or ecosystems. TCLP, developed by the United States Environmental Protection Agency (USEPA), is widely used to classify hazardous solid wastes and to evaluate the worst leaching conditions in a landfill (USEPA, 1989). ANC and ELT simulate the leaching characteristics caused by precipitation on improperly designed landfills (ECAEC, 1986). ELT is designed to evaluate the maximum leachate concentration under mild conditions, while ANC uses acidic solutions to evaluate the leachate (ECAEC, 1986). Both ANC and ELT are applicable to fine- to moderate-sized waste materials

(ECAEC, 1986). Based on the particle sizes of HOFA, an ELT and ANC method was selected for this study. Pollutants from a landfill are mainly leached by rainwater or acid rain. To simulate the appropriate leaching environment, distilled water (p^H = 6.3) and acid solution (p^H = 3.0 using distilled water with nitric acid) were used as leaching media. All test apparatus were cleaned with an acid solution (e.g., 15% HNO_3 solution) and rinsed with distilled water prior to the leaching experiments. The batch extraction procedures and liquid to solid (L/S) ratios are reported in Table 3-4. To ensure continuous stirring of the samples, a PHIPPS & BIRD stirrer model 7790-400 with 10 revolutions per minute (rpm) was used over the test period.

Table 3-4 Experimental conditions of batch leaching test

Method	**Leachant**	**L/S Ratio**	**Extraction time (h)**	**Temperature (°C)**	**Reference**
ELT	Distilled water (p^H=6.3)	4:1	7 days	25	(ECAEC, 1986)
ANC	HNO_3 solutions (p^H=3.0)	3:1	48 hours	25	(ECAEC, 1986)

Among the trace metals originally present in the HOFA samples (Table 3-2), a significant percentage (i.e., 0-3345 mg/L) was obtained through leaching tests under different conditions (Table 3-5). In this case the maximum leachate concentration (MLC) is 3345 mg/L for V followed by Ni at 2494 mg/L. All elements showed higher leaching rates under an acidic medium than with distilled water, except for V and Cd in sample FA-NB. This test proved that the leachability of the metals is affected by the acidity of the leaching solution. Similar results were observed by Van der Sloot (2002). From this test it is also clear that pH has a significant impact on the mobility of the trace elements present in HOFA. Leach from an HOFA dumping site may have polluted the groundwater or a nearby surface-water body. In

many developing countries people still use untreated groundwater and surface water for household purposes. To manage the possible environmental impacts associated with HOFA dumping, a local authority may need a maximum leaching concentration (MLC). In order to evaluate the possible impacts of HOFA on the portable water, MLCs were compared with the drinking-water threshold values set by United Kingdom (DWT, 2001) and USEPA (1993). Table 3-5 shows that the MLCs (6.94, 0.242, 9.988, 15.60, 0.006, 1442.98, 1.559, and 74.867 mg/L) respectively for As, Cd, Cr, Cu, Hg, Ni, Pb, and Zn exceed their highest environmental permissible concentrations (0.01, 0.001, 0.005, 0.02, 0.002, 0.05, 0.05, and 5 mg/L) respectively, as recommended by DWT (2001) and USEPA (1993).

Table 3-5 Results of batch experiments

Heavy metals	**Detection limit (mg/L)**		**Peak concentration levels (mg/L)**			**Permissible limit** [a]
		FA- NB	**FA- SA**	**FA- NB**	**FA- SA**	
		ANC (P^H = 3)		ELT (P^H =6.3)		
As	0.001	6.940	0.041	1.710	0.002	0.01
Cd	0.001	0.217	0.004	0.242	0.004	0.001
Co	0	31.83	0.05	29.64	0.05	-
Cr	0.005	9.988	0.283	5.854	0.162	0.05
Cu	0	15.60	0.600	12.30	0.700	0.02
Hg	0	ND	0.006	ND	0.003	0.002
Ni	0	1442.98	77.91	1395.51	55.86	0.05
Pb	0	0.568	0.116	0.273	0.025	0.05
Se	0.027	1.559	0.031	1.446	0	-
V	0.001	2494.155	303.912	3345.546	102.626	-
Zn	0.002	74.867	0.894	65.623	0.652	[b]5.00

Note: ND = not detectable; [a](DWT, 2001); [b](USEPA, 1993)

BLT results indicate that the elements in the HOFA easily leach into the environment by rainwater or acid rain. The amount of toxic metals released through HOFA is hazardous to the environment and to human health. Because of this, the proper management of HOFA is

crucial. Although particle-removal devices in power plants effectively minimize air pollution by capturing fine particles, this experiment reveals that toxic elements in HOFA are introduced to the environment by land-based dumping.

3.4 Summary

The physical and chemical properties of two different HOFA samples have been examined. Standard batch leaching tests were conducted in order to identify the mobility of potentially hazardous elements within HOFA. The results indicated that most of the toxic elements in HOFA can easily leach into the environment, which might result in toxicity to ecosystems and humans through contamination of the surface and groundwater.

The two HOFA samples presented both differences and similarities in their properties. However, characteristics analysis showed a high percentage of unburned carbon, less toxic metals, and an extremely porous particle surface of the Saudi Arabian HOFA, which could be a feasible source of raw material for producing a good quality natural adsorbent for industrial use. This reuse would have environmental and economic benefits and also reduce HOFA management costs.

Chapter 4

Methodology for Health Risk Assessment Associated with Fly Ash Dumping

4.1 Introduction

The goal of health risk assessment is to estimate the severity and likelihood of damage to human health from exposure to pollutants. Risk assessment models are used to identify human exposure limits to contaminants via multiple exposure routes such as inhalation, ingestion, and dermal contact. Regulatory agencies use health risk assessment processes for a variety of situations: (i) to set standards for toxic chemicals in air, water, soil, or food, (ii) to conduct baseline analyses of contaminated sites or facilities and determine remedial actions, (iii) to develop cleanup goals at contaminated sites, and (iv) to evaluate the effectiveness of existing and new technologies used for the prevention, control, or mitigation of hazards and risks. There are two primary methods of risk analysis. Qualitative analysis, which helps to identify the resources at risk, uses simple calculations and expert assumptions and procedures. It does not quantify the hazards or frequencies of risk. Different qualitative scales are used to assess an acceptable level of risk and develop awareness procedures. On the other hand, quantitative analysis, which identifies the magnitudes of losses associated with hazards, involves exposure dose estimates against a benchmark of toxicity, such as a cancer slope factor (SF) or a reference dose (RfD). For example, the quantitative analysis is generally used to estimate the probability of risk in a community where the chemical was

suddenly spilled or to calculate the health risks associated with the presence of metals in the air or the drinking water.

Risk assessment provides an effective framework for determining the relative importance of problems and the allocation of resources to reduce the risks. The results of risk assessment help to develop target prevention, remediation, and control efforts for areas, sources, or situations in which the greatest risk reductions can be achieved with available resources. This study develops an integrated risk assessment methodology to assess human health risks associated with the airborne metals (AM) released from a fly ash (FA) dumping site. The methodology involves (a) dispersion of AM in the ambient environment, with a consideration of source uncertainties, (b) human exposure and response assessment, and (c) characterization of the human health risk. The ground-level inhalable dust concentration was predicted using an Industrial Source Complex (ISC3) air dispersion model (ISC, 1987). The exposure concentration of arsenic (As), cadmium (Cd), and chromium (Cr) were established by chemical analysis of the source FA dust. The possible health risk to residents living near a FA dumping site in Saudi Arabia is addressed through this analysis. Several models are available for a health risk assessment. The application of such methods depends on the nature and availability of data. In general, a risk assessment process consists of four basic steps.

4.1.1 Hazard identification

The purpose of hazard identification is to identify the adverse effects of a substance (USEPA, 1991). Initially, a Preliminary Hazard List (PHL) is generated for a specific assessment. Based on toxicity analysis the PHL is grouped into classes. Sometimes a consequence assessment (i.e., a possible undesired event) resulting from a hazard is needed prior to risk analysis. Hazard scenarios may address questions related to exposures and

levels: who (exposed), what (levels), where (exposed), when (exposed), why (exposed), and how (USEPA, 1991). For example, identifying the level of a chemical contaminant like arsenic or benzene and documenting its toxic effects on humans are part of hazard identification.

4.1.2 Exposure assessment

Exposure assessment evaluates the contaminant's concentration in the environment and its intake rate by the target organisms. It also identifies the potential pathways (e.g., inhalation, ingestion, and dermal contact) of human exposure and chemical intake associated with each pathway (USEPA, 1989, 1991).

4.1.3 Dose-response assessment

Based on the degree of exposure, a dose-response assessment quantifies the adverse effects arising from exposure to a hazardous agent (USEPA, 1991). It is usually expressed mathematically as a plot showing the response in living organisms to different doses of a chemical agent.

4.1.4 Risk characterization

Risk characterization is an integral component and final step of a risk assessment process. Risk characterization estimates the potential impact of a hazard based on the severity of its effects and the amount of exposure (USEPA, 1991). After the characterization of risk, sometimes regulatory options are evaluated in a process called risk management. Social, political, and economic issues, as well as engineering knowledge, are used in risk management.

4.2 Background of the study

Due to its local availability and relatively low cost some power production facilities in Saudi Arabia use heavy fuel oil (HFO) to generate electricity. HFO is the main fuel contributing to more than 70% of Saudi Arabia's national energy production (ECRA, 2009). Chemical analysis (Chapter 3) showed that a significant amount of heavy metals such as arsenic (As), cadmium (Cd), mercury (Hg), copper (Cu), vanadium (V), and nickel (Ni) is present in HOFA. HOFA consists of airborne particles with very low bulk density which varies from 0.250 g/cm^3 to 0.50 g/cm^3 (Chapter 3). In Saudi Arabia, thousands of tonnes of HOFA are generated yearly and dumped into landfills. HOFA production will continue to increase in the future; therefore, power plants in the Kingdom may face difficulties with their HOFA disposal. The current industrial management practices of HOFA in the Kingdom mainly follow a dry disposal procedure: FA is transported by truck or conveyor from power plant to disposal site. Land disposal of FA creates ever-growing environmental problems, including the pollution of air, surface water, and groundwater. Air pollution is caused by direct emissions of windblown ash from the disposal facilities. Airborne dust can fall in, and contaminate, the surface water or soil. Dumping FA involves different activities (i.e., handling, transportation, and disposal) which lead to the formation of airborne dust. This metal-contaminated dust can be inhaled and swallowed by exposed humans and animals. Long-term exposure to AM can lead to many human diseases, which are well documented in the literature (IARC, 1980; Comba et al., 2006;). Effective evaluation is crucial in assessing the health risk associated with FA dumping. Risk assessment results can be used for improving FA management systems. However, the quality of information available for the health risk assessment of AM released from HOFA disposal sites is often inadequate; this

lack prompted the present study. Risk assessment generally describes the origin of pollutants, their movement within the environment, and their exposure pathways. The resulting human health risk can then be calculated by using data, models, and necessary assumptions related to the exposure.

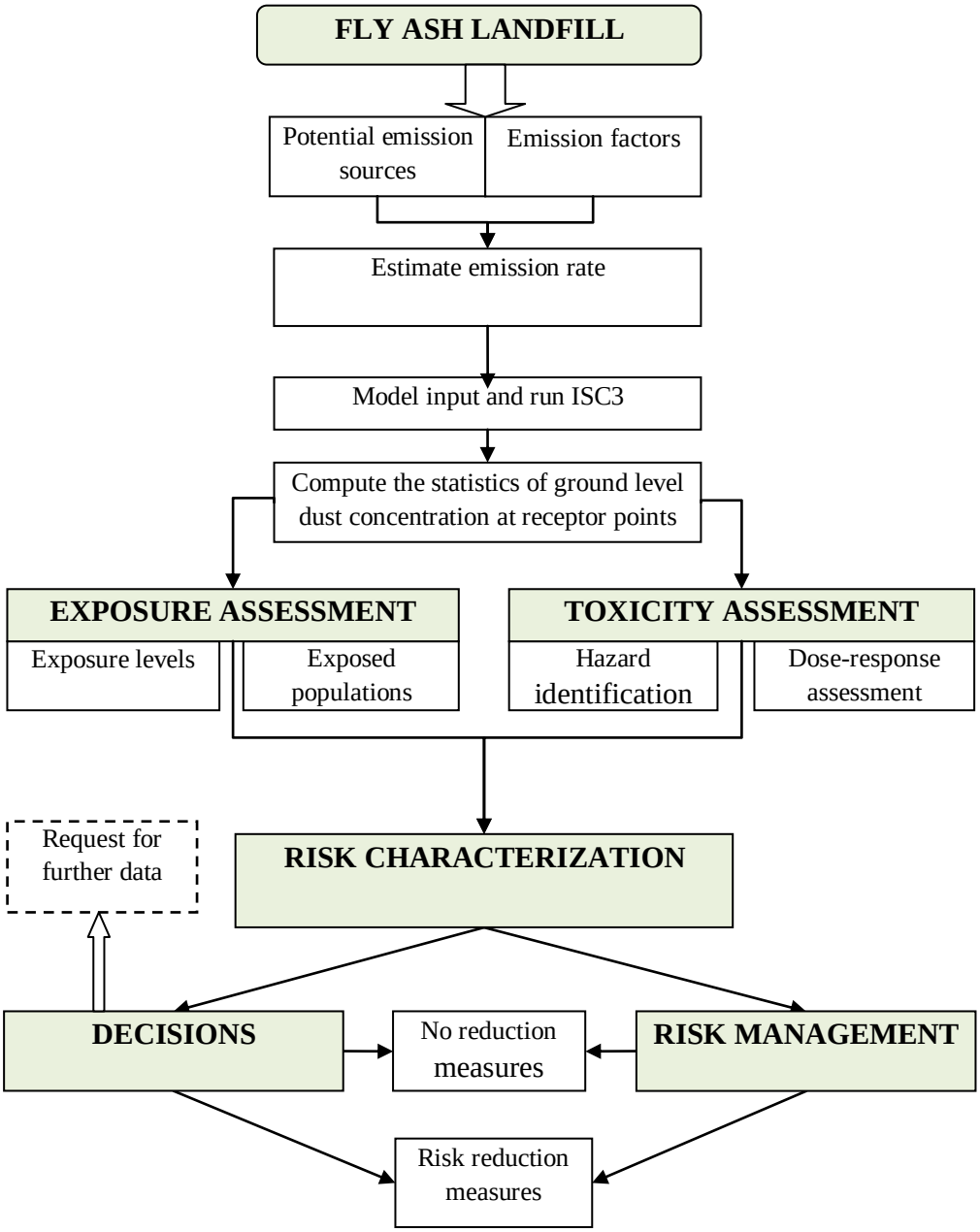

Figure 4-1 Health risk assessment procedure for landfill dust emissions

The goal of risk assessment is to estimate the severity and likelihood of harm to human health from exposure to a substance or activity (USEPA, 1991). Using an inhalation pathway, Christopher et al. (2006) conducted a quantitative human risk assessment of the air pollution released from landfills. This study observed that landfill pollutants have a negative impact on human health. The significant health effects of heavy metals are reported in the literature (IARC, 1973, 1980; WHO, 2003). Various studies which have assessed the health risk to residents living near landfills demonstrate a significant health risk for the exposed population (Jarup et al., 2002; Redfearn and Roberts, 2002; Comba et al., 2006). Several models are available for health risk assessment (Mofarrah and Husain, 2011; Cohrssen and Covello, 1989; USEPA, 1991). The application of such methods depends on the nature and availability of the data. Uncertainties in risk estimates may arise from sources such as the measurement or estimation of parameters, natural variability in individual response, variability in the environmental concentration of toxicants over time and space, and unverifiable assumptions in dose-response models or extrapolations of the results of these models (Kentel, 2004). Environmental conditions may change the pollutant concentration in the ambient air; it may vary as a function of air temperature, wind circulation, or humidity. The point estimate of risk always acknowledges the existence of these uncertainties in the output results. Recently, probabilistic risk assessment (PRA) methodology has become well accepted in analyzing uncertainties in risk estimates. PRA is the general term for risk assessment that uses probability theory and models to represent the likelihood of different risk levels in a population or to characterize the uncertainty in risk estimates (Maxwell and Kastenberg, 1999). The most widely used PRA approach to characterizing uncertainty in risk assessment studies is the Monte Carlo (MC) simulation (USEPA, 1996). The result of a PRA

approach is a probability distribution which reflects the combination of all input distributions. However, in a PRA approach, if input distributions provide variability, then output risks may provide some variability. If input distributions reflect uncertainty, then output risk distributions may provide information about the uncertainty in the estimated risk (USEPA, 2001).

The objective of this study is to model human exposure to airborne metals released by the dumping of HOFA into landfill sites, with the aim of providing safe and effective FA management options. In order to quantify the health risk associated with airborne metals released from a fly ash dumping site, this study uses a PRA approach. Potential exposure routes for nearby residents may be the inhalation of particles, the ingestion of contaminated home-grown food, drinking water from wells contaminated with leachates, and skin contact with contaminated soil.

However, for this study the evaluation of exposure pathways was based on site-specific situations. As the region has a low precipitation, the mobility of metals in the environmental media via surface or subsurface water movement was assumed to be insignificant. On the other hand, fugitive dust is a dominant environmental phenomenon in this area, and airborne metals from the FA dumping site have long been considered a potential health hazard for the surrounding population. Based on the toxicity level, three heavy metals, arsenic (As), cadmium (Cd), and chromium (Cr), were chosen to demonstrate the proposed methodology for evaluating risks to adult receptors.

4.3 Methodology

The major steps that contribute to the risk assessment paradigm are shown in Figure 4-1. The different steps of the methodology are illustrated below.

4.3.1 Prediction of exposure concentration

The exposure concentrations at receptor points were estimated by using an air dispersion model. An air dispersion model is a tool that simulates the release and dispersion of air pollutants in the atmosphere. It is used to study air pollution or changing the amount of pollutants released into the air from existing emission sources. Several models are available for urban air dispersion modeling: industrial source complex (ISC) modeling system (USEPA, 1995), AERMOD atmospheric dispersion modeling system (Cimorelli et al., 1998; USEPA, 2002), and CALPUFF dispersion modeling system (Scire et al., 2000). The applicability of these models depends on regulatory needs and input data requirements. Model application also depends on underlying physical concepts, temporal and spatial scales, the type of source, and the type of component, etc. Among others, industrial source complex (ISC3) model developed by USEPA (1995) is a popular air dispersion modelling system. The ISC3 dispersion model is based on a modified form of the Gaussian plume equation, which uses empirical dispersion coefficients and includes adjustments for plume rise, limited mixing height, and elevated terrain. Pollutant levels are computed from measured hourly values of wind speed and direction and estimated hourly values of atmospheric stability and mixing height. The ISC3 model can incorporate point, area, and volume sources. The ISC3 model uses hourly meteorological records to define the conditions for plume rise, transport, diffusion, and deposition (USEPA, 1995). It calculates the hourly concentration or deposition value for each source and receptor and is summed to obtain the total concentration produced at each receptor by the combined sources emissions (Mofarrah and Husain, 2010). To calculate the ground-level dust concentration at receptor points, this study used the ISC3 air dispersion model. The study area was divided into an equal grid system and all receptor

points converted to Cartesian (x, y) coordinates prior to performing the dispersion calculations.

4.3.2 Source identification and dust emission rate estimation

Many activities or situations contribute to dust generation in FA landfills: (i) a new dumping area, (ii) the operation of vehicles, and (iii) the uncovered surfaces of the landfill (USEPA, 1994). Fugitive dust easily results from a new dumping area through the process of wind erosion once the wind speed is greater than 2.5 m/sec on a sunny day (Howell et al., 1998; Etyemeziana et al., 2003; Jorkevic et al., 2004). Operation activities are another important source as moving vehicles in the landfill site often release large amounts of dust from the road, especially at speeds higher than 20 km/hr (Etyemeziana et al., 2003). Dust from uncovered surfaces could easily be created by wind at speeds above 5.0 m/sec (Clausnitzer, 1996; Ho et al., 2003). Since dust emission greatly depends on source and activity, it is important that the dust emission rate be predicted for each event separately. Dust emission from a dumping site can be calculated by using the emission factors suggested by the AP-42 guidebook (USEPA, 1994). Emissions from a FA dumping site are highly variable; they depend on such factors as the local environment, operation activities, and the movement of vehicles. For this study, (i) uncovered surfaces, (ii) new dumping spots, and (iii) operation activities were considered potential dust emission sources.

The calculation of an emission factor for FA handling (including loading, unloading, etc.) was based on the wind velocity, particle size, and moisture content of FA using Equation 4-1 (USEPA, 1994):

$$E = k(0.0016)\frac{\left(\frac{U}{2.2}\right)^{1.3}}{\left(\frac{M}{2}\right)^{1.4}} \times 10^{3} \qquad (4\text{-}1)$$

where, E is the emission factor g/ton, k is the particle size multiplier (dimensionless), U is the mean wind speed, meters per second (m/ sec), M is the material moisture content %. The particle size multiplier k varies with particle size range. However, for this investigation the average particle size of FA = 56.25 µm and the multiplier k = 0.74 were used as suggested by USEPA (1994). Using the emission factor (E), the total dust emission calculation was based on the amount of FA dumped per day into the landfill using the following relationship:

$$Q = \frac{(E \times M_{FA})}{CF} \qquad (4\text{-}2)$$

where, Q is the emission rate in g/s, M_{FA} is the amount of FA dumping to the site on a daily basis in ton/day, CF is the conversion factor (86400 second/day); E is the dust emission factor in the source in g/ton, calculated by Equation 4-1.

According to USEPA (1989a), the total dust emission from an active storage area due to wind erosion can be calculated as follows:

$$Q_{(A)} = 1.7 \times \frac{s}{1.5} \times \left\{\frac{365(365-p)}{235}\right\} \times \frac{f}{15} \qquad (4\text{-}3)$$

where, s is the silt content of the material (weight %), p is the number of days per year with at least 0.01 inch of precipitation, f is the percentage of time the wind speed is greater than 12

miles per hour (mph), $Q_{(A)}$ is the total dust emission from an active storage area in lb/year/acre of surface, which was converted to g/m^2/s.

4.3.3 Risk characterization

The average chronic daily intake (CID) of metals via the inhalation of airborne dust particulate was calculated by the following equation (USEPA, 1991):

$$CID = \frac{C_m \times C_d \times IRA \times AF_{Inh} \times EF \times ED \times CR}{BW \times AT} \quad (4\text{-}4)$$

C_m is the metal concentrations in dust, from the laboratory experiment in mg/kg, C_d is the dust concentration in the air at receptor points in μg/m^3 determined by an ISC3 air dispersion model, *IRA* is the inhalation rate of air m^3/hr, AF_{Inh} is the absorption factor for the lungs (unit less), used a value of 1 for conservative risk assessment as recommended by USEPA (1991), *EF* is the exposure frequency in days/year, *BW* is the human body weight in kg, *ED* is the exposure duration in year, *CR* is the conversion factor (10^{-9}), *AT* is the average time in number of day.

The combined non-carcinogenic risk is normally expressed by a dimensionless term called a hazard index (HI). This is simply the ratio of the CID to the reference dose (RfD) (mg/kg day) as follows:

$$HI = \sum_{i=1}^{4} \frac{\mathrm{CID_i}}{\mathrm{RfD_i}} \quad (4\text{-}5)$$

The cumulative cancer risk (CR) was calculated by adding the chronic daily intake values multiplied by the corresponding slope factors of the respective heavy metals as follows:

$$CR = \sum_{i=1}^{n} CID_i \times SF_i \quad (4\text{-}6)$$

where, SF_i is the carcinogenic slope factor of ith pollutant $(mg/kg/day)^{-1}$, n is the number of pollutants, CID_i is the chronic daily intake value for the pollutant i (mg/kg/day), i equal to 1,2,3,4... represents the heavy metals.

Table 4-1 Parameters used in human risk analysis

Parameters	**Symbol/Unit**	**Distribution**	**Values**	**References**
Body weight	BW (kg)	Triangle	Triangle (63,70,77)	Mofarrah and Husain, 2013
Inhalation rate	IRA (m^3/hour)	Log normal	LN (0.8334,0.108334)	Section 4.3.4
Metal concentrations in FA	Cm (mg/kg)	Normal	As = N (2.51, 1.75) Cd = N (0.824, 0.511) Cr = N (3.02, 2.32)	Lab analysis
Exposure frequency	EF (days/year)	Constant	350	USEPA, 1991
Exposure duration	ED (years)	Log normal	$\mu = 5.32$, $\sigma = 3.09$	Benekos et al., 2007
Number of year the person is likely to be exposed	LE (days)	Constant	25,550; for cancer risk estimation 10,950; for non-cancer risk estimation	USEPA, 1991
Carcinogenic slope factor (SF)	Inhalation SFs $(mg/kg/day)^{-1}$	Constant	As = 1.5E+01 Cd = 6.30E+00 Cr = 42	IRIS, 1995 IRIS, 1995 IRIS, 1995
Reference dose (RfD)	Inhalation RfDs (mg/kg/day)	Constant	As = 8.6E-06 Cd = 8.00E-04 Cr = 1.0E-03	IRIS, 1995 IRIS, 1995 Health Canada, 2007

4.3.4 Evaluations of risk assessment parameters

Metal concentration in FA

A quantitative chemical analysis was performed to determine the metal concentrations in the HOFA samples. An inductively coupled plasma-mass atomic spectrometry (ICP-MS) was

used. The mean and standard deviations of different metal concentrations are shown in Table 4-1.

Inhalation rate

The inhalation rate varies from person to person. According to USEPA (1991), the average inhalation rate for adult receptors was 0.8334 m^3/hour. For this study, a log normal distribution with geometric mean and geometric standard deviation LN (0.8334, 0.1083) was selected for the adult inhalation rate.

Body weight (BW)

According to USEPA (1991), the body weight for adult receptors was 70 kg. This value may differ for the population near the FA dumping site. The present risk assessment study assumed a triangle distribution, with the most likely value 70 kg, a minimum 63 kg, and a maximum 77 kg for adult body weights.

Life expectancy (AT)

At present, there is no human characteristics data for this risk assessment study. According to USEPA (1991), an average human life expectancy is 70 years for a carcinogenic risk assessment. For this study, life expectancy is assumed to be a triangle distribution (63, 70, and 77), with minimum 63, most likely value 70, and maximum 77 years respectively. All other parameters used in the risk assessment are reported in Table 1.

4.4 Case study

The Rabigh power plant (RPP), which is situated near Jeddah city, is one of the largest power generation facilities in Saudi Arabia. About 10,000 tonnes of FA are generated yearly by this plant, which dumps into the landfill. The Rabigh area has a typical arid climate. A very low rainfall (i.e., 0-10 mm) is observed from May to December, and precipitation ranging from

14 mm to 30 mm is observed from January through April (SEC, 2007). The average temperature of this region varies from 14°C to 35°C respectively in the winter and summer seasons (SEC, 2007). There is no air quality monitoring station in this area; the closest reliable metrological recording station for the area is the Jeddah airport. As shown in Figure 4-2, the prevailing wind direction is north-west, which was estimated by using the meteorology data of 2006 from the Jeddah airport metrological monitoring station.

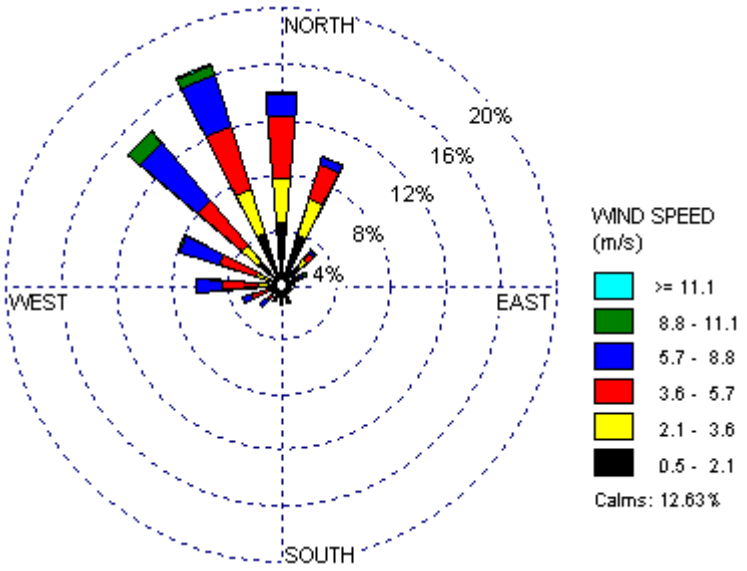

Figure 4-2 Prevailing wind direction in the study area

There is no surface-water body near the FA dumping site. Because the groundwater table is very deep, the mobility of metals in environmental media via surface or subsurface water movement was assumed to be insignificant. Therefore, this investigation was undertaken in order to provide information about the human health risk associated with the FA dumping site through an inhalation pathway only. The exposure assessment was modeled by an ISC3 air dispersion model to predict the risk agent to the nearest receptor point.

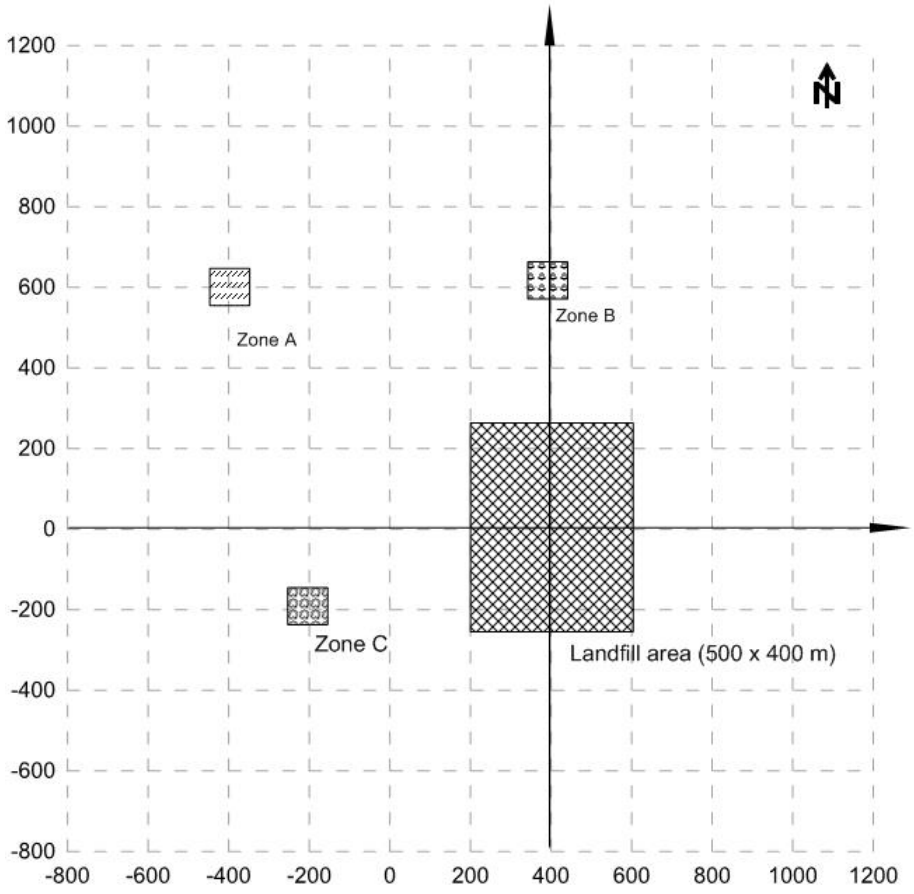

Figure 4-3 Configuration of risk assessment study area

The FA dumping site was modeled at 500 × 400 m (Figure 4-3). Based on the dominant wind directions, three points (i.e., zones A, B, and C) were assumed to be receptor locations which are sensitive to airborne metals released from the FA dumping site.

Fugitive dust easily results from the new dumping area through a process of wind erosion on a sunny day or landfill activity. This analysis assumed that a 30 m^2 new dumping area will be created by routine operations. Operation activities are another important source of fugitive dust, since moving vehicles and the loading and unloading of FA often releases large amounts of particles into the atmosphere. For this assessment, a 30 m wide and 200 m long road is considered a daily operation area in the landfill site. Although a good practice in a

landfill operation is to cover a new dumping area regularly, this may not be possible for each case. For a conservative analysis, a 100 m^2 area was assumed to be a daily basis uncovered surface from where air particles could be stirred up by the wind. The estimates of FA dust emissions from these three sources were based on the amount of FA dumped on a daily basis. From the investigation, it was found that the Rabigh power facility generates about 25-30 tonnes of FA per day.

Table 4-2 Evaluation of emission rate for different activities in the FA landfill

Sources	**Unit**	**Symbol**	**Emission rate**
Uncovered surfaces	$g/m^2/s$	(μ, σ)	(6.28E-5, 2.51.14E-5)
New dumping area	$g/m^2/s$	(μ, σ)	(6.28E-5, 2.51.14E-5)
Operation activities	g/s	(μ, σ)	(0.000136, 3.87E-5)

μ = arithmetic mean ; σ = standard deviation

To minimize uncertainty in the study a variable FA dumping rate with a mean and standard deviation of 28 tonnes /day and 8 tonnes /day respectively was assumed. Using Equations 4-1 and 4-2 the emission dust rate was calculated for various activities. The wind erosion dust for uncovered and new dumping areas was calculated by Equation 4-3. The silt content of FA was assumed to be 75% by weight, and only 10 days per year considered to experience precipitation within a certain rang. Based on the metrological information 60% of the time with a standard deviation of 10% was considered to be when there was a wind speed greater than 12 mph over the FA dumping area. Table 4-2 shows the emission factors calculated for this assessment. A Monte Carlo simulation (MCS) with 1000 iterations was used to generate the cumulative distribution of emission rates for each scenario.

Using the emission rates (Table 4-2), an ISC3 model predicted 24-hour maximum ground-level dust concentrations at three receptor points (i.e., zones A, B, and C) in Figure 4-3. To minimize the influence of parameter uncertainty, especially the emission rate estimation, MCS was used. The MCS approach involves the repeated generation of random values for uncertain input parameters. With a known emission rate probability distribution, 1000 sets of possible values were generated. Consequently, using the 2006 metrological data from the Jeddah airport, at each receptor point 1000 sets of maximum ground-level dust concentration values were generated (Table 4-3). The spatial distribution of the FA dust over the study area (for #1 simulation) is shown in Figure 4-4. The cumulative distribution function (CDF) of FA dust concentrations at different receptor points is shown in Figure 4-5. The maximum and minimum values of the predicted ground-level dust concentrations at zone A are 239.15 and 194.76 $\mu g/m^3$, respectively. The histogram of the 1000 simulation runs shows a normal distribution. The produced mean and standard deviation values were 218.25 and 7.05 $\mu g/m^3$, respectively. The maximum and minimum values of the predicted ground-level dust concentrations at zone B are 648.33 and 527.99 $\mu g/m^3$, respectively. Similarly, the mean and standard deviation values of the predicted ground-level dust concentrations at zone C are 535.80 and 17.28 $\mu g/m^3$, respectively.

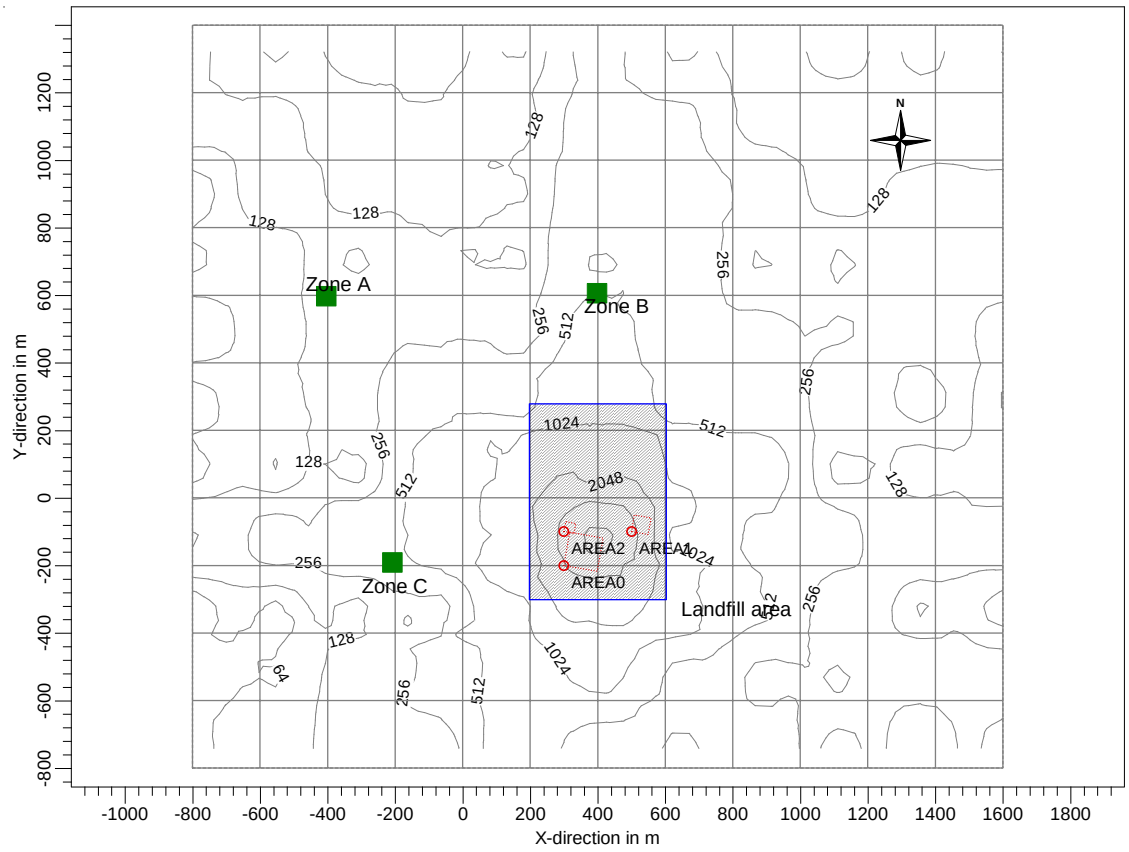

Figure 4-4 FA dust distribution over the study area (for #1 simulation)

To estimate the human risk for the selected metals associated with FA dust, MCS was used to propagate the information supplied by the probability distribution functions and constant variables. A 1000 times iteration was used to calculate the risk distributions.

A determination of the non-cancer risk associated with the pollutants is based on a hazard quotient (HQ), which is simply the ratio of the estimated CID to RfD. The sum of HQs for all pollutants with similar toxic effects is the HI. A HI less than 1 indicates that the predicted risk is unlikely to pose potential human health risks. On the other hand, a HI greater than 1 indicates potential adverse health effects (USEPA, 1991).

Table 4-3 FA dust concentrations at different receptor zones (for 1000 simulations)

Number of simulation	**Zone A**	**Zone B**	**Zone C**
1	214.22	580.74	524.94
2	226.32	613.52	554.57
3	213.96	580.02	524.29
4	206.34	559.36	505.61
5	220.30	597.20	539.82
6	227.40	616.47	557.24
.	.	.	.
994	206.01	558.47	504.81
995	214.42	581.28	525.43
996	227.18	615.85	556.68
997	207.27	561.87	507.89
998	221.14	599.49	541.89
999	216.60	587.19	530.77
1000	215.64	584.57	528.40

For this study, the CDF of HI associated with arsenic (As), cadmium (Cd), and chromium (Cr) were generated. The predicted minimum and maximum HI was found to be 0.00121 and 0.00396 respectively for zones A and B as shown in Figure 4-6.

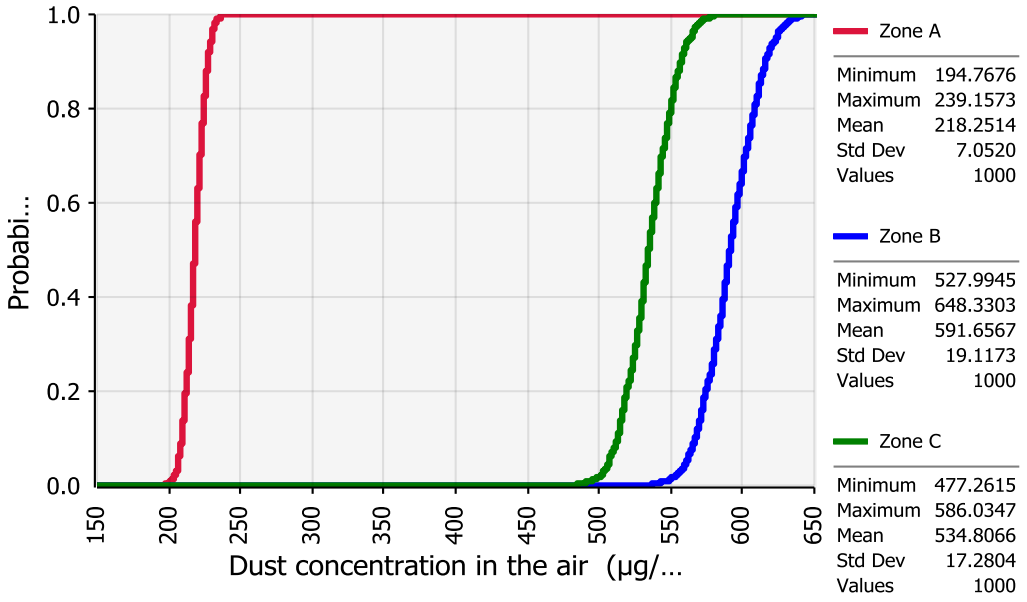

Figure 4-5 Cumulative distribution of dust concentration at receptor zones

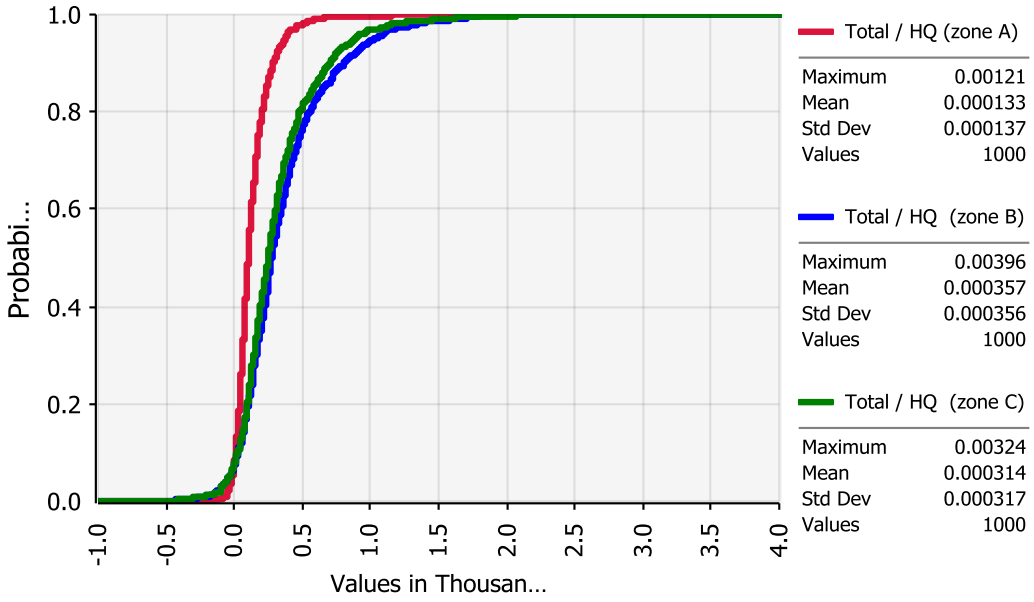

Figure 4-6 Cumulative HQ at different receptor zones

The CDF of the total cancer risk associated with As, Cd, and Cr is shown in Figure 4-7. The maximum individual risk was found to be 1.86E-07, 5.81E-07, and 5.55E-07 respectively for zones A, B, and C.

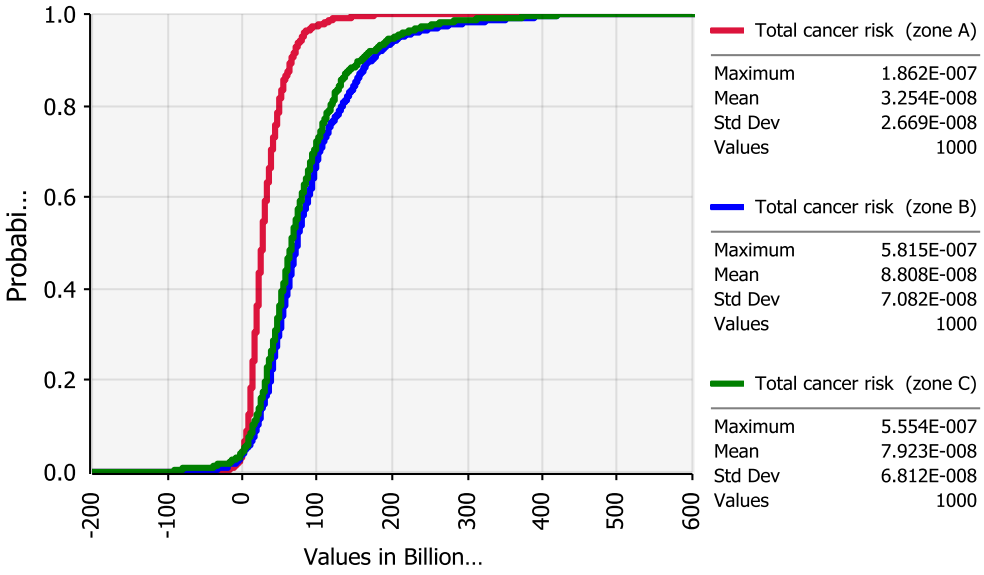

Figure 4-7 Cumulative cancer risk at different receptor zones

Although different regions worldwide use a 1 in 1 million (10^{-6}) lifetime cancer risk as the most acceptable human health risk posed by carcinogenic agents, USEPA (1991) considers a range from 1 in 10,000 (or 1 x 10^{-4}) to 1 in 1,000,000 (1 x 10^{-6}) as the acceptable risk. Comparing the risk levels shown in Figure 4-6 with the tolerable ranges (e.g., 1 x 10^{-6}), it was found that the lifetime risk associated with inhalation of dust-borne metals is below the acceptable level.

4.5 Summary

The human health risks presented in this study are estimated based on the direct inhalation of dust by the population living surrounding the FA dumping area. The deposition of dust is another factor that may cause nearby soil and water pollution. The study offers an initial screening, which is of value in addressing concerns about the potential risks to human health from the bulk disposal of FA at strategic locations. For a comprehensive investigation, other

exposure scenarios such as the ingestion of contaminated soil and home-grown food, and skin contact with contaminated soil should be considered.

Chapter 5

Potential Use of Heavy Oil Fly Ash as Construction Material

5.1 Overview

Characteristics analysis (Chapter 3) showed that HOFA could be used as a primary material for such uses as soil stabilizer/ fill material for construction, a colour ingredient for ornamental concrete, or an adsorbent for industrial pollutions control (Mofarrah et al., 2012; Hsieh and Tsai, 2003). The goal of the present study (in this chapter) is to use HOFA in such construction activities as (i) fill soil stabilizer/ fill material , and (ii) a colour ingredient for ornamental concrete. FA from coal combustion (e.g., pozzolanic fly ash) has been used extensively in engineering applications including fill materials and as an admixture in the cement industry (Jones, 1995); however, due to different characteristics of HOFA such applications are limited.

In order to explore the possible use of HOFA in engineering applications, this chapter describes the experimental procedures and outcomes from deferment experiments using Saudi Arabian fly ash (i.e., FA-SA). Two sets of experiments were conducted: (i) the first experiment described the possible use of HOFA as a soil stabilizer/fill material, and (ii) a second experiment investigated the use of HOFA as a black pigment or admixture in ornamental concrete. Batch and column leaching tests were also conducted to study their environmental effects.

5.2 Possible use of HOFA as soil stabilizer/fill material

Soil stabilization refers to the process of changing soil properties and improving its physical stability and durability. Many techniques are available for soil stabilization: compaction, dewatering, and adding admixture materials to the soil (Neopaney et al., 2012). Among others, the addition of cementitious or pozzolanic materials to improve soil properties is well established. Due to its pozzolanic properties, coal fly ash has proven applications as a soil stabilizer in many engineering projects (Kumpiene et al., 2007; Edil et al., 2006). However, such application is limited to carbon-rich HOFA (Mofarrah et al., 2012). This experiment focuses mainly on the potential use of HOFA as a soil stabilizer by mixing it with Portland cement.

5.2.1 Preparation of fill/stabilized materials

Three stabilized ash samples (i.e., FA20, FA30, and FA40) were prepared by mixing 160 g of oven-dried wel-mixed (i.e., 105℃ for 24 hrs) HOFA with 32 g (i.e., 20% by weight), 48 g (i.e., 30% by weight), and 64 g (i.e., 40% by weight) of Portland cement, respectively. The moisture content of the mixture was increased by adding 40% water by weight to each sample. The prepared samples were kept in a dessicator for 28 days to allow sufficient reaction time (Mofarrah et al., 2012). After 28 days, each sample was divided into two equal parts in order to obtain samples for batch and column leaching tests.

5.2.2 Batch leaching test

Leaching tests generally evaluate the worst-case environmental scenario associated with solid waste (Querol et al., 1996; Praharaj et al., 2002; Fytianos et al., 1998). The goal of this test is to investigate the leaching behaviour of toxic components in solid waste. Various batch leaching test (BLT) were discussed in Chapter 3.

Table 5-1 Properties of batch leaching tests

Method	Leachate	Maximum particle size	L/S ratio	Extraction time (h)	Number of steps	Temperature (°C)	Reference
ELT	distilled water (pH=6.3)	150 μm	4:1	7 days	1	25	USEPA, 1989
ANC	HNO_3 solutions (pH=3.0)	150 μm	3:1	48 hours	1	25	ECAEC, 1986

For this study, a BLT was conducted on three stabilized samples (i.e., FA20, FA30, and FA40) to determine the metals' leaching characteristics. Considering the particle size distribution of the HOFA sample, an ELT and an ANC method were selected.

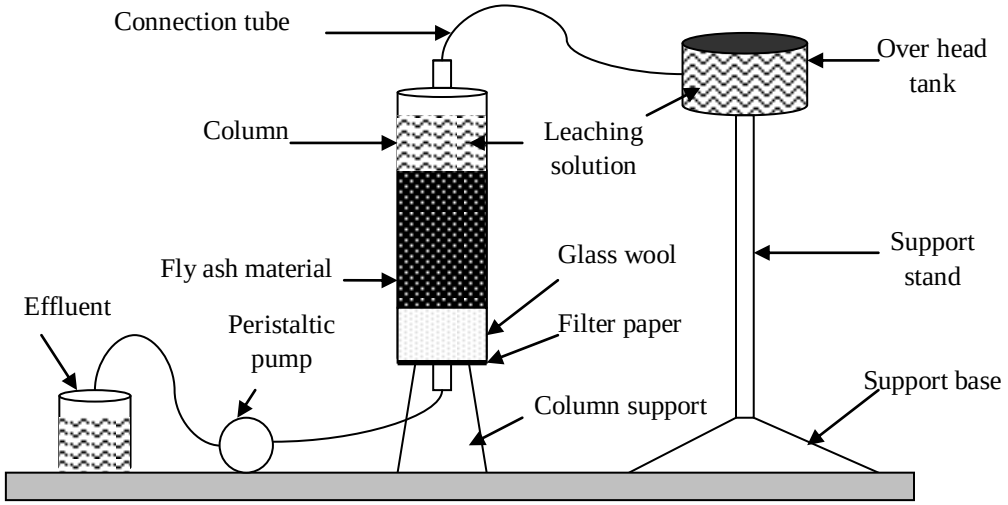

Figure 5-1 Column leaching test device

Distilled water (p^H=6.3) and an acid solution (p^H=3.0, using distilled water with HNO_3) were used as leaching media. All test apparatus and glass were cleaned with an acid solution (e.g., 15% HNO_3 solution) and rinsed with distilled water prior to the leaching experiments. The

batch extraction procedures and liquid to solid (L/S) mixing ratio are shown in Table 5-1. To ensure continuous stirring of the samples, a PHIPPS & BIRD stirrer model 7790-400 at 10 rpm was used over the test periods. The mixtures from the above experiments were filtered through 0.45 µm Whatman filter paper and acidified with a nitric acid solution to make pH < 2 for the chemical analysis.

5.2.3 Column leaching test

To evaluate the realistic leaching characteristics, a column leaching test (CLT) was conducted on three stabilized samples (i.e., FA20, FA30, and FA40) and an HOFA sample following the test procedures described in the literature (Francis and White, 1987; Reemtsma and Mehrtens, 1997). The stabilized samples (i.e., FA20, FA30, and FA40) and 80 g of HOFA were separately transferred into a fixed Pyrex glass column (40 mm in internal diameter and 30 cm in length) for the leaching test. A small amount of glass wool with a filter paper was also packed at the bottom of the column to prevent the loss of fine particles during leaching. To simulate the possible field conditions, the specimen was compacted inside the column by a 5 mm rod in two layers with 5-10 blows in each layer. This compaction was conducted because materials could be compacted after being placed in a field. The leachability of metals is highly affected by the acidity of the leaching solution; it decreases with an increase in pH values (Mofarrah et al., 2012). To evaluate the maximum leach conditions only an acidic solution (pH = 3.0, using distilled water with HNO_3) was used in the column test. The outflow velocity of the resulting leachate was controlled in such a way that the cumulative liquid to solid (L/S) ratio did not exceed the values in Table 5-1. A flow rate of 5 ml/hr was maintained, which is equivalent to L/S ratios of 1.5 and 3.0 at the end of 24 hrs and 48 hrs, respectively. A leaching solution was passed through the column in

a down flow motion and pumped from the outlets by a peristaltic pump. The main advantage of this pump is that there is no chance for fluids to come in contact with the moving parts of the pump, because the fluid is pumped through an interior tube. The test was conducted at room temperature, and approximately 5 cm of liquid was maintained above the sample placed inside the column. Figure 5-1 shows the experimental setup used for this study.

The resulting leachates were collected after 24 h and 48 h and stored in polyethylene bottles. The leachate from the above experiments was filtered through 0.45 μm filter paper and acidified with a nitric acid solution to make the pH < 2 for the chemical analysis. The element concentrations of the resulting leachates and leaching solutions (blank value) were determined by an ICP-MS. Finally, the concentrations of the elements were obtained by calculating the differences between the blank value and the concentration value for the leachates.

Table 5-2 Results of batch experiments

Heavy metals	**Detection limit (mg/L)**		**Peak concentration levels (mg/L)**						
		HOFA	**FA20**	**FA30**	**FA40**	**HOFA**	**FA20**	**FA30**	**FA40**
			Acid solution (pH = 3)			Distilled water (pH = 6.3)			
As	0.001	0.041	0.002	0.001	ND	0.002	0.001	0	ND
Cd	0.001	0.004	0.004	0.001	ND	0.004	0.001	0.002	ND
Co	0	0.05	0	0	0	0.05	0	0	0
Cr	0.005	0.283	0.225	0.129	0.083	0.162	0.301	0.036	0.093
Cu	0	0.600	0.2	0.2	0.1	0.7	0.2	0.2	0.1
Hg	0	0.006	0.002	0.001	0	0.003	0.001	0.001	0
Ni	0	77.91	0.42	0.05	0.04	55.86	0.18	0.01	0.01
Pb	0	0.116	0.005	0.003	0.002	0.025	0.003	0.013	0.006
Se	0.027	0.031	0.009	0.001	0.001	ND	0.001	ND	ND
V	0.001	303.912	0.702	0.594	0.079	102.626	0.507	0.021	0.019
Zn	0.002	0.894	0.093	0.031	0.048	0.652	0.057	0.037	0.063

5.2.4 Outcomes and discussion

Among the trace metals originally present in the HOFA, only a minor percentage was obtained through leaching tests under various conditions. The batch experiments had a concentration range of 0-303.91 mg/L (Table 5-2). In this case, the maximum leachate concentration is 303.91 mg/L for V, followed by Ni at 77.91 mg/L.

Table 5-3 Results of column leaching experiments

Heavy metals	**Detection limit (mg/L)**	**Peak Concentration Levels (mg/L) with pH =3.0**							
		HOFA	**FA20**	**FA30**	**FA40**	**HOFA**	**FA20**	**FA30**	**FA40**
		After 24 hrs				After 48 hrs			
As	0.001	0.031	0.006	0.004	ND	0.005	ND	ND	ND
Cd	0.001	0.006	0.001	ND	ND	0.001	ND	ND	ND
Co	0	0.08	0.01	0.01	0	0.010	0.0012	0	0
Cr	0.005	0.343	0.149	0.094	0.026	0.006	0.020	0.005	0.005
Cu	0	14.2	0.40	0.2	0	0	0.001	0.001	0
Hg	0	0.007	0.002	0.001	0	0.001	0.001	0	0
Ni	0	76.94	0.04	0.03	0.02	0.02	0.003	0.003	0.001
Pb	0	0.553	0.0978	0.0643	0.0535	0.014	0.0011	0.001	0.001
Se	0.027	0.033	0.004	0.004	0.012	0.018	0.002	0.002	0.002
V	0.001	307.54	0.007	0.083	0.007	2.235	0.001	0.001	ND
Zn	0.002	3.471	0.124	0.938	0.592	0.061	0.0024	0.0015	ND

Note: ND = not detectable

The peak concentration levels of heavy metals obtained from the CLT over a period of 48 hr are shown in Table 5-3. The results show that the overall leach concentrations of trace metals are relatively less in the batch tests compared with the column tests. In CLT, the leaching concentration (LC) of the elements is high at the initial stage (i.e., 0-24 hrs). After an initial high LC, the concentration then significantly decreases (24-48 hr sampling). The water soluble elements and fraction of elements attached to the solid surface may easily leach in the first stage of the experiment; this could be one reason for a high LC in the initial stage.

As leaching continues, the concentration of the water soluble fraction gradually decreases. However, this does not confirm that LCs will continually decrease with time. Many trace elements may be dissolved by physical and chemical reactions and then leach from residues after a long period of time (Wang et al., 2008).

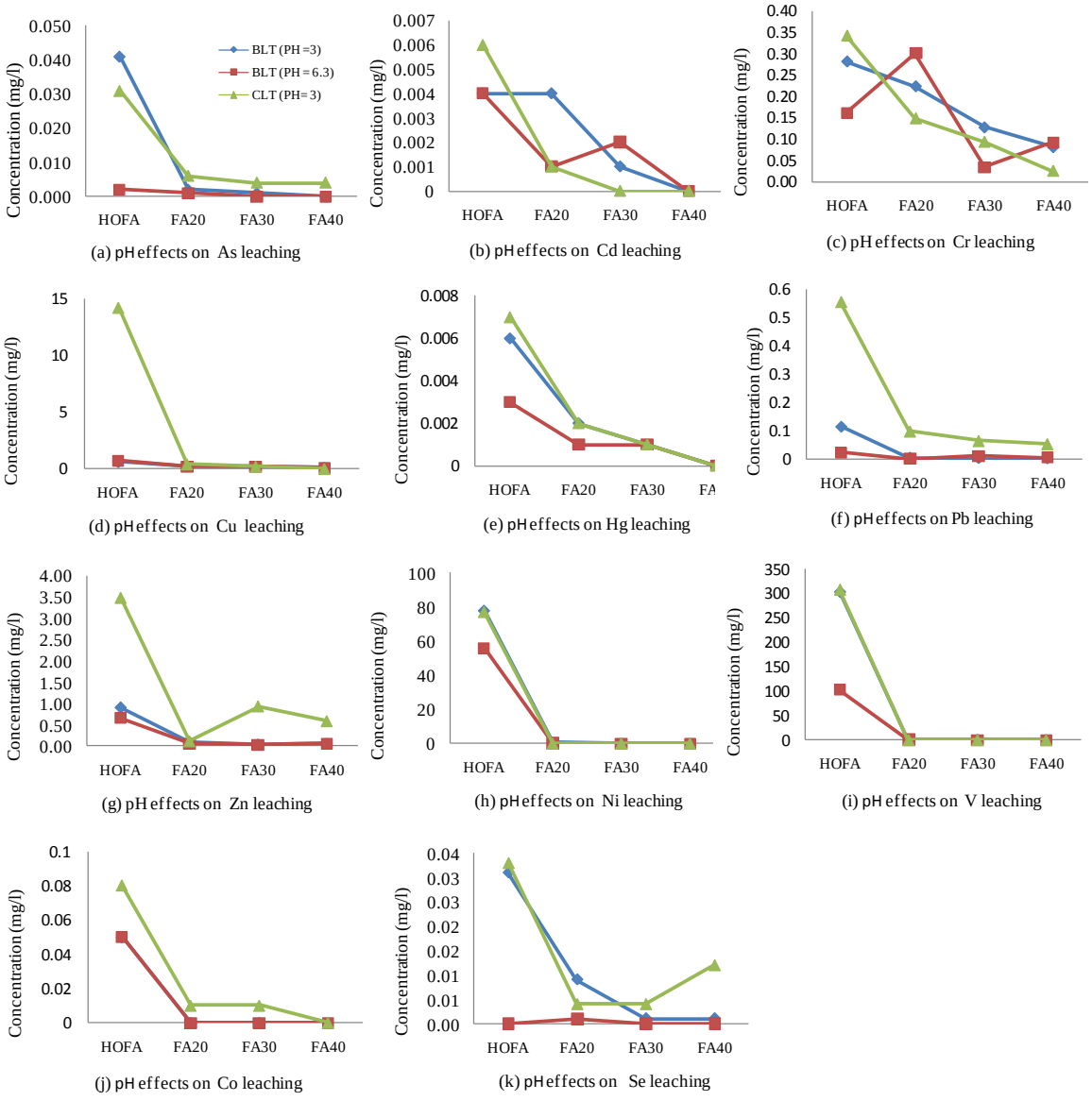

Figure 5-2 pH effects on leaching behaviour of 11 trace elements

The leaching behaviour of many trace elements from HOFA and stabilized ash is affected by the acidity of the solution. Figure 5-2 exhibits information about the change in leaching behaviour of 11 elements. The leachability of As (Figure 5-2a) was found to be dependent on the pH of the solution, i.e., its LCs decreased with an increase in the solution's pH. In this case, the HOFA has a higher LC in BLT compared to CLT, but the stabilized ash showed a maximum LC in CLT.

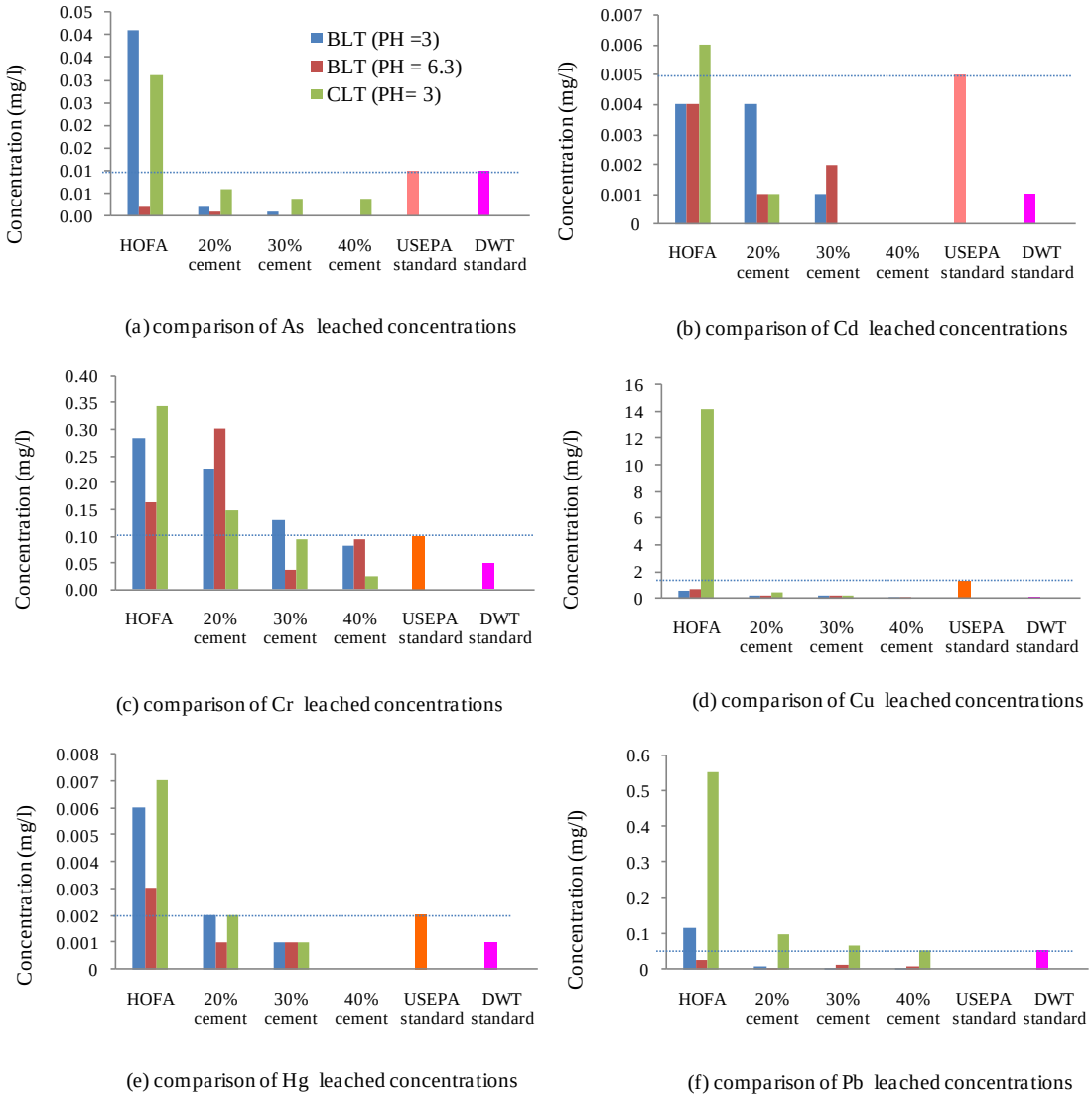

Figure 5-3 MLC of the six heavy metals related to the environmental standard

The leachability of Cd and Cr (Figures 5-2b and c, respectively) decreased with an increase in the p^H of the leaching solution. In this case, the HOFA has a higher LC in CLT compared to BLT, but the stabilized ash showed a maximum LC in BLT. The leaching behaviours of Cu, Hg, Pb, Zn, Ni, V, and Co (Figures 5-2d, e, f, g, h, i, and j, respectively) increase with a decrease in the leaching solution's pH. These metals showed higher LCs in CLT than in BLT for both HOFA and stabilized ash. The leachability of Se (Figure 5-2k) decreases with an increase in the leaching medium's pH. In this case, the HOFA has a higher LC in CLT compared to BLT, but the stabilized ash (i.e., FA20) showed a maximum LC in BLT. As shown in Figure 5-2, the addition of cement with HOFA dramatically decreased the LCs of all the metals. It also proved that the amount of cement has a significant influence on the LC.

The maximum leaching concentration (MLC) of the heavy metals is compared with the permissible concentration recommended by environmental agencies (Table 5-4). The LCs of six toxic heavy metals (i.e., As, Cd, Cr, Cu, Hg, and Pb) from HOFA and stabilized ash were compared with drinking-water threshold values suggested by USEPA (1993) and the United Kingdom's Drinking Water Threshold (DWT, 2001). As can be seen from Figure 5-3, the maximum LCs (0.041, 0.006, 0.343, 14.20, 0.007, and 0.535 mg/L respectively) of As, Cd, Cr, Cu, Hg, and Pb from HOFA exceeds the highest environmental permissible concentrations recommended by USEPA and DWT.

In addition, leachate from HOFA (e.g., Cu, Ni, Zn) also exceeded the landfill drainage standard (Table 5-4) set by the Council of the European Communities (CEC, 1991). On the other hand, the addition of cement to HOFA significantly decreased the LC of most of the elements to below permissible levels. It also shows that the amount of cement has an

influence on the LC. However, the addition of 20% and 30% cement to HOFA does not decrease the metals' LCs below permissible levels in all cases (e.g., Cr, Hg, and Pb respectively, Figures 5-3c, e, and f). Furthermore, if we compare the metals' LCs with environmental regulations (Figure 5-3), it is clear that the addition of 40% cement to HOFA is adequately safe for the environment.

Table 5-4 Permissible limits of heavy metals in drinking water and leachates

Heavy metals (mg/L)	**USEPA[a] limit, maximum**	**Leachates[b]**	**Landfill drainage[c]**
As	0.01	0.01	0.2-1.0
Cd	0.005	0.001	0.1-0.5
Cr	0.1	0.05	0.1-0.5
Cu	1.3	0.02	2-10
Hg	0.002	0.001	0.02-0.10
Ni	-	0.05	0.4-2.0
Pb	0.0	0.05	0.4-2.0
Zn	5.00[b]	-	2-5

[a]USEPA (1993); [b]DWT (2001); [c]CEC (1991)

In addition, the metals' LCs for this stabilized material is well below the landfill drainage standard set by CEC as reported in Table 5-4. Based on the comparative results, the stabilized material prepared from HOFA with 40% Portland cement would not be classified as a hazardous waste. The results of this study indicate that the use of HOFA with 40% cement as fill material has no significant impact on the environment, as most of the toxic metals present in the HOFA may not leach beyond threshold limits.

5.3 Use of HOFA as a colour ingredient in concrete mortar

The objective of this experiment is to investigate the use of HOFA (i.e., sample FA-NB) as a black pigment in ornamental concrete. Due to its naturally black colour, the FA sample (i.e., sample FA-NB) has the potential to be used as a black pigment in ornamental concrete. Ornamental concrete can be used in landscaping, driveways, walkways, patios, planters, and

retaining walls. Since HOFA contains a significant amount of leachable metals, the use of HOFA mixed concrete in the landscape may leach toxic elements into the environment through rainwater or acid rain. Therefore, leaching tests were conducted to evaluate the environmental impact associated with the use of HOFA in concrete.

5.3.1 Preparation of concrete samples

To evaluate the compressive strength of concrete when HOFA is added as a colour ingredient, 50 mm concrete mortar cubes were prepared by mixing Portland cement, sand, and HOFA at different ratios according to a standard method (i.e., ASTM C109). The cubes were prepared by mixing one part Portland cement to 2.75 parts of graded standard sand by weight. The HOFA was mixed with mortar at 0% (reference sample), 2%, 5%, 10%, 20%, 30%, and 50% by weight. The water to cement ratio was maintained at 0.45 for all cases. Different groups of cube samples were prepared: OC_0, OC_2, OC_5, OC_{10}, OC_{20}, OC_{30}, and OC_{50} (four in each group, a total of 28 cubes prepared).

Table 5-5 Variations of compressive strength of different concrete cubes

% HOFA	Compressive **strength after 28 days (MPa)**			
	Sample 1	**Sample 2**	**Sample 3**	**Average**
2	41.15	40.95	42.59	41.56
5	38.75	37.95	39.82	38.84
10	28.63	28.49	29.02	28.71
20	24.07	25.02	24.00	24.36
30	8.24	8.89	9.15	8.76
50*	NA	NA	NA	NA
Reference cubes	42.96	41.32	42.59	42.29

**NA sample OC_{50} was broken during handling*

The prepared cube specimens were stored into air for 24 hours. After this period each group of samples was kept in a separate tray and cured by cotton moistened with distilled water for

28 days. Moist cotton was applied in order to minimize the leaching of metals during the curing process. After 28 days, three cubes from each group were placed on the Automax 5 automatic concrete compression test machine to measure the compressive strength. Load was applied and gradually increased at a rate of 0.2 Mpa/sec until the specimen failed. The remaining one sample from each group was separately placed in the leaching solution (mentioned in Table 5-1) in order to perform a BLT.

5.3.2 Results and discussion

When considering the use of FA as a black pigment or admixture in concrete, this material should possess suitable concrete properties such as compressive strength. To investigate the possibility of HOFA use in ornamental concrete, changes in compressive strength are measured by making cube blocks. The compressive strength of the study cubes after 28 days is shown in Table 5-5. The change of compressive strength of the concrete cubes is shown in Figure 5-4. This figure demonstrates that the addition of 2% or 5% HOFA to concrete results in no major difference in strength compared to the reference block; but compressive strength significantly decreases by adding 10% to 20% HOFA to the mortar. The addition of 30% HOFA to the mortar did not provide sufficient compressive strength. The compressive strength was dramatically reduced by adding 30% HOFA with the mortar: sample OC_{50} was not hard enough, and broke during handling and processing; for these reasons this sample was not considered for further studies.

The results show that the addition of 2% or 5% HOFA to concrete does not affect its quality.

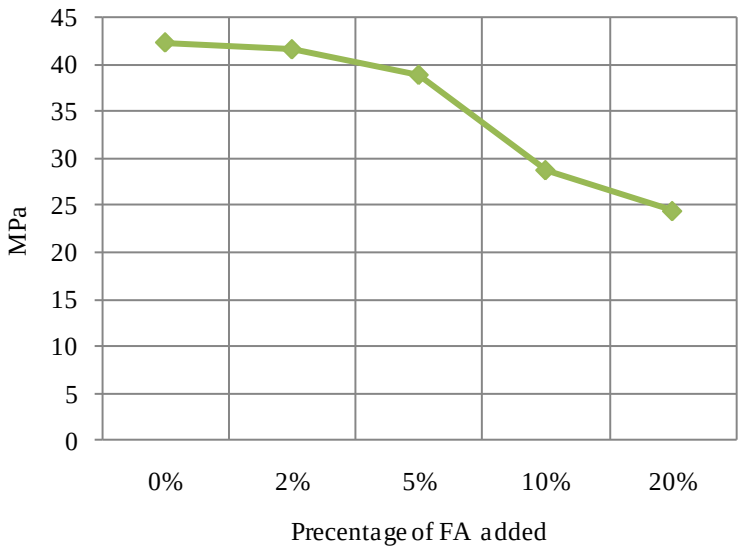

Figure 5-4 Change of compressive strength in concrete cubes

Among the trace metals originally present in HOFA (Chapter 3), only minor concentrations were obtained through a batch leaching test (BLT). A BLT (Table 5-2) indicated that the toxic elements in HOFA easily leach into the environment through rain water or acid rain. The study also pointed out that metal leaching increased with an increase in acidity. To evaluate the maximum leach condition only an acidic solution (p^H = 3.0 using distilled water with HNO_3) was used in this test. The leaching behaviour of the 11 elements from the HOFA mixed concrete blocks is shown in Table 5-6. The results indicate that mixing HOFA with concrete significantly decreases the LC of most of the elements to below the permissible level set by environmental agencies (Table 5-4). The results also show that the quantity of FA in the concrete influences the LC. Increasing the percentage of HOFA in the concrete increases the LC of the metals. However, the addition of 10% and 20% HOFA to concrete shows a higher LC of some metals (i.e., Ni) than the permissible level.

Table 5-6 Results of batch experiments of cement mortar with HOFA

Heavy metals	**Detection limit (mg/L)**	**Peak Concentration Levels (mg/L) rounded to 3 digits**			
		OC_2	**OC_5**	**OC_{10}**	**OC_{20}**
As	0.001	ND	ND	0.001	0.001
Cd	0.001	ND	ND	0.001	0.001
Co	0	ND	ND	0	0
Cr	0.005	ND	ND	ND	0.006
Cu	0	ND	0	0	0.002
Hg	0	ND	ND	ND	ND
Ni	0	ND	0.001	0.07	0.091
Pb	0	ND	0.001	0.003	0.003
Se	0.027	ND	0.001	0.001	0.001
V	0.001	ND	0.005	0.086	0.195
Zn	0.002	ND	0.001	0.003	0.006

Furthermore, by comparing LCs with the environmental standards (Table 5-4), it is clear that the use of 2% or 5% HOFA in concrete is adequately safe for the environment. In addition, 2% or 5% HOFA in concrete does not pose any significant change in its compressive strength (Figure 5-4). Based on the comparative results, it can be concluded that 2% or 5% HOFA can be added to ornamental concrete as a black pigment. However, further experiments with the quality of the concrete colour are recommended.

5.4 Summary

Batch and column leaching tests have been carried out in order to evaluate the leaching behavior of trace elements within the HOFA and stabilize ash prepared from HOFA mixing with cement. The results of this study indicate that the use of HOFA with 40% cement as fill material has no significant impact on the environment, as most of the toxic metals present in the HOFA may not leach beyond threshold limits.

A possible utilization of HOFA as a black pigment for concrete material was also investigated. Environmental risk that may pose by concrete made with HOFA was studied by laboratory BLT. The results show addition of 2% or 5% HOFA with concrete is adequately safe for the environment. As well, the use of 2% or 5% HOFA in concrete does not pose any significant change in the concrete's compressive strength.

Chapter 6

Production and Characterization of Fly Ash Activated Carbon

6.1 Introduction

The characteristics study of HOFA (Chapter 3) showed that Saudi Arabian HOFA has a higher percentage of carbon and a lower percentage of pollutants such as heavy metals than the FA-NB, which prompted the present study to produce fly ash activated carbon (FAC) from Saudi Arabian HOFA. After this point all analysis was conducted with the Saudi Arabian HOFA unless otherwise stated. The process involved in FAC production is shown in Figure 6-1. The cleaning of HOFA and the recovery of unburned carbon are covered the first stage of the process. The production and characterization of FAC were discussed in the second stage of the experiment.

6.2 Recovery of unburned carbon

To recover unburned carbon, raw HOFA was treated by several washing and leaching processes to remove impurities. For this study, raw HOFA was treated with an aqueous acid solution at a ratio of 10 g of HOFA per 50 ml of nitric acid (28% HNO_3) at 60°C for 2 hr as suggested by Hsieh and Tsai (2003). The mixture was continuously stirred by a PHIPPS & BIRD stirrer model 7790-400 at 10 rpm over the test period. The photograph in Appendix B shows the HOFA sample cleaning process. During the stirring process, a magnetic bar was immersed in the solution to capture those impurities which had magnetic properties.

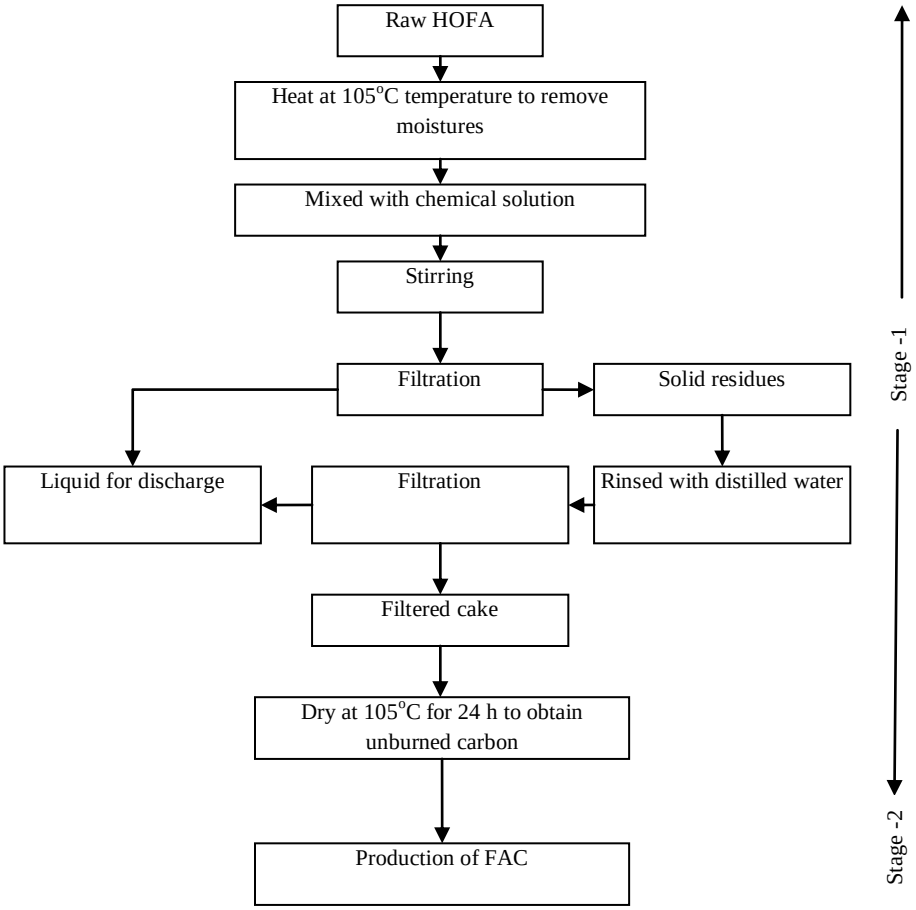

Figure 6-1 General flow diagram for FAC production from HOFA

After filtration, the residues were washed with distilled water several times to eliminate NO_3^- ions. Subsequently, the filtrate residue was treated with 15% HCl solution at a solid to liquid ratio of 1:5 at 60°C for 1 hr. The solution was then filtered to obtain a filtered cake. The filtered cake was rinsed repeatedly with distilled water to eliminate chloride ions. Finally, the filtered cake was dried at 105°C for 24 hr to obtain the unburned carbon. Figure 6-1 shows the process flow diagram of unburned carbon recovery from HOFA.

Table 6-1 Metals found in cleaned HOFA

Metals	Raw HOFA (mg/kg)	Cleaned HOFA (mg/kg)	[a] USEPA maximum limit
Arsenic (As)	2.239	0.006	0.01
Bromide (Br)	370.9	2.5	-
Cadmium (Cd)	3.275	ND	0.005
Cobalt (Co)	*3.28*	0.039	-
Chromium (Cr)	4.056	0.014	0.1
Copper (Cu)	170.4	0.4	1.3
Iron (Fe)	981	8.25	-
Mercury (Hg)	0.245	*Not detectable*	0.002
Manganese (Mn)	20.675	0.23	
Molybdenum (Mo)	26.047	0.526	
Nickel (Ni)	1762.22	1.231	
Lead (Pb)	10.995	0.014	
Selenium (Se)	11.592	ND	
Tin (Sn)	17.274	0.406	
Vanadium (V)	2957.701	4.53	
Zinc (Zn)	130.84	0.61	5.00

[a]*USEPA (1993)*

During the washing process impurities as metals, ash remove from raw HOFA and ncreases the pore volume. This is due to the extraction of mineral matter from the carbon structures. As shown in Table 6-1, the washing process noticeably reduces metal concentrations but increases the pore volume and surface area of the samples.

6.3 Preparation of FAC by physical activation process

In physical activation, 10 g of clean unburned carbon from the washing process (Section 6.2) was activated under a nitrogen (N_2) environment at an average flow rate of 5 ml/ minutes. To expedite the burning process a constant flow of CO_2 at a ratio of 1:5 (e.g., 1.0 g carbon with 5 ml/ minutes CO_2 STP) was applied to the system. The activation was done in a

programmable Lindberg/Blue M tube furnace (Figure 6-2) at 800-900°C with 60-120 minutes holding time. The furnace was programmed in such a way that the heating rate was increased 5°C/ minutes until it reached the final temperature.

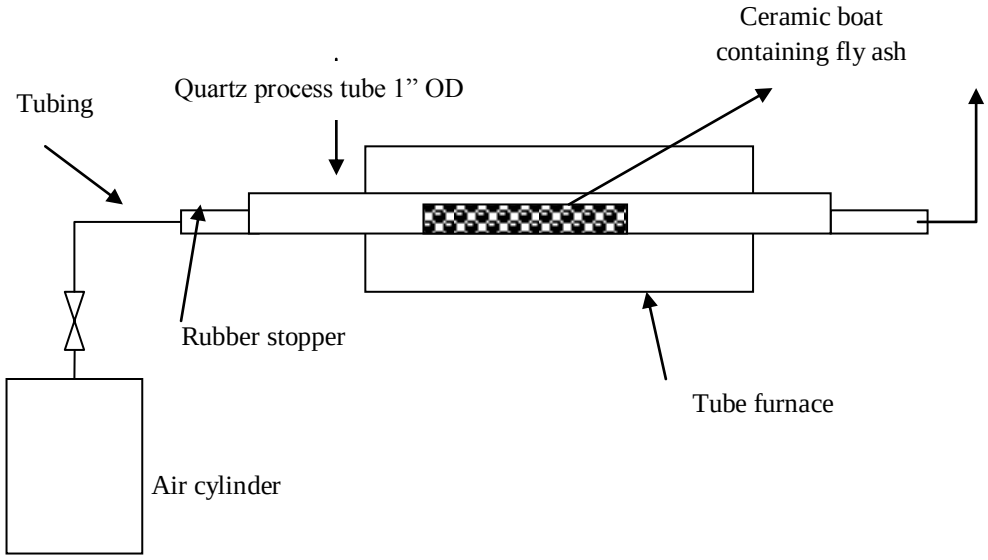

Figure 6-2 Experimental setup used to produce FAC

Table 6-2 Burning temperatures and times used in physical activation process

Parameters	**FAC-P01**	**FAC-P02**	**FAC-P03**	**FAC-P04**	**FAC-P05**	**FAC-P06**	**FAC-P07**
Activation Temperature (°C)	900	900	900	900	700	800	850
Activation Time (minutes)	45	90	120	60	120	120	120

The furnace then remained at final temperature for the desired period. At the end of the heating period the furnace was left to cool to room temperature. By changing temperatures and burning times as shown in Table 6-2, different sets of FAC, namely FAC-P01, FAC-P02, FAC-P03, FAC-P04, FAC-P05, FAC-P06, and FAC-P07, were produced. The produced

FAC was characterized by iodine number (IN), methylene blue number (MBN), BET surface area, and pore volume.

6.4 Preparation of FAC by NaOH and KOH

Sodium hydroxide (NaOH) and potassium hydroxide (KOH) were used separately as chemical agents. Ten grams of clean unburned carbon (Section 6.2) was mixed with NaOH or KOH (40% aqueous solution) at different ratios (5-25% w/w). The mixing process was performed at 80°C for 30 minutes. The impregnated sample was dried in an oven at 105°C for 24 hrs. The sample was then placed inside a quartz tube and inserted horizontally into the middle of a tubular electric furnace (Figure 6-2). The activation was performed at 900°C under a nitrogen (N_2) gas flow at an average rate of 5 ml/ minutes for 2 hr followed by a CO_2 gas flow (i.e., average 20 ml/ minutes) for the last 1 hour. The resulting FAC was washed with 250 ml 0.5 N HCl at 80°C for 30 minutes followed by distilled water washing until the p^H of the mixture exceeded 6. During activation the furnace was programmed in such a way that the heating rate was increased 5°C/ minutes until reaching the final temperature. It then remained at that temperature for the desired period. At the end of the heating period the furnace was left to cool to room temperature.

Table 6-3 Different mixing doses of NaOH and KOH

Parameters	**KOH**				**NaOH**			
	FAC-1	**FAC-3**	**FAC-5**	**FAC-7**	**FAC-2**	**FAC-4**	**FAC-6**	**FAC-8**
Chemical agents used by weight	25%	15%	10%	5%	25%	15%	10%	5%

To investigate the effects of chemical doses, different sets of FAC were produced by changing the dose of NaOH and KOH as shown in Table 6-3. Among them were four sets of

FAC (e.g., FAC-2, FAC-4, FAC-6, and FAC-8) produced by NaOH and four sets of FAC (e.g., FAC-1, FAC-3, FAC-5, and FAC-7) produced by KOH.

6.5 Production of FAC by H_3PO_4

The dried unburned carbon from the washing processes (Section 6.2) was activated by mixing it with H_3PO_4. The mixing ratio, temperature, and activation times were varied according to a factorial design. The unburned carbon and chemicals were stirred continuously at 80°C for 30 minutes and dried at 100°C for 24 hrs. After this process, the carbonization process was applied to the product obtained. The effect of temperature was investigated by varying burning temperatures between 550°C and 800°C. Carbonization was conducted in a programmable Lindberg/Blue M tube furnace (Figure 6-2), which provides the versatility and control accuracy to meet the critical temperature required for the system. The furnace was programmed in such a way that the heating rate was increased 5°C/ minutes until reaching the final temperature. It then remained at that temperature for 30 or 60 minutes, according to Table 6-4. At the end of this period the furnace was left to cool to room temperature. During the heating period a constant air flow of 5 ml/ minutes was applied to the system to expedite the burning process, as suggested by Rahman et al. (2006). The carbonized product was cleaned with 0.5 N HCl by mixing 10 g of carbonized product to 250 ml acid at 85°C for 30 minutes. The filtered cake was then rinsed with distilled water several times until the p^H of the mixture exceeded 6. Finally, the FAC was dried at 100°C for 24 h and its characteristic properties determined. This experiment was varied according to a two-level full factorial design (Montgomery, 1997), where the impacts of the following three factors were studied based on the surface area (m^2/g) of the produced FAC.

a. Effect of temperature

b. Impact of reaction time

c. Impact of chemical reagent (H_3PO_4) dose

A two-level factorial design is the most widely used experimental design for estimating the main as well as the interaction effects of different variables (Singh et al., 2002).

Table 6-4 Design parameters for chemical activation process

Sample	Coded values			Actual			Unburned carbon (g)
	A	B	C	Temperature (°C) A1	Heating time (minutes) B1	H_3PO_4 (ml) C1	
AC1	-	-	-	550	30	2	10
AC2	+	-	-	800	30	2	10
AC3	-	+	-	550	60	2	10
AC4	+	+	-	800	60	2	10
AC5	-	-	+	550	30	5	10
AC6	+	-	+	800	30	5	10
AC7	-	+	+	550	60	5	10
AC8	+	+	+	800	60	5	10

For this study, the effects of three variables on surface area development were quantified based on a two-level full 2^3 factorial design of the experiment suggested by Montgomery (1997). The experimental design involved three variables at two levels (i.e., low and high). In this case the total 8 experiments were conducted. The variables and levels for the experiment, along with actual and coded scales, are given in Table 6-4. The higher level variable was designated as +1, the lower level as -1. In Table 6-4, A1, B1, and C1 represent the burning temperature, heating time, and the amount of H_3PO_4 added to a fixed 10 g of unburned carbon, respectively, and A, B, and C are the corresponding values in coded forms. The maximum and minimum levels are expressed in coded form as +1 and -1, respectively. The

coded values are used to convert the absolute quantity into a dimensionless factor, which is convenient for handling experimental data.

6.6 Characterization of FAC

6.6.1 Surface area and pore volume

The FAC was characterized by its surface area, porosity, and adsorption capacity of methylene blue and iodine. The surface area (m^2/g) was estimated by the BET equations described in Chapter 3. Total pore volume, V_T, was obtained from a N_2 adsorption isotherm at $p/p_0 = 0.99$.

6.6.2 Measurement of pH

The pH of FAC was measured according to procedures suggested by Belen et al. (2009) and described in Chapter 3.

6.6.3 Iodine number

Iodine number (IN) of FAC was determined using the standard method described in Chapter 3.

6.6.4 Methylene blue number

The methylene blue number (MBN) is defined as the maximum amount of dye adsorbed on 1 g of adsorbent. MBN was determined by the method described by Raposo et al. (2009). In this assay, 10 mg of FAC was placed in contact with 10 mL of a methylene blue solution at various concentrations (10, 25, 50, 100, 250, 500, and 1000 mg/L) for 24 h at room temperature (approximately 22°C). The remaining concentration of methylene blue (MB) was analyzed by a UV/Vis spectrophotometer (Hewlett-Packard Model 8453) at 665 nm. This wavelength corresponds to the maximum absorption peak of the MB monomer

(Bergman and O'Konski, 1963). The amount of MB adsorbed (q_{eq}) from each solution is calculated as:

$$q_{eq} = \left(\frac{C_0 - C_e}{w} \right) \times v \qquad (6\text{-}1)$$

where *C*o (mg/L) is the concentration of the MBsolution at starting time (t = 0), *Ce* (mg/L) is the concentration of MB solution at equilibrium time, *V* is the volume of the solution treated in L, and *w* is the amount of FAC used in g.

A calibration curve (Figure 6-3) was obtained by using standard MB solutions of known concentrations at pH 8.5. The unknown concentration was estimated by using Beer's law, as shown in Equation 6-2.

$$A = \varepsilon.c.l \qquad (6\text{-}2)$$

where, *A* is the absorbance, ε is the the molar extinction coefficient, *c* is the concentration of dye (mg/L), *l* is the path length of the absorbing solution (in cm), the cells used are 1 cm^2 in cross-section, so *l* is considered 1 cm.

A calibration curve (Figure 6-3) with a high determination coefficient (R^2 = 98.7) allows us to consider that the molar extinction coefficient is constant over the concentration range being investigated. The molar extinction coefficient value obtained from the slope is 7.314 x 10^{+4}; this value lies within the broad range reported in the literature, (3.9-9.5) x 10^{+4} (Bergman and O'Konski, 1963).

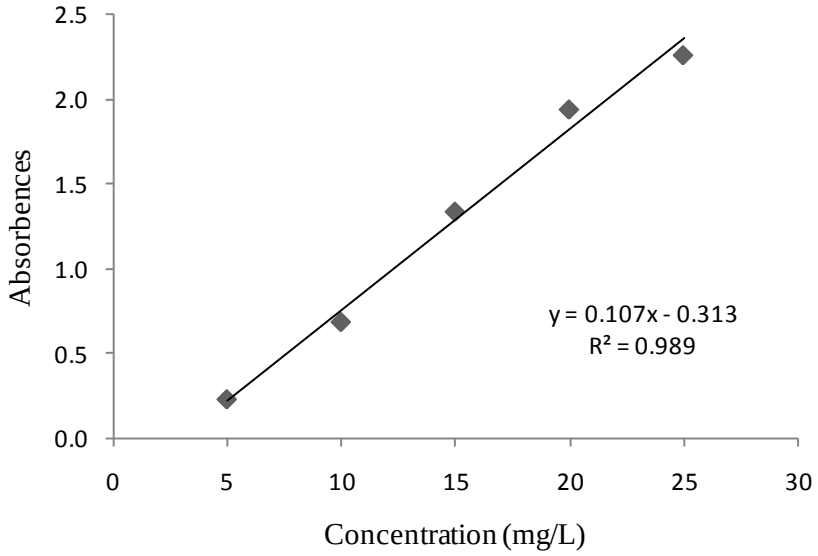

Figure 6-3 MB adsorption calibration curve

6.6.5 Ash content

Ash content determination was done according to the ASTM D2866-94 method. In this case, 1.0 g of FAC was dried at 105°C for 24 h and placed in weighed ceramic crucibles. The sample was heated in an electric furnace at 1000°C for 1 h after which the crucible and its contents were transferred to a desiccator and allowed to cool. The crucible and its contents were reweighed and the weight loss recorded as the ash content of the FAC sample. The percentage of ash was calculated as follows:

$$\text{Ash}(\%) = \frac{W_{si} - W_{sf}}{W_i} \times 100 \qquad (6\text{-}3)$$

where, W_{Si} (g) is the weight of crucible containing ash, W_{Sf} (g) is the weight of the crucible, and W_i (g) is the weight of the original FAC used.

6.6.6 Bulk density

The bulk density of the resulting FAC was determined using the method of Ahmedna et al. (1997), which consists of placing a known weight of FAC in a 25 ml cylinder to a specified volume and tapping the cylinder for at least 1-2 minutes and measuring the volume of carbon. The bulk density was determined as:

$$\rho = \frac{W_s}{V_s} \qquad (6\text{-}4)$$

where, ρ is the bulk density in g/cm^3, *Ws* is the weight of FAC sample in g, and *Vs* is the volume of packed dry sample in cm^3.

6.6.7 Percentage yield

The percentage yield (%) of FAC was determined by the ratio of weight before and after the activation process. The percentage yield was calculated as follows:

$$\text{Yield (\%)} = \frac{W_f}{W_i} \times 100 \qquad (6\text{-}5)$$

where, W_i is the initial weight of HOFA originally used in g, W_f is the weight of FAC finally produced in g.

6.7 Determination of BET surface area and pore volume by using IN and MBN

The surface area of AC is usually measured by the BET method (Brunauer et al., 1940), which employs nitrogen adsorption at different pressures at the temperature of liquid nitrogen (77 K). Determination of pore volume also uses nitrogen adsorption isotherm data, and the micropore volume is calculated from the nitrogen adsorption isotherms using the Dubinin-Radushkevich equation (Blanco et al., 2000). The above methods for surface area and pore volume determination are time-consuming and require the use of expensive

equipment. However, the adsorption characteristics of FAC for different adsorbates, such as methylene blue and iodine, can be used to estimate surface area and pore volume by means of statistical models. The MB molecule has an area of 2.08 nm^2 (Alaya et al., 2000) and can only enter large micropores and mesopores (Baçaoui et al., 2001). The iodine molecule is relatively small, with an area of 0.4 nm^2 (Alaya et al., 2000), and can enter smaller micropores (Baçaoui et al., 2001). These characteristics present the potential for their use in a study of the surface area and pore volume of porous materials. In this section an empirical relationship between methylene blue number (MBN), iodine number (IN), and the BET surface area of FAC was studied.

6.7.1 Surface area modeling

To describe the behaviour of the MBN and IN in relation to the BET surface area, a linear model was developed based on information from the 12 FAC samples produced by this study (Appendix A). The surface area (m^2/g) of the samples was estimated by the BET equation described in Chapter 3. The BET surface area of 12 FAC samples varied from 2.0 to 161.0 m^2/g. The MBN and IN of these samples ranged from 3.5 to 25.5 mg/g and 5 to 110 mg/g, respectively. Figure 6-4 shows the interaction of the MBN, IN, and BET surface area of the 12 samples used in the modeling: both MBN and IN have a positive effect on BET development. The maximum set condition can be described by a linear regression model as shown in Equation 6-6.

$$BET = -5.31939+0.118321*IN+4.03959*MBN \qquad (6\text{-}6)$$

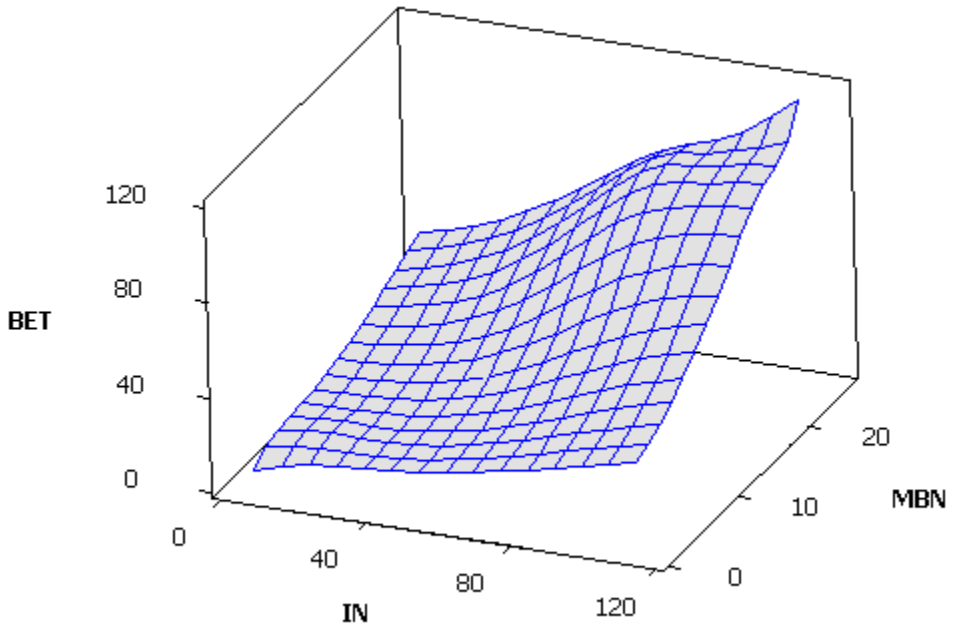

Figure 6-4 Interactions between BET, MBN, and IN for FAC

Table 6-5 Analysis of variance for surface area modeling

Source	**DF**	**Sum of squares**	**Mean squares**	**F**	**Pr > F**	**R-Sq**	**R-Sq (adj)**
Model	2	19464.0	9732.0	840.4	< 0.05	99.47%	99.35%
Error	9	104.2	11.6				
Corrected total	11	19568.2					

The BET surface area prediction by Equation 6-6 was tested. A comparison between predicted and experimentally obtained values is shown in Figure 6-5. The model presented a high determination coefficient (R^2 = 0.8798), claiming 87.98% of the variation in surface area development can be explained by the independent variables. The analysis of variance (Table 6-5) shows that the probability corresponding to the F value is lower than 0.05. Therefore, it is concluded with confidence that the developed model can be used to estimate an unknown BET surface area when MBN and IN information is given.

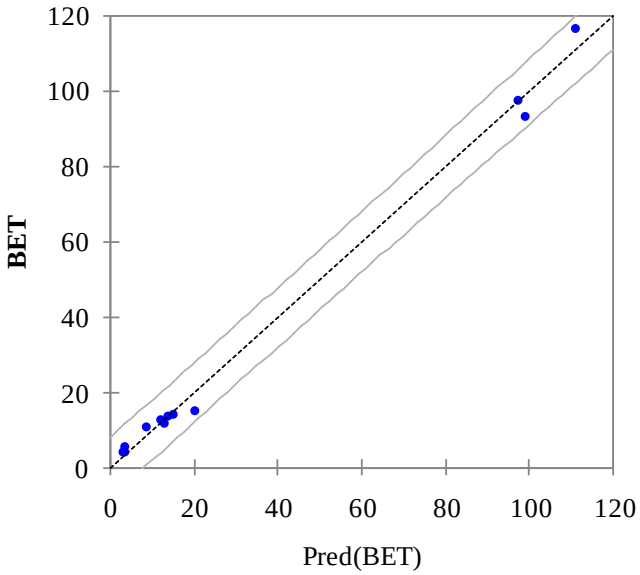

Figure 6-5 Correlation between measured and predicted BET surface areas (m^2/g)

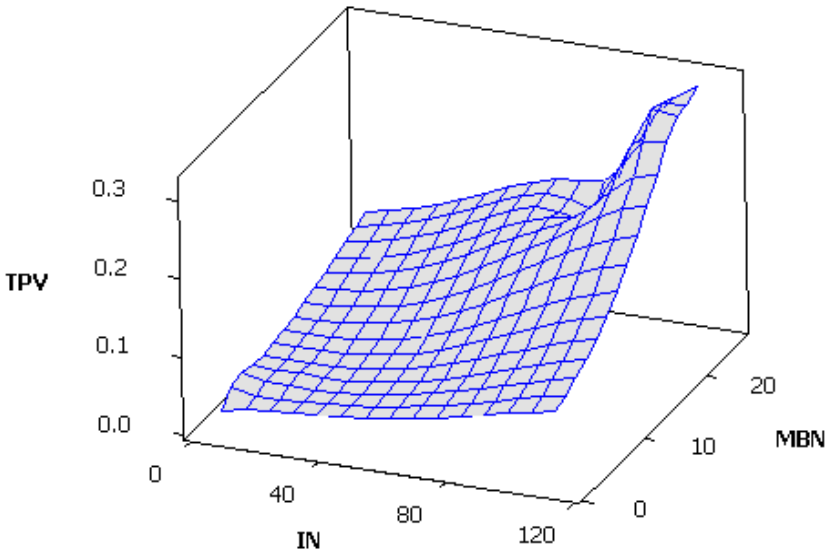

Figure 6-6 Interactions between TPV, MBN, and IN for FAC

6.7.2 Total pore volume modeling

The relation between MBN and IN and total pore volume (TPV) was established through a linear regression model. The model was developed by using the 12 FAC samples described in Section 6.7.1. Figure 6-6 shows the interaction of the MBN and IN in relation to the TPV of the 12 samples used in the modeling. It can be seen that both MBN and IN have a positive effect on TPV development. A linear model regression (Equation 6-7) was developed to describe the relation between MBN, IN, and TPV.

$$TPV = 5.747681E\text{-}03+5.68739E\text{-}03*IN-1.324098E\text{-}02*MBN \quad (6\text{-}7)$$

Table 6-6 Analysis of variance for TPV modeling

Source	DF	Sum of squares	Mean squares	F	Pr > F	R-Sq	R-Sq (adj)
Model	2	0.1	0.1	87.5	< 0.05	95.11%	94.02%
Error	9	0.0	0.0				
Corrected total	11	0.1					

A comparison of the values predicted by Equation 6-7 and the TPV values experimentally obtained is shown in Figure 6-7. The model presented a high determination coefficient (R^2 = 0.95.11), claiming 95.11% of the variation in TPV development can be explained by the independent variables. The analysis of variance (Table 6-6) shows that the probability corresponding to the F value is lower than 0.05. Therefore, the developed model can be used to estimate unknown TPV when MBN and IN are known.

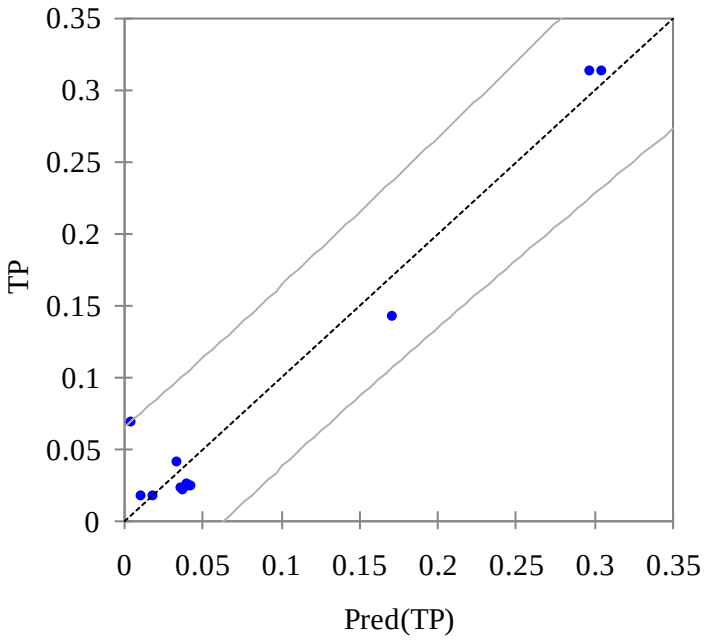

Figure 6-7 Correlation between measured and predicted TPV

6.7.3 Micropore volume modeling

Using a linear model, micropore volume (MPV) was estimated as a function of MBN and IN. The model was built with the 12 FAC samples described in Section 6.7.1. The MPV of the samples was measured from the nitrogen adsorption isotherms described in Chapter 3. Figure 6-8 shows the interaction of IN and MBN in relation to MPV. It can be seen that both IN and MBN have a positive effect on MPV development. A linear model (Equation 6-8) was developed to describe the effect of IN and MBN on MPV development.

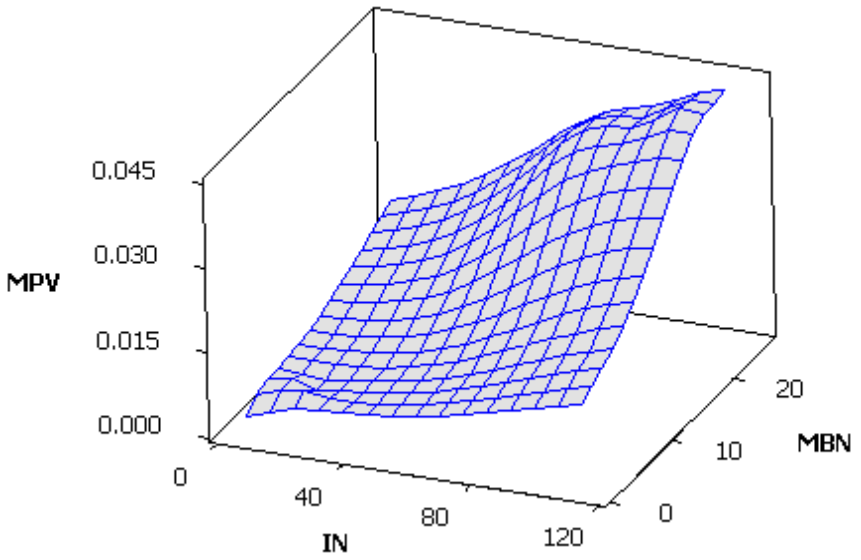

Figure 6-8 Interactions between MPV, MBN, and IN for FAC

A comparison of the values predicted by Equation 6-8 and the MPV values experimentally obtained is shown in Figure 6-9. The model presented a high determination coefficient (R^2 = 0.9511), claiming 95.11% of the variation can be explained by the independent variables. The analysis of variance (Table 6-7) shows that the probability corresponding to the F value is lower than 0.05. Therefore, the model can be used to estimate unknown TPV when IN and MBN information is given.

MPV = -1.222681E-03+2.618721E-04*IN+6.905555E-04*MBN (6-8)

Table 6-7 Analysis of variance for MPV modeling

Source	**DF**	**Sum of squares**	**Mean squares**	**F**	**Pr > F**	**R-Sq**	**R-Sq (adj)**
Model	2	0.0	0.0	247.1	< 0.05	98.21%	97.81%
Error	9	0.0	0.0				
Corrected total	11	0.0					

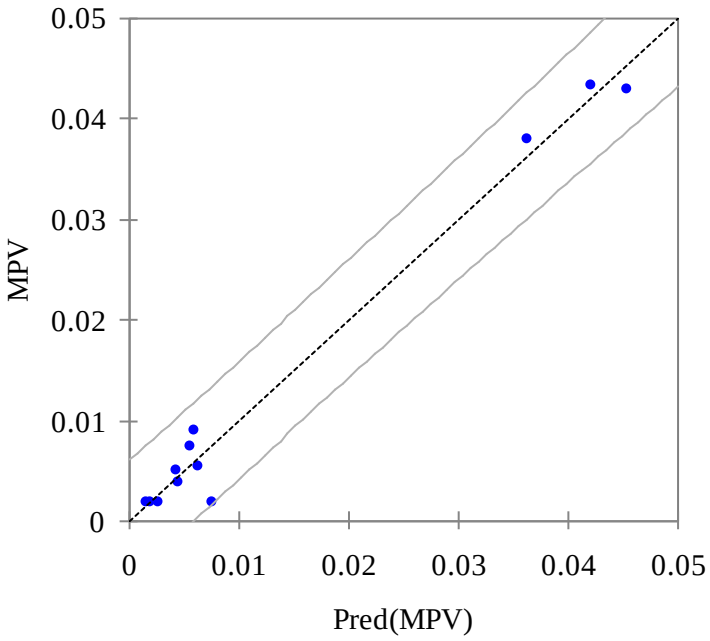

Figure 6-9 Correlation between measured and predicted MPV

6.8 Characterization of FAC produced by physical activation

A scanning electron microscope (SEM) study showed that the carbonization process has a significant influence on the particle's porosity development. Figure 6-10 shows that the surface porosity of HOFA dramatically increased after activation.

Bulk density of AC is an important property, especially when used it as an adsorbent. AC with a high density is good to use as a filter media . AWWA (1991) suggested that the lower limit of bulk density is 0.25 g/cm^3 for granular activated carbon. The bulk density of all FAC produced from physical activation ranged from FAC-P01 (0.325 g/cm^3) to FAC-P07 (0.285 g/cm^3). FAC produced at a higher temperature showed a higher bulk density (Table 6-8).

Table 6-8 Characteristics of FAC produced by physical activation

Parameters	**FAC-P01**	**FAC-P02**	**FAC-P03**	**FAC-P04**	**FAC-P05**	**FAC-P06**	**FAC-P07**
BET surface area (m^2/g)	4.1266	12.6990	14.0380	10.7370	5.8500	8.7500	10.2300
Total pore volume, (cm^3/g)	0.0182	0.0239	0.0221	0.0248	0.0119	0.0250	0.0222
Micropore volume (cm^3/g)	0.0019	0.0074	0.0054	0.0039	0.0011	0.0040	0.0029
Mesopore volume (cm^3/g)	0.0163	0.0166	0.0167	0.0209	0.0108	0.0210	0.0193
Meanpore diameter (nm)	17.6310	7.5414	6.3060	9.2503	-	-	-
Iodine number	6.5200	15.2300	16.2500	13.3000	7.1000	11.2500	13.3000
Methylene blue number	1.8500	3.8200	4.5800	3.0500	2.1000	3.2500	3.8900
Yield %	65.23	60.36	55.55	62.75	66.21	64.36	60.77
Ash content (%)	13.75	14.75	15.25	13.12	10.15	11.80	12.10
Bulk density (g/cm^3)	0.325	0.315	0.331	0.31	0.322	0.281	0.285
P^H	6.65	6.85	6.80	6.60	6.50	6.50	6.55

Note: BET, Total pore volume and Mesopore volume of FAC-P05, FAC-P06, FAC-P07 were estimated by developed model Equation 6-6 to 6-8

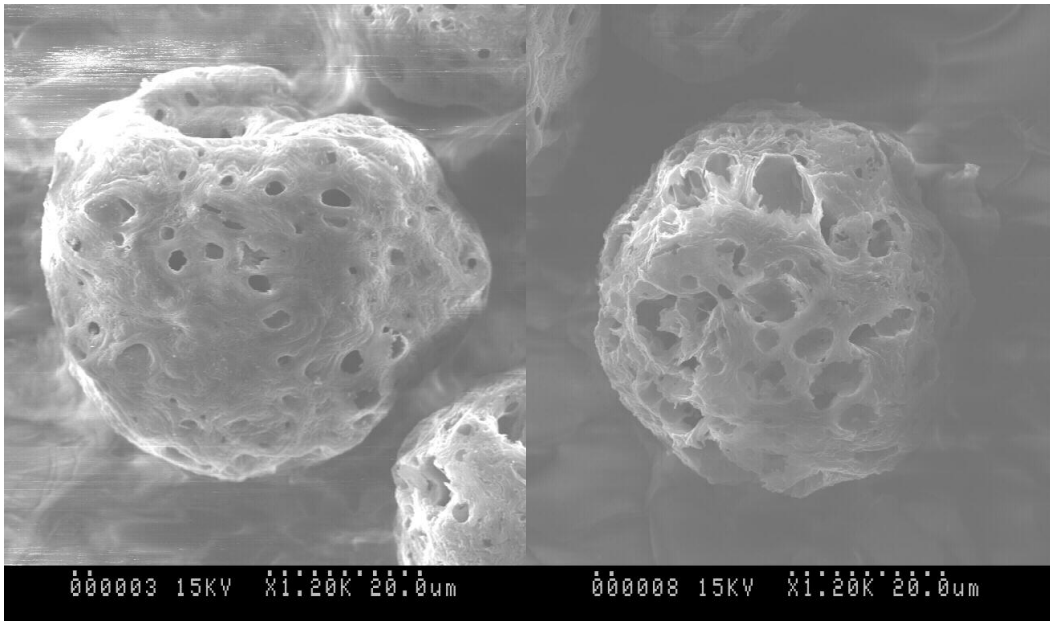

(a) (b)

Figure 6-10 SEM analysis of (a) HOFA (b) after heating at 900°C

IN is the amount of iodine, in milligrams, adsorbed per gram of AC at an equilibrium concentration (e.g., 0.02 M). It provides an indication of the surface area (m^2/g) and porosity of AC (Gergova et al., 1994; Collin et al., 2008). The IN of FAC prepared by physical activation (Table 6-8) ranged from 6.52 mg/g to 16.25 mg/g, which is generally low and indicates low porosity. A lower IN generally represents low porosity with a pore size narrower than 1.0 nm (Collin et al., 2008).

The pH of produced FAC ranged from 6.55 (FAC-P07) to 6.85 (FAC-P02), which is close to acidic conditions. The burning temperature and reaction time was found to have an insignificant effect on the pH of FAC. The pH of carbon materials ranging from 6 to 8 is practical for most industrial applications, especially for the adsorption of pollutants from an aqueous solution (Qureshi et al., 2007). Therefore, FAC prepared by physical activation could be acceptable in most applications involving adsorption from aqueous solutions.

The ash content indicates the quality of the ash in AC. It is the residue that remains when the carbonaceous portion is burned off. The ash consists mainly of minerals such as silica and oxides of aluminium, iron, magnesium, and calcium (oxides). The ash content of the produced FAC ranged from 10.15 (FAC-P05) to 15.25 (FAC-P03). The effect of the activation temperature on BET surface area, iodine number (IN), and methylene blue number (MBN) was studied. From Figure 6-11 it is clear that BET, IN, and MBN were increased gradually by increasing the activation temperature from 700°C to 900°C.

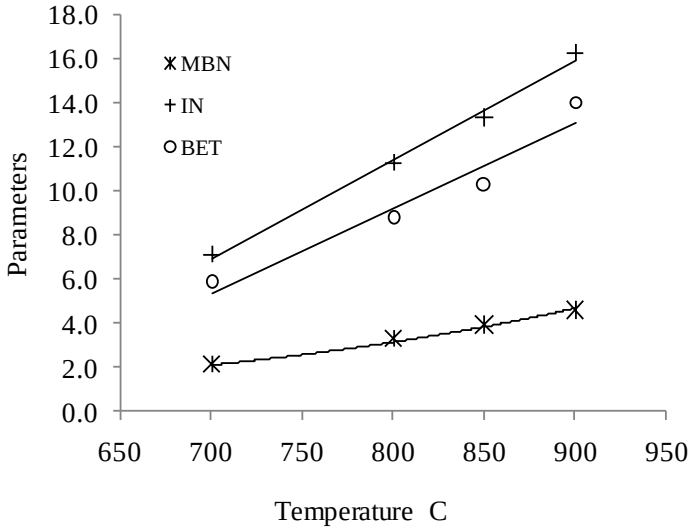

Figure 6-11 Effects of temperature on FAC development (at 120 minutes activation)

Figure 6-12 shows that BET, IN, and MBN are gradually increased by activation times from 45 to 90 minutes; after that, a decreasing trend is observed with increasing the activation time. Based on this experiment an activation time of 90 minutes could be considered the optimum activation time for this case. FAC yield ranged from 60% to 70%. Both temperature and heating time have a significant effect on the final yields. The effect of activation temperature on the yield was evaluated at an activation time of 120 minutes. This is evidence that FAC yield decreases by increasing the activation temperature (Figure 6-13).

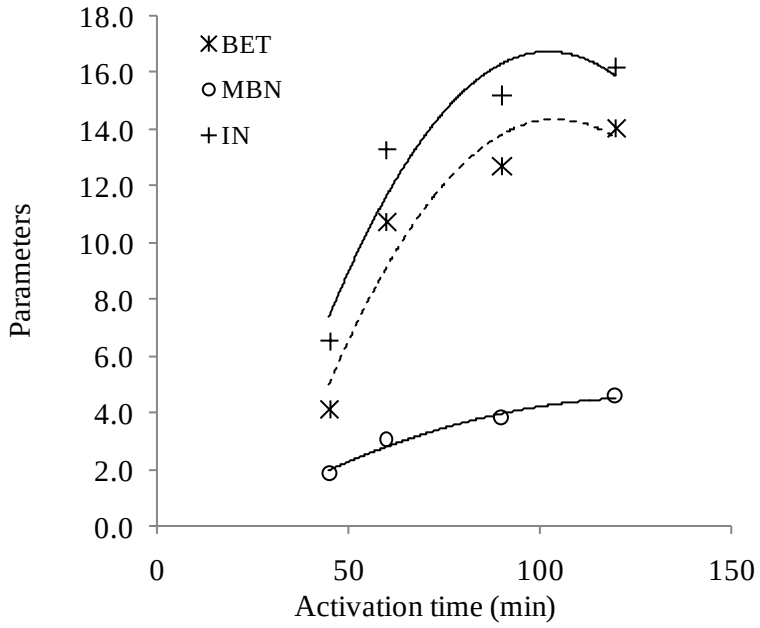

Figure 6-12 Effects of activation time on FAC development (at 900ºC)

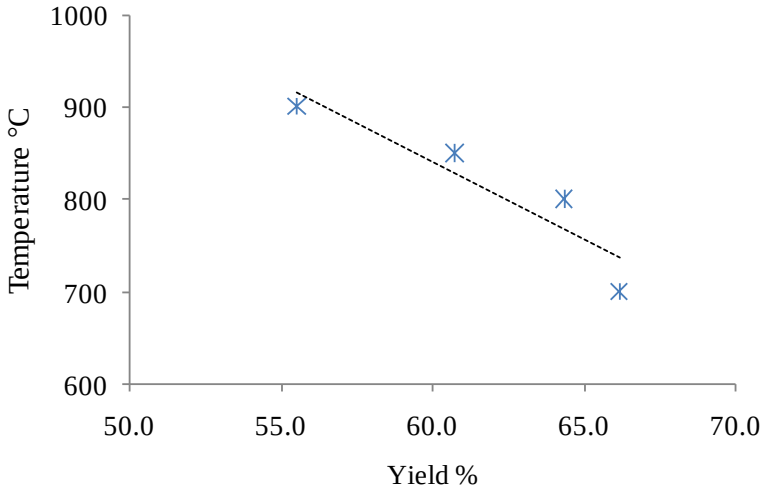

Figure 6-13 Effects of activation temperature (at 120 minutes) on FAC yield

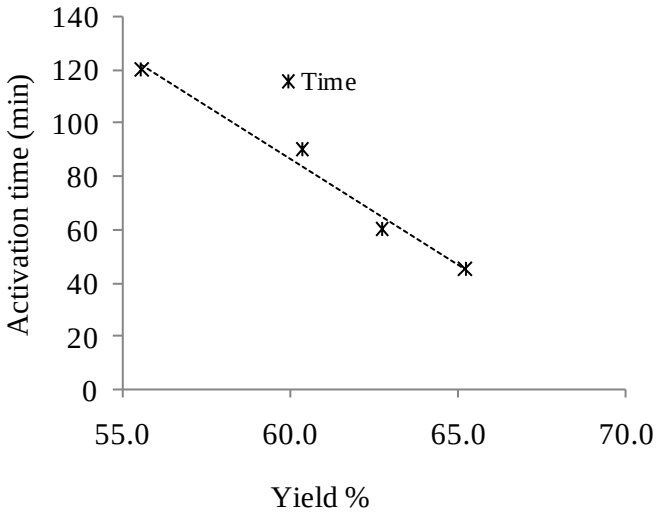

Figure 6-14 Effects of activation time (at 900ºC) on FAC yield

The effect of activation time on FAC yield was also evaluated at 900°C. Figure 6-14 shows that the yield decreased by increasing the activation time.

6.9 Characterization of FAC produced by NaOH and KOH

The BET surface area of FAC produced by NaOH and KOH was evaluated by N_2 adsorption isotherms, MBN, and IN (Table 6-9). FAC prepared by NaOH and KOH (Table 6-9) showed a higher surface area than that obtained by physical activation (Section 6.8). This is probably due to the development of more pores on the particle surface. The FAC yield was estimated by the weight difference of the original materials and the quantity after activation treatment. Under test conditions, FAC yield was 60% to 75%. Figure 6-15 shows that the FAC yield decreased as the percentage of chemical dose increased. Burn-off is the weight loss of char during the activation process (Davini, 2002). Higher burn-off values were observed by increasing chemical doses. High burn-off generally provides a better surface area, which may lead to a higher adsorption capacity of AC. The burn-off for the produced FAC was

between 10% and 25% (Figure 6-15), which could be considered low burn-off compared to the reported values (Caramuscio, 2003).

A high microporosity and a large surface area are the most desired properties of AC. These properties may be affected by varying the amounts of activation reagents and other reaction parameters such as temperature and reaction time. The effect of chemical agents on the surface area development of the produced FAC is shown in Figure 6-16. In this case, adding 25% by weight chemical agent to HOFA with a reaction time of 2 h at 900^{o}C was found to be the best condition for surface area development. However, high burn-off values and consequently low yields were found at this condition.

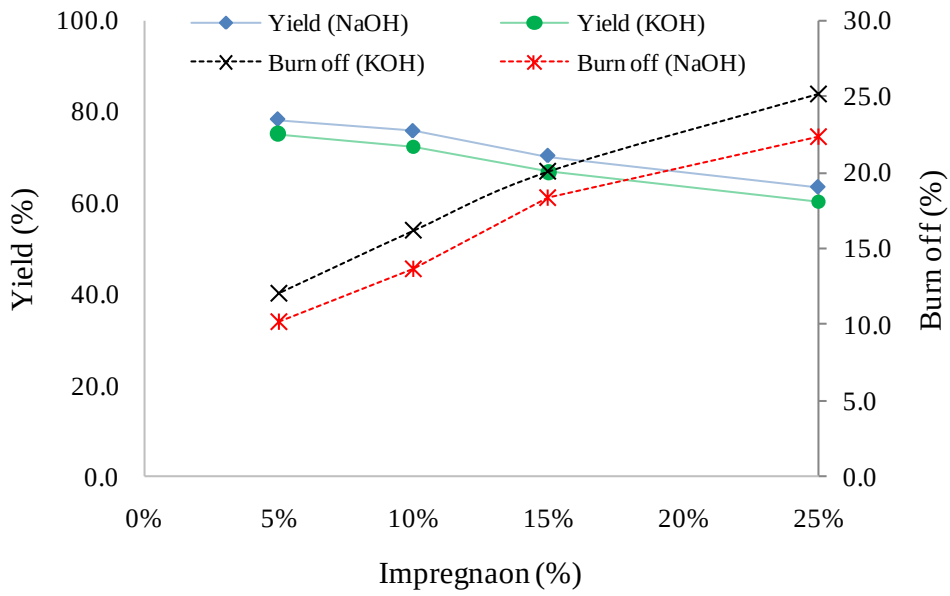

Figure 6-15 Effect of impregnation type and ratio on the yield of FAC

The maximum surface areas of FAC were found to be 116.4 and 97.6 m^2/g respectively with 25% KOH and NaOH. The BET surface area of the FAC was much lower at a low dose of chemical agent, and it increased dramatically with increased chemical doses. However, the increment rate of BET surface area was found to be insignificant with a KOH dose between

15% and 25%. On the other hand, a larger BET surface area was observed at a higher dose of NaOH (Figure 6-16). Micropore volumes also increased by increasing the percentage of chemical agents (Table 6-9). Higher INs and MBNs were found for FAC prepared by KOH compared to those obtained with NaOH (Table 6-9).

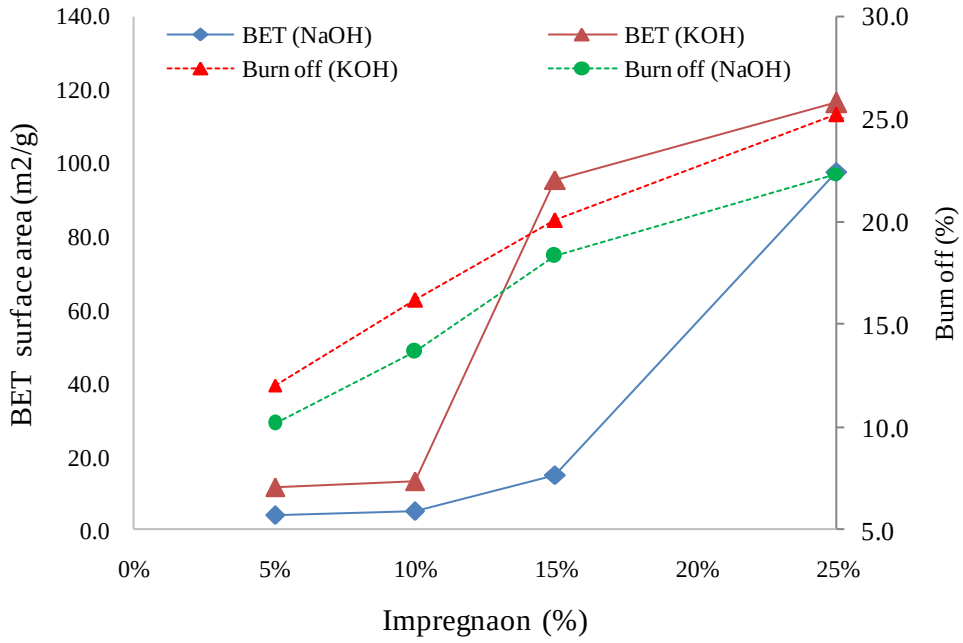

Figure 6-16 Effect of chemical dose on the surface area development of FAC

A high ash content is undesirable for AC since it reduces the mechanical strength of carbon and affects the adsorptive capacity. The ash content of the produced FAC ranges from 12% to 14% and indicates good mechanical strength (ASTM D2866-94, 2000). The pH of FAC generated by NaOH and KOH ranges from 7.25 to 7.90 as shown in Table 6-9.

Table 6-9 Textural properties of fly ash activated carbon

Parameters	**KOH**				**NaOH**			
	FAC-1	**FAC-3**	**FAC-5**	**FAC-7**	**FAC-2**	**FAC-4**	**FAC-6**	**FAC-8**
BET surface area (m^2/g)	116.410	92.9150	13.496	11.864	97.612	15.041	5.390	4.127
Total pore (cm^3/g)	0.313	0.3128	0.026	0.069	0.065	0.041	0.023	0.018
Micropore (cm^3/g)	0.043	0.0434	0.009	0.005	0.038	0.002	0.002	0.002
Mesopore (cm^3/g)	0.269	0.2694	0.017	0.065	0.027	0.040	0.021	0.016
Meanpore (nm)	13.467	13.4670	7.675	23.367	12.654	10.967	16.722	17.631
IN	110.59	85.68	15.88	9.56	105.86	18.26	9.52	5.36
MBN	25.50	18.75	5.12	4.25	22.98	5.75	6.12	3.78
Yield %	60.32	66.73	72.36	75.2	63.4	70.25	75.67	78.232
Ash content (%)	14.50	14.20	13.95	13.12	14.10	13.80	13.10	12.75
Bulk density (g/cm^3)	0.35	0.33	0.325	0.321	0.332	0.321	0.295	0.289
pH	7.90	7.75	7.50	7.20	7.85	7.65	7.30	7.25

**Note: BET, total pore volume and mesopore volume of FAC-3, to FAC 8 were estimated by developed model Equation 6-6 to 6-8*

6.10 Characterization of FAC produced by H_3PO_4

The carbonization process has a significant influence on the particle's porosity development. A SEM micrograph, as shown in Figure 6-17b, indicates that, compared to clean HOHA, the surface porosity of the HOFA is increased by a chemical activation process (Figure 6-17a). Table 6-10 shows the different properties of FAC produced by H_3PO_4. The maximum BET surface area (i.e., 144 m^2/g for AC-8) was achieved at 800°C with 60 minutes reaction time by 5 ml H_3PO_4. The second highes surface area was estimated for AC-6 (i.e., 130 m^2/g), which was produced by 5 ml of H_3PO_4 at 800°C with a holding time of 30 minutes. It shows that heating time has a significant influence on AC yield. For example, the yield of AC-8 and AC-1 achieved 66% and 82%, respectively, at 60 minutes and 30 minutes reaction time.

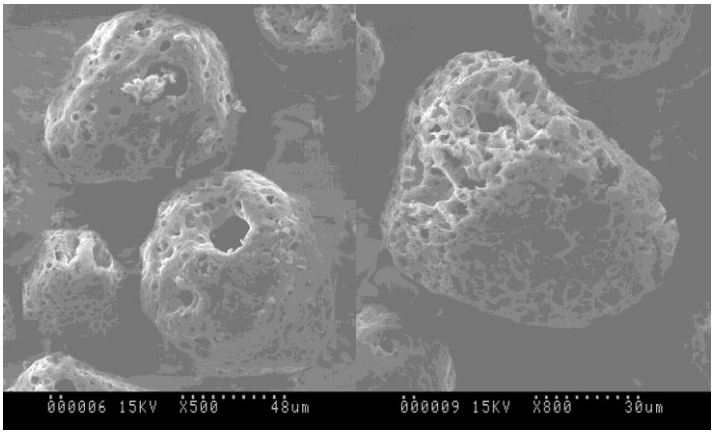

(a) (b)

(a) after washing treatment (b) after heating at 800°C (AC-8)

Figure 6-17 SEM analysis of FAC

Table 6-10 Properties of FAC produced by H_3PO_4

Parameters	**AC-1**	**AC-2**	**AC-3**	**AC-4**	**AC-5**	**AC-6**	**AC-7**	**AC-8**
BET surface area (m^2/g)	75.38	82.674	91.22	123.19	79.48	130.06	102.778	143.888
TP (cm^3/g)	0.1219	0.1329	0.1440	0.2215	0.1285	0.1662	0.2105	0.2326
MPV (cm^3/g)	0.0536	0.0548	0.0588	0.0976	0.06158	0.05747	0.08699	0.10951
Mesopore (cm^3/g)	0.0682	0.0780	0.08518	0.12389	0.06691	0.10872	0.12350	0.12308
IN	80.50	95.50	110.20	130.25	90.75	140.45	120.50	160.85
MBI	19.75	21.48	23.58	31.45	20.71	33.10	26.41	36.36
% Yield	82.8	78.33	74.32	79.15	78.25	75.22	72.12	66.25
Ash content (%)	12.75	12.52	13.10	13.02	14.1	13.75	12.81	12.25
Bulk density (g/cm^3)	0.332	0.328	0.315	0.322	0.312	0.321	0.325	0.354
pH	7.50	7.55	7.35	7.25	6.95	6.75	7.10	6.90

In order to examine the main factors and their interactions for BET surface area development, a 2^3 factorial design was used. The regression analysis was performed to fit the experimental data. A Design-Expert version 8 software trial package was used in this case. The main interaction effects of each parameter were analyzed and are listed in Table 6-11. In this case, all main factors and their interactions have a positive effect on surface area

development except BC and ABC (Table 6-11). Among the parameters, temperature has the highest effect (about 46% contribution) in surface area development followed by the heating time (24% contribution).

Table 6-11 Contribution of different parameters on surface area development

Parameters	**Effects**	**% Contribution**
A (Temperature)	32.65	45.74
B (Heating time)	23.28	23.26
C (H_3PO_4)	21.03	18.97
AB	3.89	0.65
AC	13.02	7.27
BC	-4.90	1.03
ABC	-8.45	3.06

Table 6-12 shows the experimental and predicted values of BET surface area from the Design-Expert version 8 trial software. The normal probability plot of residuals (Figure 6-18) shows that the residual distribution is approximately normal, and there is no abnormality in the data set. Figure 6-19 shows that the distribution residuals are approximately constant. All these diagnostic proved that the analysis is satisfactory.

Table 6-12 Predicted values of BET surface area (m^2/g) of FAC

Order	**Experimental BET**	**Predicted BET**
AC1	75.42	65.15
AC2	82.58	97.80
AC3	91.24	88.43
AC4	123.27	121.08
AC5	79.41	86.18
AC6	130.05	118.83
AC7	102.79	109.46
AC8	143.46	142.11

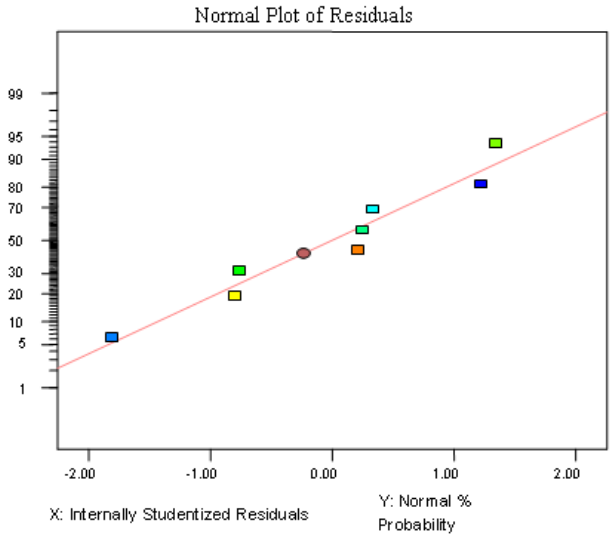

Figure 6-18 Normal probability plot of residuals

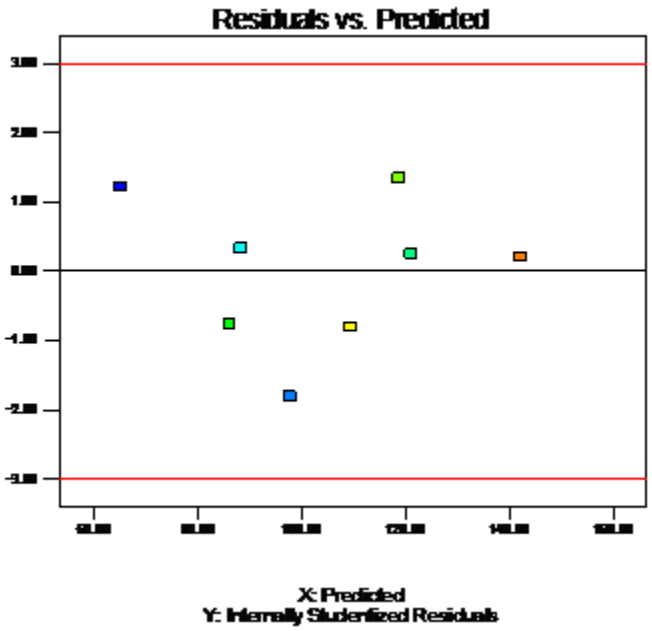

Figure 6-19 Residuals vs. predicted plot

In order to determine the optimum value of each variable, 3D plots were generated. Figure 6-20 shows the interaction of temperature and heating effects on surface area development: both factors have a positive effect on the final output. At maximum set conditions,

temperature has more influence than heating time. Similarly, if we compare the interaction effect of temperature and H_3PO_4 (Figure 6-21), both have a positive effect and the degree of temperature influence is higher than with H_3PO_4.

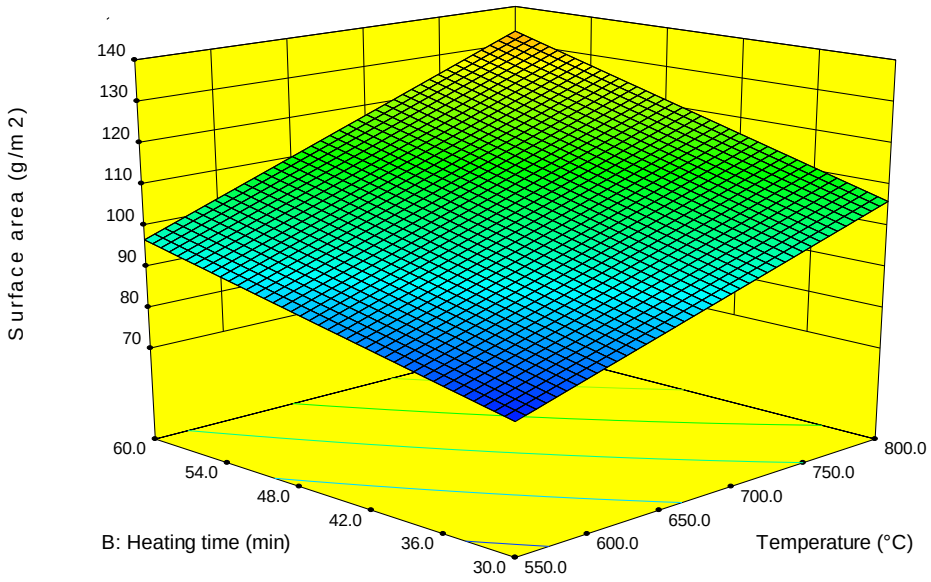

Figure 6-20 Effect of heating time and temperature on surface area development

Figure 6-22 shows that heating time and H_3PO_4 have a positive effect on BET surface area development. By analyzing the 3D response plots, it is easy to evaluate the optimum values of the variables.

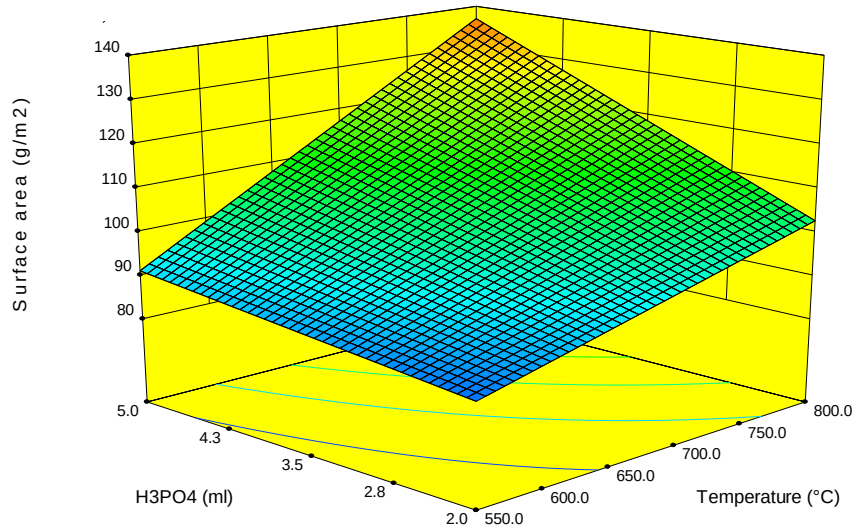

Figure 6-21 Effect of temperature and H_3PO_4 on surface area development

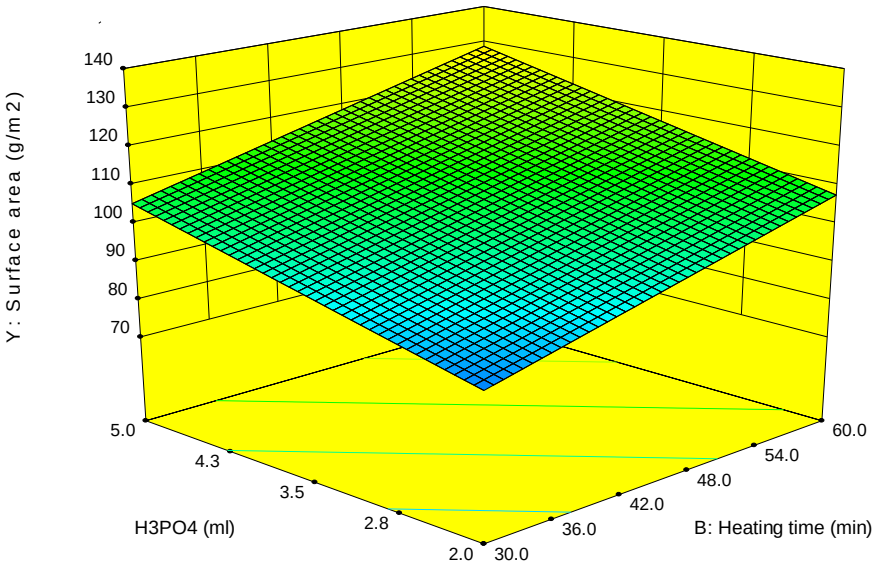

Figure 6-22 Effect of heating time and H_3PO_4 on surface area development

Each contour line (e.g., bottom of 3D surface diagram) represents an infinite number of combinations of two-test variables. The maximum predicted value can be found by the surface confined with the smallest ellipse in the contour. Elliptical contours are obtained when there is a perfect interaction between independent variables (Montgomery, 1997). The surface plot in Figure 6-20 indicates that BET surface area increased by an increase in temperature and time. Similar patterns were observed for Figures 6-21 and 6-22. However, at high temperatures cause shrinkage of AC, which may result in poor surface area (Guo and Lua, 1998). The higher temperature and holding time also reduced the percentage yield of FAC. Thus, increasing the temperature above 800°C may not be feasible for this case.

6.11 Summary

Different methods are available to clean the impurities in FA. However, the selection of chemicals and its dose depend on the raw material characteristics. Based on the literature and different trial experiments, this study found that 28% HNO_3 and 15% HCl treatment lowered the metal concentration in HOFA to an acceptable level. A case by case study is required in order to develop appropriate washing and cleaning procedures.

To produce FAC, physical and chemical activation was used in this study. Three different types of chemicals, such as NaOH, KOH and H_3PO_4, were used as chemical agents during the chemical activation process of this study. Based on the surface area analysis, it is clear that chemical agent has significant influence on the development of surface area of final product. During the activation process the chemical agent react with the impurities present the in particle and produce extra pores on the particle surface, which may lead the higher surface area of the produce FAC, compared with the physical activation. The produced FAC was compared with AC produced from various raw materials (Table 6-13) reported in the

literature. Based on a comparative analysis, it can be concluded that HOFA has the potential to be used as a raw material for AC production.

This study revealed that Saudi Arabian HOFA can be used as an effective and inexpensive (since the FA is very cheap at generation points) raw material for AC production, which has the potential for various industrial applications, especially in the adsorption process for the removal of pollutants with large molecules where a mesopore volume is required.

Table 6-13 Characteristics of activated carbons obtained from various precursors

Raw Material	**Activation agent**	**BET (m^2/g)**	**Total pore volume (cm3/g)**	**References**
Plum kernels	NaOH	113	0.083	Tseng, 2007
Anthracite	NaOH	334	0.140	Lillo-Rodenas et al., 2004
Corn cob	NaOH	446	0.420	Tseng, 2006
E. rigida	NaOH	396	0.202	Kilic et al., 2012
HOFA	NaOH	97.612	0.065	This study (Maximum BET)
HOFA	KOH	116.41	0.191	This study (Maximum BET)
HOFA	H_3PO_4	143.46	0.439	This study (Maximum BET)
HOFA	Physical	14.03	0.0221	This study (Maximum BET)
Oil FA	NH_4OH	318.00	-	Yaumi et al., 2013
Indulin lignin	KOH	514	-	Hayashi et al., 2000
Lignite	KOH	1594	0.71	Lillo-Rodenas et al., 2007
Coconut	KOH	1740	0.74	Lillo-Rodenas et al., 2007
Bagasse fly ash		2316	1.27	Purnomo et al., 2011

Chapter 7

Potential Use of Fly Ash Activated Carbon in Wastewater Treatment

7.1 Background

Industrial development and modernization have exerted a significant pressure on water demand all over the world, and it is expected to grow at a high rate. Recurring water-related problems are becoming even more worrisome. Improved recycling and wastewater reuse could be alternative sources to meet future water demands, especially in agriculture, landscaping, and aquifer recharge. Due to the presence of significant toxic compounds, pre-treatment is needed before wastewater is reused.

Without treatment the direct disposal of wastewater into the environment may have a negative impact on ecosystems and human health. Only 42% of the wastewater generated by global industries receives some kind of treatment (Doan et al., 2009). The improper discharge of wastewater into water bodies over a long period of time can cause the deterioration of these environments and liver and kidney damage, diarrhoea, and other waterborne diseases in humans and animals (Sarkar and Acharya, 2006).

A range of wastewater treatment technology is available in the market. However, research is being conducted on the development of sustainable and cost-effective technology. The most common wastewater treatment systems are biological treatment (Gernjak et al., 2003), chemical oxidation (Ahn et al., 1999), biodegradation (Massot et al., 2012), and adsorption

(Lin and Juang, 2009; Xue et al., 2009). Of these, the adsorption process is the most favourable method for removing pollutants from wastewater due to its simple design and easy operation (Ahmed and Dhedan, 2012). With the selection of a proper adsorbent, this process could be an alternative and cost-effective technique for wastewater treatment. Adsorption techniques can be used in treating dyes, metals, and other organic pollutants in wastewater. Activated carbon (AC) is a widely used adsorbent for wastewater treatment (Ahmad et al., 2007). However, the use of commercially available activated carbon (CAC) for wastewater treatment involves a high treatment cost, which has led researchers to develop alternative and cost-effective adsorbents. The use of industrial by-products to treat wastewater could be an innovative and sustainable alternative. Many researchers have focused on low-cost adsorbents from industrial and or agricultural by-products (Ozcan et al., 2004; Suteu and Bilba, 2005; Voudrias et al., 2002). A recent review by Mohan and Pittman (2006) showed that low-cost adsorbents can be divided into three categories: (i) biomass, (ii) agriculture and industrial wastes, and (iii) nano-sized particles. Recently, FA has gained popularity for use in the adsorption of pollutants from waste streams because of its relatively low cost, good mechanical stability, and high adsorption capacity. Many researchers have investigated the adsorption capacity of FA (Sarkar and Acharya, 2006; Gupta and Ali, 2004). Using Turkish coal FA, Bayat (2002) investigated the removal efficiency of aqueous Cr (VI) ions. Banarjee et al. (2004) used chemically modified coal FA to remove Cr (VI) from an aqueous solution. Gupta and Ali (2004) used bagasse FA to remove lead and chromium from wastewater. All this research has found that the thermal activation of FA offers a satisfactory adsorption performance.

The study presented in this chapter investigates the possible application of FAC to the removal of different pollutants from aqueous solutions. Three separate adsorption experiments such as (i) the adsorption of polycyclic aromatics hydrocarbons (PAHs) (e.g., naphthalene), (ii) the adsorption of Cr (VI), and (iii) the adsorption of dye from simulated wastewater (prepared in the laboratory) were conducted to study the adsorption efficiency of the FAC prepared in Chapter 6.

PAHs, one of the most widespread organic pollutants, are mainly produced by the incomplete combustion of carbon-containing fuels such as wood, coal, diesel, fat, and tobacco. PAHs are lipophilic: they mix more easily with oil than water (Nagpal, 1993; Schwarzenbach et al., 2003). PAHs are found in soil, sediment, and oily substances (Pitt et al., 1999). It is considered environmental persistent and is composed of low biodegradable compounds (Yuan et al., 2010). Because of their toxicity, the fate of PAHs in the environment is of great concern (Maloni and Samara, 1999; Holoubeki et al., 2000). Due to its aromatic characteristics, PAH compounds are easily adsorbed on fine carbonic particles (Gong et al., 2007). The adsorption capacity depends on the molecular size of the PAH; generally, the larger molecular size has less affinity to attach onto particles (Gong et al., 2007). In wastewater, the presence of PAHs mainly depends on the source of the wastewater. PAHs in wastewater may produce a high chemical oxygen demand (COD) and a low biological oxygen demand (BOD). The treatment of wastewater containing PAHs is essential to preserving the standard quality of the receiving water.

Various methods are used for the removal of PAHs in water: biodegradation, adsorption, and ion exchange resins (Xia et al., 2006; Liu et al., 2011; Sponza and Oztekin, 2010). Among others, adsorption provides a simple approach to removing PAHs from aqueous solutions.

With the selection of a proper adsorbent, this process can be a viable alternative and cost-effective technique for the removal of PAHs from wastewater. AC has a proven application in environmental purification. It has been broadly applied in different studies to the removal of organic pollutants, including PAHs, from wastewater (Qianqian et al. 2012; Yuan et al., 2010; Gong et al., 2007).

Heavy metals are considered to be the most toxic environmental pollutants because of their non-degradability and their threat to human life and the ecosystem (Ahalya et al., 2003). Metals enter the environment when metal-bearing streams are not treated properly. Of the heavy metals, chromium (Cr) is one of the most important, as it is widely used in many industrial processes. The major sources of Cr in aquatic systems are effluents from electroplating, metal finishing and processing, magnetic tapes, pigments, leather tanning, wood protection, chromium mining and milling, brass, paint, electrical and electronics equipment manufactures, and catalysis (Mohan and Pittman, 2006). Chromate poisoning can cause skin disorders and liver damage (Sawyer et al., 2004). The United States Environmental Protection Agency (USEPA, 2006) has fixed an enforceable maximum contamination level for Cr in drinking water of 0.1 mg/L for public water systems. The World Health Organization (WHO) also recommends a maximum allowable Cr (VI) concentration in drinking water of 0.05 mg/L (WHO, 2003, 2007). Improper treatment of Cr effluents may pose a serious problem to ecosystems and public health. Methods available for the removal of metal ions from aqueous solutions include ion exchange, electro dialysis, electrochemical precipitation, evaporation, solvent extraction, reverse osmosis, chemical precipitation, and adsorption (Patterson, 1985; Mahvi et al., 2005). Most of these methods suffer from such disadvantages as high capital and operational costs and are not suitable for

small-scale industries. Of these techniques, adsorption seems to be one of the most effective methods for removing heavy metals and dyes from wastewater because of its simple operation and easy handling (Weng et al., 2000; Sharma and Forster, 1994). With the selection of a proper adsorbent, this process can be a viable alternative and cost-effective technique for the removal of Cr ions from wastewater (Mor et al., 2007; Tan et al., 1993; Gode and Pehlivan, 2006; Mohan et al., 2005).

Methylene blue (MB) ($C_{16}H_{18}N_3SCl.3H_2O$), a dye commonly used in the textile industry, has a molecular weight of 373.9 g/mol (Ardizzone et al., 1993). It is mainly discharged from textile, rubber, paper, cosmetic, and plastics industries. Because of their poor biodegradability and toxicity, dyes may pose a serious environmental concern (Pala and Tokat, 2002; Yao et al., 2010). In water, MB, even at very low concentrations, is highly visible. Because of reduced light penetration, the presence of MB in water may affect photosynthetic activity in aquatic life (Allen and Koumanova, 2005). MB can cause eye burns, which may result in permanent injury to the eyes of humans and animals (Ghosh and Bhattacharyya, 2002). Therefore, the treatment of effluent containing MB is essential to preserving the standard quality of the receiving water. Various methods have been developed to remove dyes from wastewaters, including chemical oxidation (Chengtang et al., 2011), photo degradation (Fatimah et al., 2011), and adsorption (Vargas et al., 2011). Due to the complex nature of organic dyes, the commonly used biological treatment process is not very effective in treating them (Pala and Tokat, 2002). Among other techniques, the adsorption process is the most favourable method for removing dyes from wastewater (Ahmed and Dhedan, 2012). AC is a widely used adsorbent for dye removal from wastewater (Ahmad et

al., 2007). For this study MB was selected because of its known strong adsorption onto solids.

7.2 Adsorption of naphthalene on FAC

Naphthalene is the simplest and most abundant polycyclic aromatic hydrocarbon (PAH) compound found in wastewater. It is a natural constituent of coal and tar, and is commonly used as a wood preservative, moth repellent, and synthetic resin (Chang et al., 2004). The objective of this experiment is to explore the performance of FAC in removing naphthalene from wastewater. Different batch adsorption experiments were conducted by simulated wastewater prepared in the laboratory. The equilibrium state of adsorption process was also studied to understand the mechanism of naphthalene adsorption onto FAC.

7.2.1 Adsorbents used in naphthalene adsorption

For this experiment FAC-1 and FAC-2 (see Chapter 6 of this thesis) were used as representative adsorbents to evaluate the effects of naphthalene adsorption onto FAC. The properties of FAC were reported in Chapter 6.

7.2.2 Naphthalene adsorption experiments

Adsorption experiments were performed at room temperature in a stirred batch system. In this study naphthalene ($C_{10}H_8$) with a molecular weight of 128.16 was used. To prepare a naphthalene stock solution 200 mg of naphthalene was dissolved in reagent grade ethanol, the mixture was carefully swirled together for approximately 15 to 20 min to allow proper dissolution, and subsequently diluted with distilled water to make total volume of 1000 ml as suggested (Cabal et al., 2009; Owabor et al., 2012). The ethanol concentration in the stock solution was maintained approximately 3% of the volume. A series of naphthalene solutions with concentrations ranging from 25 mg/L to 120 mg/L was prepared by diluting stock

solutions with distilled water. Batch experiments investigated the effects of such parameters as FAC dose, initial naphthalene concentration, temperature, and pH. The experiments were performed in a series of 250 ml Erlenmeyer flasks, where 50 ml of naphthalene solutions with known initial concentrations (i.e., 25-120 mg/L) were agitated at a constant rate (i.e., 120 rpm) by 0.025-0.15 g of FAC. An equilibrium contact time was selected based on kinetic studies. In this case, 50 ml of naphthalene solution of known concentration (i.e., 50 mg/L) and pH (6.5) was agitated by 0.1 g of FAC on a Fisher stirrer model 11-500-7SH at a rate of 120 rpm. At given time intervals, the solutions were filtered on Whatman No. 42 filter paper. The naphthalene concentration in each solution was measured by a UV-visible spectrometer (Hewlett-Packard Model 8453) at a wavelength of 276 nm (Qianqian et al., 2012; Belen et al., 2009). To eliminate error due to the adsorption of naphthalene onto the filter paper, a parallel control set (without FAC) was run in an identical manner. To evaluate the effect of pH on the adsorption process, the original pH of the naphthalene solution was adjusted to the desired value by adding the required quantities of 0.5 N NaOH or 0.5 N HCl solutions. At equilibrium, the amount of naphthalene adsorbed on FAC (i.e., q_e, mg/g), was calculated as follows:

$$q_e = \left(\frac{C_0 - C_t}{w} \right) \times v \qquad (7\text{-}1)$$

where, *C*o (mg/L) is the initial naphthalene concentration, *Ct* (mg/L) is the equilibrium naphthalene concentration in the solution, *V* is the volume of the naphthalene solution in litres, and *w* is the amount of FAC used in *g*. The percentage removal of naphthalene (R_{cn}) from the solution was calculated as follows:

$$R\,\% = \left(\frac{C_0 - C_t}{C_0}\right) \times 100 \qquad (7\text{-}2)$$

The effects of pH and temperature on the adsorption process were also investigated by varying the temperature and pH in the fixed equilibrium experiments.

7.2.3 Adsorption isotherm models

Freundlich and Langmuir models were used to study the adsorption process of naphthalene onto FAC. The method of least squares was used for finding the parameters of the isotherm models. The Freundlich model (Freundlich, 1906) (Table 5-1) represents the relation between the amount of ions adsorbed per unit mass of adsorbent and the equilibrium concentration of ions in solution. The Freundlich constant, K_f, which indicates the relative adsorption capacity of the adsorbent related to the bonding energy, q_e, is the amount adsorbed per unit mass of the adsorbent (mg/g), C_e, equilibrium concentration (mg/L), and 1/n a factor representing the deviation of the absorption process from its linearity.

Table 7-1 Isotherms and their linear forms

Isotherm		**Linear form**	**Plot**
Freundlich	$q_e = K_f \cdot C_e^{1/n}$	$\log q_e = \log K_f + \frac{1}{n}\log C_e$	log *(qe)* vs log *(Ce)*
Langmuir-1	$q_e = \frac{\alpha\beta C_e}{1+\alpha C_e}$	$\frac{C_e}{q_e} = \frac{1}{\alpha\beta} + \frac{C_e}{\beta}$	(C_e/q_e) vs C_e
Langmuir-2		$\frac{1}{q_e} = \frac{1}{\alpha\beta}\left(\frac{1}{C_e}\right) + \frac{1}{\beta}$	($1/q_e$) vs ($1/C_e$)
Langmuir-3		$\frac{q_e}{C_e} = \alpha\beta - \alpha q_e$	q_e/ C_e vs q_e

The Freundlich coefficients can be determined from a plot of log (q_e) versus log (C_e), which has a slope of *1/n*, and an intercept of log K_f. The value of *1/n* < 1 indicates positive adsorption, while high K_f values indicate greater adsorption intensity. *n* < 1 represents unfavourable conditions, and 1<n<10 represents favourable conditions for adsorption.

The Langmuir isotherm (Langmuir, 1916) is valid for a monolayer adsorption process. It can be linearized as different types, and the parameter estimates may differ in each case (Kinniburgh, 1986). To evaluate model uncertainty, the three most popular linear forms of Langmuir isotherm (Table 7-1) were used in this study.

Langmuir isotherm parameters α (L/mg) and β (mg/g) are constants related to the apparent energy of adsorption and the adsorption capacity, respectively. The constants α and β can be determined from the intercept and slope of the plot of (i) (C_e/q_e) versus C_e for Langmuir-1, (ii) ($1/q_e$) vs. ($1/C_e$) for Langmuir-2, and (ii) $q_{e/}$ C_e vs q_e for Langmuir-3. The essential characteristic of the Langmuir isotherms can be expressed in terms of the dimensionless parameter (Weber and Chackravorti, 1974) as:

$$\Delta = \frac{1}{1+\alpha C_0} \qquad (7\text{-}3)$$

where, Δ is indicative of the isotherm shape. Δ > 1.0 indicates that an adsorption system is unfavourable, whereas a favourable adsorption take place within 0< Δ <1.0.

7.2.4 Effect of contact time and concentration on naphthalene removal

In order to establish the time needed to reach equilibrium and to find the kinetic properties, the adsorption of naphthalene on FAC was studied as a function of contact time. The results are shown in Figure 7-1.

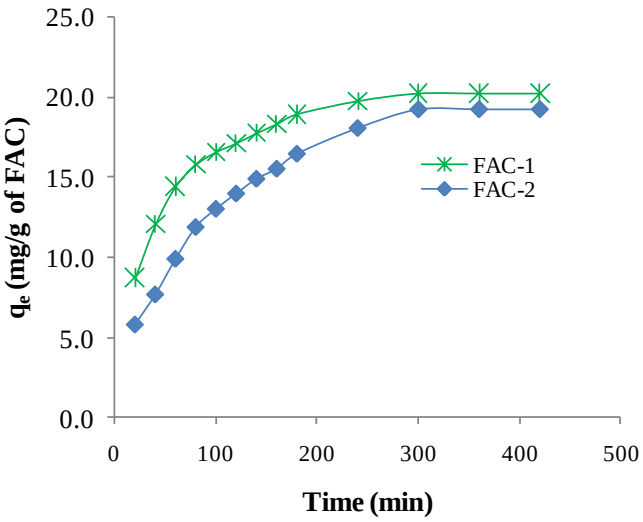

Figure 7-1 Effect of contact time on naphthalene removal (Co = 50 mg/L, adsorbent dosage = 0.1 g/50 ml, pH = 6.5 at room temperature T = 22±1^{o}C)

Table 7-2 Pseudo-first- and second-order constants for naphthalene removal

FAC	qe, experimental (mg/g)	Pseudo-first-order model			Pseudo-second-order model		
		k_1 (per minutes)	q_e	R^2	k_2 (g/mg. minutes)	q_e	R^2
FAC-1	20.221	0.013	14.498	0.987	0.0014	22.222	0.999
FAC-2	19.220	0.011	17.921	0.986	0.0006	23.256	0.996

Based on the kinetics study (Figure 7-1), the required time for equilibrium adsorption was selected as 300 minutes. This equilibration time was used for all other experiments. The study shows that the rate of naphthalene uptake is high at the beginning: about 50% of the adsorption was completed within the first 2 hr.

Pseudo-first- and pseudo-second-order models were used to analyze the kinetics of naphthalene adsorption on the FAC. The linear form of pseudo-first-order equation is generally expressed (Lagergren, 1898) as:

$$\ln(q_t - q_e) = \ln(q_e) - K_1 t \quad (7\text{-}4)$$

where, q_e and q_t (mg/g) are the amounts of naphthalene adsorbed at equilibrium, respectively at time t (minutes), and K_1 (L/ minutes) is the adsorption rate constant. The values of ln (q_e − q_t) were linearly correlated with *t.* The plot of ln(*q*e − *qt*) vs. *t* (Figure 7-2) provided a linear relationship. The factors k_1 and *q*e were determined from the slope and intercept of this plot, respectively. The conformity between the experimental data and the model predicted values was expressed by correlation coefficients (R^2). Least-squares regression was used to fit these models to the experimental data. A relatively high R^2 value indicates that the model successfully describes the kinetics of naphthalene adsorption.

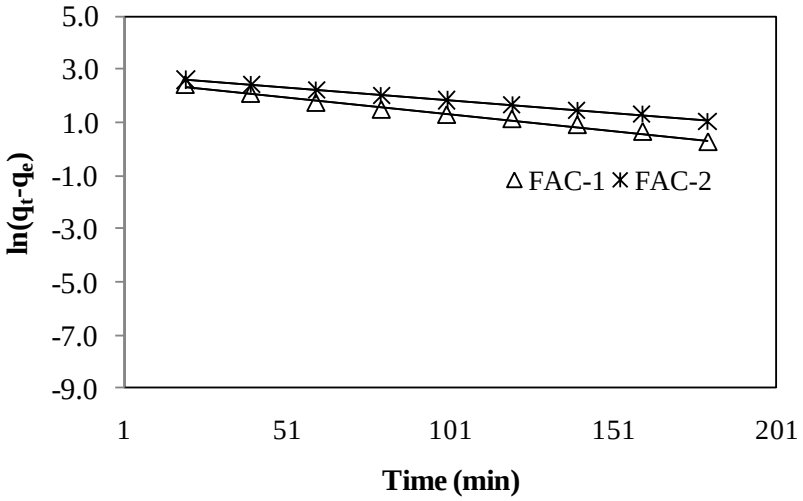

Figure 7-2 Pseudo-first-order kinetics plots for naphthalene adsorption (Co = 50 mg/L, adsorbent dosage = 0.1 g/50 ml, pH = 6.5 at room temperature T = 22±1^{o}C; $\ln(q_t-q_e) = 0.012t + 2.599$ for FAC-1& $\ln(q_t-q_e) = -0.009t + 2.805$

The pseudo-second-order equation is based on the adsorption equilibrium. The linear form of this equation can be expressed as (Ho and Mckay, 1999):

$$\frac{t}{q_t} = \frac{1}{K_2 q_e^{\,2}} + \frac{t}{q_e} \qquad (7\text{-}5)$$

where, K_2 (g/mg. minutes) is the rate constant of the second-order equation. The plot of (t/qt) vs. t (Figure 7-3) given a linear relationship. The factors q_e and k_2 were determined from the slope and intercept of this linear plot, respectively.

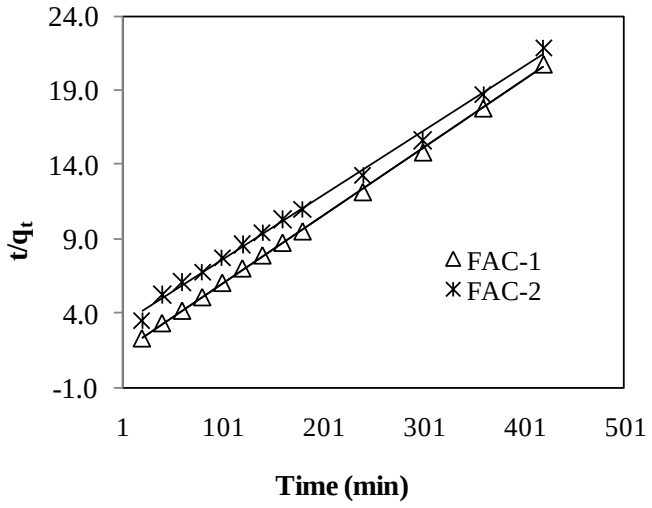

Figure 7-3 Pseudo-second-order kinetics plots for the removal of naphthalene (Co = 50 mg/L, adsorbent dosage = 0.1 g/50 ml, pH = 6.5 at room temperature T = 22±1^{o}C; (t/q_t = 0.045t + 1.433 for FAC-1& t/q_t = 0.043t + 3.217 for FAC-2)

The different factors obtained from the pseudo models are reported in Table 7-2. It can be observed (Table 7-2) that regression correlation coefficient R^2 is smaller for the pseudo-first-order equation compared to pseudo-second order equation. These results indicate that the adsorption of naphthalene on FAC better follows pseudo-second-order model.

When compared with other non-conventional adsorbents (Table 7-3), the results of the present study indicates that FAC has a promising adsorption capacity compared to other AC prepared from different raw materials.

Table 7-3 Summary of naphthalene adsorption capacity of various adsorbents

Raw Material	**Maximum adsorption capacity (mg/g)**	**References**
Biomass-derived carbons	300.000	Belen et al., 2009
Biomass-derived carbons	85.000	Belen et al., 2009
Flamboyant pod	294.118	Alade et al., 2012
Milk bush kernel shell	21.692	Alade et al., 2012
HOFA	20.221	This study
Activated carbon	200.200	Alina et al., 2011
Charcoal	1.700	Tryba et al., 2003

7.2.5 Analysis of naphthalene adsorption isotherms

The effects of the equilibrium concentration on adsorption are presented in Figure 7-4. The initial concentration varied from 25 mg/L to 120 mg/L at a pH of 6.5. The isotherms showed an upward trend when the equilibrium concentration was increased. The adsorption of naphthalene on FAC follows the Freundlich model, with correlation coefficients greater than 0.97 (Table 7-4). The values of n did not change significantly for FAC-1 and FAC-2. It is obvious that this model represents a good fit with the highest R^2. In the case of Langmuir models, the parameter (Δ) was found to be less than 1 and greater than 0 in all cases, which proved a favourable adsorption process.

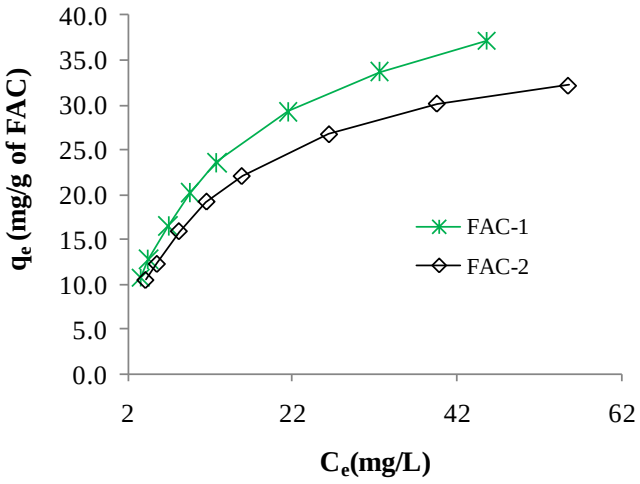

Figure 7-4 Adsorption of naphthalene onto FAC

Table 7-4 Isotherm constants and correlation coefficients for naphthalene adsorption

Models	**Parameters**	**FAC-1**	**FAC-2**
Freundlich coefficients	1/n	0.485	0.437
	kf	2.226	2.192
	R^2	0.980	0.972
Langmuir-1	α (L/mg)	0.081	0.083
	β (mg/g)	47.619	40.000
	R^2	0.999	0.999
Langmuir-2	α (L/mg)	0.083	0.087
	β (mg/g)	46.434	38.563
	R^2	0.995	0.994
Langmuir-3	α (L/mg)	0.087	0.089
	β (mg/g)	45.455	38.462
	R^2	0.999	0.997

The pH of the naphthalene solution can influence the adsorption progress by changing the solubility of the adsorbate (Ania et al., 2007). To evaluate the effects of pH, batch experiments were carried out by varying the pH of the solution. The results show that pH has

no remarkable effect on naphthalene adsorption, except for minor variations over a range of pH 3 to pH 11 (Figure 7-5).

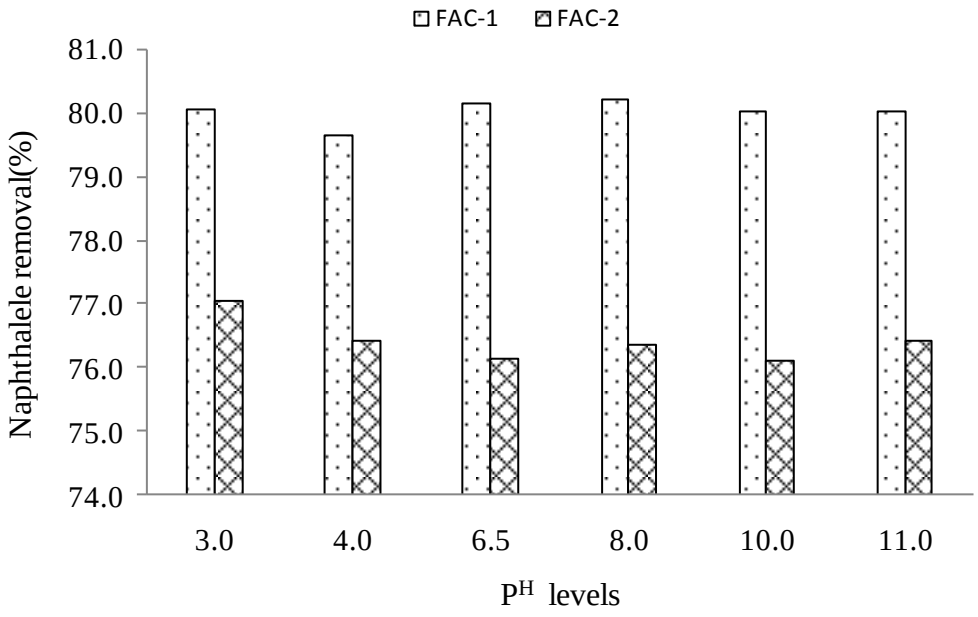

Figure 7-5 pH effects on naphthalene removal
(C_o = 50 mg/L, adsorbent dosage = 0.2 g/50 ml, at room temperature T = 22±1^oC)

7.2.6 Regeneration of FAC saturated by naphthalene

The spent FAC saturated by naphthalene was taken out and immersed in absolute ethanol for 90 minutes at a dosage of 1.3 g/L as suggested by Qianqian et al. (2012). After filtration, FAC was washed twice by distilled water and dried at 105ºC for 12 hr. Subsequently, the naphthalene adsorption experiment was carried out as described in Section 7.2.2. The regeneration of FAC was repeated twice. At equilibrium, the amount of naphthalene adsorbed on the regenerated FAC was estimated. Results show that after regeneration the adsorption efficiency of FAC was reduced. According to the experimental conditions, naphthalene adsorption was reduced about 15.0% and 20.0%, respectively, for first- and second-cycle regeneration (Figure 7-6).

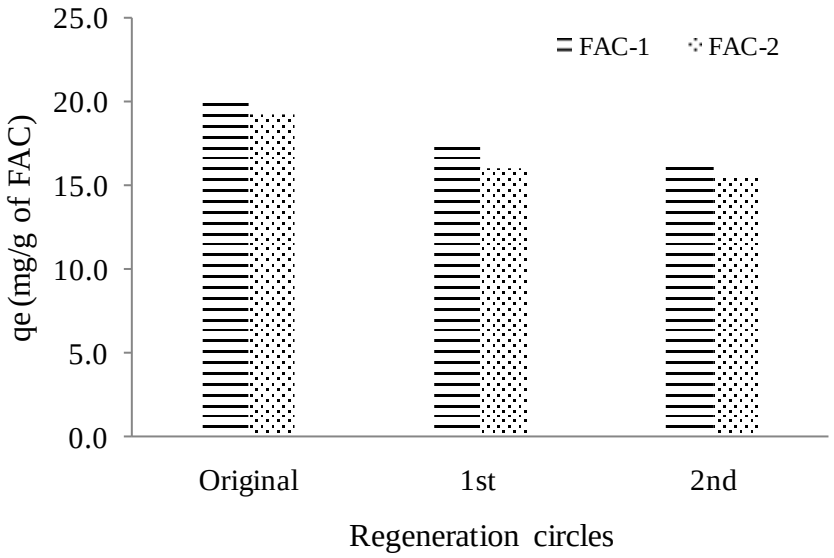

Figure 7-6 Regeneration effects on naphthalene removal (C_o = 50 mg/L, adsorbent dosage = 0.1 g/50 ml, pH = 6.5 at room temperature T = 22±1^oC)

7.3 Adsorption of heavy metals onto FAC

The objective of this study is to investigate the use of FAC as an adsorbent for removing Cr (VI) ions from aqueous solutions. For this experiment a response surface methodology (RSM) was used to determine the optimal Cr (VI) adsorption on FAC. The effects of various parameters such as FAC dose, initial Cr (VI) concentration, and pH of the solution were studied.

A well-known tool, RSM is used to identify the response of a process as a function of independent variables (Montgomery, 1997). This methodology is particularly applicable in situations where several input variables potentially influence the performance of the process.

7.3.1 Design of Cr (VI) adsorption experiments

A three-level factorial design was established using Design Expert software (8.0 trial version) following the Box-Behnken methodology (Montgomery, 1997). Three independent

variables were designated: A (dose of FAC, g), B (initial Cr (VI) concentration, mg/L), and C (pH). Low, middle, and high levels of each variable are designated as -1, 0, + 1. The range and levels used in the experiment are listed in Table 7-5.

Table 7-5 Experimental factor levels used in the metal adsorption tests

Variables	**Factor**	**Coded levels**		
		+	0	-
FAC dose (g)	A	2	1	0.5
Initial Cr (VI) concentration (mg/L)	B	150	100	25
pH	C	9	5.5	2

In order to understand the process, some preliminary experiments were conducted to determine the contact time and other conditions used in this investigation. The Box-Behnken method was selected for this experiment as it requires relatively few combinations of the variables to estimate the response function. A total of 17 experiments were found to be sufficient for calculating the coefficients of the second-order polynomial regression model. Employing RSM, the second-order polynomial equation that fits the experimental data can be written as:

$$Y = \lambda_0 + \sum \lambda_i x_i + \sum \lambda_{ii} x_{ii}^2 + \sum \lambda_{ij} x_i x_j + \varepsilon \qquad (7\text{-}6)$$

where, Y is the predicted response, i.e., percent of Cr (VI) adsorption by the FAC, λ_0 is the constant coefficient, λ_i is the 1st linear coefficient of the input factor x_i, λ_{ii} is the ith quadratic coefficient of the input factor x_i, λ_{ij} is the interaction coefficients between the input factors x_i and x_j, and ε is the error of the model.

7.3.2 Adsorbents used in Cr (VI) adsorption

For this experiment AC-4 (see Chapter 6 of this thesis) was used as the representative adsorbent to evaluate the effects of Cr (VI) adsorption. The properties of AC-4 were also reported in Chapter 6.

7.3.3 Cr (VI) adsorption experiments

A series batch experiment was carried out in 250 ml conical Erlenmeyer flasks by agitating a pre-weighed amount (0.5-2.0 g) of FAC with 50 ml of an aqueous solution containing Cr (VI) concentrations ranging from 25 mg/L to 150 mg/L at a pH range of 2-9. A predetermined contact time of 120 minutes was selected based on kinetic studies. All flasks were maintained at room temperature (22±1°C) and a continuous shaking of 100 rpm was provided by a Fisher stirrer model 11-500-7SH. A chromium (VI) stock solution (500 mg/L) was prepared by dissolving 1.4144 g of 99.9% potassium dichromate ($K_2Cr_2O_7$) in 1 L of distilled water. This solution was diluted as required to obtain 25-150 mg/L Cr (VI) standard solutions. The pH of the Cr (VI) standard solutions was adjusted by using 0.5 N NaOH or 0.5 N HCl solutions. All chemicals used for this study were analytical grade. After the required contact time, the solutions were filtered on Whatman No. 42 filter paper, and the residual concentrations of Cr (VI) in the filtrate solution were determined.

A UV-visible spectrophotometer (Hewlett-Packard Model 8453) was used following the standard Gilcreas et al. (1965) method to determine Cr (VI) concentrations in the filtrate solution. The absorbance of the purple-violet-coloured solution was recorded at a wavelength of 540 nm. In order to eliminate error due to the adsorption of Cr (VI) on the filter paper, a parallel control set of experiments (without FAC) was run in an identical manner. The

amount of Cr (VI) adsorbed in mg/g at contact time *t* was calculated by Equation 7-1 and the percentage removal of Cr (VI) (R_{cr}) from the solution was calculated by Equation 7-2.

To study the effect of temperature and contact time, a series of batch experiments were conducted in a 250 ml conical Erlenmeyer flask with 50 ml of the aqueous solution containing 150 mg/L Cr (VI) concentration at pH 2. One gram of FAC was added at room temperature (22±1ºC) to each flask and allowed to agitate by the magnetic stirrer on Fisher stirrer model 11-500-7SH at a rate of 100 rpm. At a given time interval, the solutions were filtered and analyzed by a UV-visible spectrophotometer for Cr (VI) concentrations. Similar experiments were conducted at four different temperatures (25, 30, 40, and 50ºC) to investigate the effect of temperature.

7.3.4 Analysis of Cr (VI) adsorption isotherms

Adsorption models like those of Freundlich and Langmuir-1 (Table 7-1) were used to explain the process of Cr (VI) a**d**sorption on FAC.

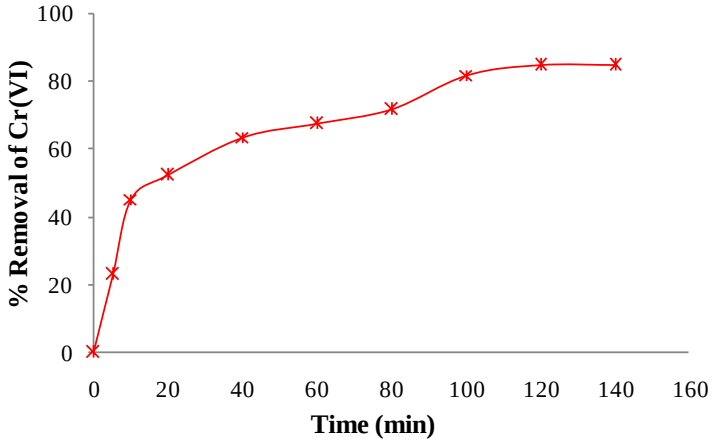

Figure 7-7 Effect of contact time on Cr (VI) adsorption

(At initial concentration 150 mg/L, pH 2, and 1 g of FAC at room temperature)

The contact time was found to be an important parameter for Cr (VI) adsorption on FAC. At the initial stage of the experiment, the rate of Cr (VI) adsorption was very high: about 68.00% of the adsorption occurred within the first hour of the experiment. However, some Cr (VI) adsorption (slow rate) was observed until 120 minutes, and reached up to 84.83% (Figure 7-7). A further increase in the contact time had a negligible effect on Cr (VI) adsorption. Therefore, a contact time of 120 minutes was selected as the equilibrium contact time for all other batch studies. The temperature effects on the Cr (VI) adsorption onto FAC were also studied by varying the temperature from 20 to 50ºC. In this case, 1 g FAC was dissolved in 50 ml of aqueous solution containing 150 mg/L Cr (VI) at a pH of 2. After 120 minutes contact time the results showed that temperature has a negligible effect on Cr (VI) adsorption. Therefore, room temperature was selected for all batch experiments.

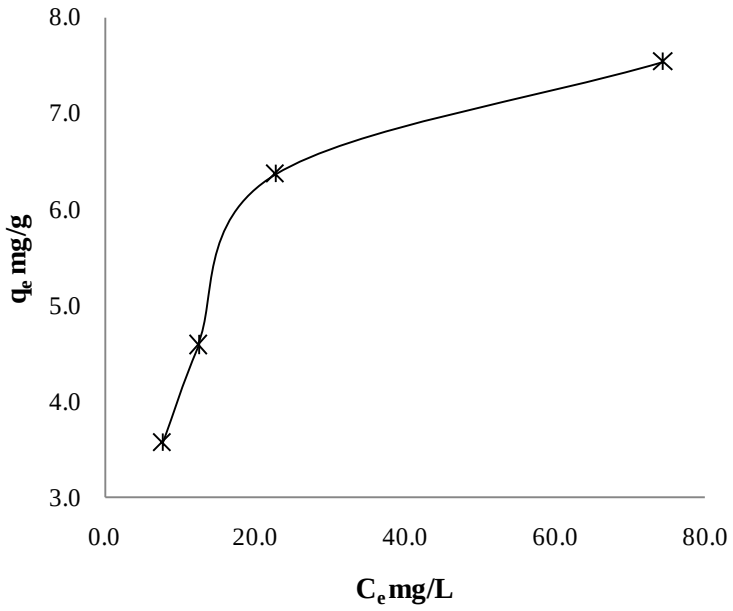

Figure 7-8 Adsorption isotherms for Cr (VI) removal (FAC equal to 0.5, 1.0, 1.50, 2.0 g/50 ml), initial concentration (150 mg/L), pH 2 and a contact time of 120 minutes

7.3.5 Cr (VI) adsorption modeling

The adsorption isotherm was used to determine the equilibrium between the concentration of Cr (VI) in the aqueous solution (*C*e) and the amount of Cr (VI) adsorbed on FAC (e.g., *q*e, mass of Cr (VI) per unit mass of FAC). This isotherm (Figure 7-8) was developed by varying the dose of FAC from 0.5 g to 2.0 g and maintaining the initial concentration of Cr (VI) at 150 mg/L at a pH of 2.0. Figure 7-8 shows that the adsorption capacity (mg/g) increased rapidly from 3.55 mg/g to 4.58 mg/g within equilibrium Cr (VI) concentrations of 7.66 mg/L to 12.50 mg/L; after that, the adsorption capacity eventually attained a constant value. In order to model the adsorption behaviour of Cr (VI) on FAC, Langmuir and Freundlich isotherm models were used. The isotherm data was linearized using the Langmuir equation shown in Figure 7-9.

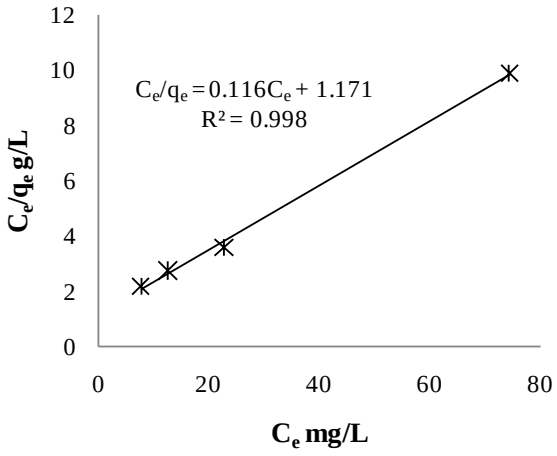

Figure 7-9 Langmuir isotherms for adsorption of Cr (VI) by FAC (0.5, 1.0, 1.50, 2.0 g/50 ml) at initial concentration 150 mg/L, pH 2 and contact time 120 minutes

The regression constants for the Langmuir model are tabulated in Table 7-6. A high correlation coefficient (R^2 = 0.998) indicated a good agreement between parameters. The

constant β, which is a measure of the adsorption capacity of a monolayer, was 9.091 mg/g. The constant *α*, which denotes adsorption energy, was determined to be equal to 0.094 L/mg.

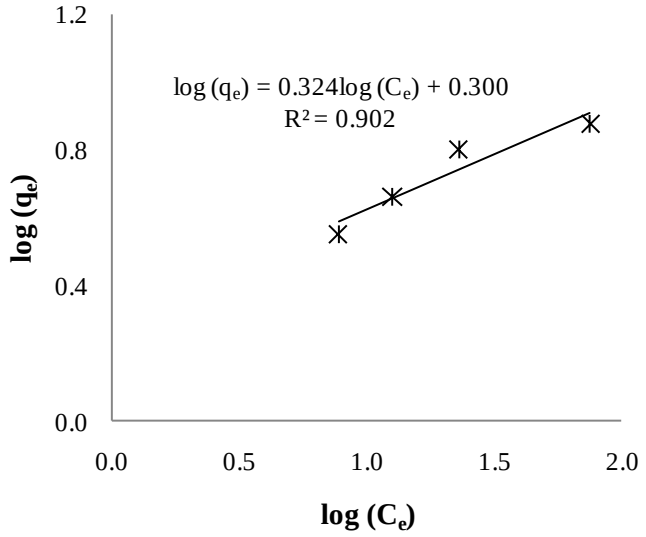

Figure 7-10 Freundlich isotherms for adsorption of Cr (VI) by FAC (0.5, 1.0, 1.50, 2.0 g/50 ml) at initial concentration 150 mg/L, pH 2 and contact time 120 minutes.

The adsorption data was also fit the Freundlich equation shown in Figure 7-10. The Freundlich regression constants are listed in Table 7-6. The correlation coefficient (R^2 = 0.902) indicated that the data conform well to the Freundlich equation. A Freundlich constant *1/n* < 1 indicated that favourable adsorption occurred during the batch experiments.

Table 7-6 Isotherm constants for adsorption of chromium (VI) on FAC

Langmuir Isotherm	**α**	**β**	**R^2**
	0.094	9.091	0.998
Freundlich Isotherm	KF	1/n	R^2
	1.995	0.324	0.902

When compared with other non-conventional adsorbents (Table 7-7), the present study's result indicate that FAC has a better Cr (VI) adsorption capacity than biomass residual slurry, Fe (III)/Cr (III) hydroxide, and walnut shells (Table 7-7).

Table 7-7 Summary of Cr (VI) adsorption capacity of various adsorbents

Adsorbents	**Maximum adsorption capacity (mg/g)**	**Reference**
Saw dust	15.823	Dakiky et al., 2002
Almond shells	10.616	Dakiky et al., 2002
Olive cake	33.44	Dakiky et al., 2002
Pine needles	21.50	Dakiky et al., 2002
Fly ash impregnated with iron	1.700	Banarjee et al., 2004
Fly ash impregnated with aluminium	1.800	Banarjee et al., 2004
Fly ash	1.400	Banarjee et al., 2004
Palm pressed-fibers	15.000	Tan et al., 1993
Maize cob	13.800	Sharma and Forster, 1994
Sugar cane bagasse	13.400	Sharma and Forster, 1994
Sugarbeet pulp	17.200	Sharma and Forster, 1994
Activated charcoal	12.870	Mor et al., 2007
FAC prepared from HOFA	9.092	Present study
Activated alumina	7.440	Mor et al., 2007
Activated carbon from coconut fibers	15.990	Mohan et al., 2005
Brown coal	50.950	Gode and Pehlivan, 2006
Activated Carbon (Filtrasorb-400)	57.70	Huang and Wu, 1997

7.3.6 RSM analysis of Cr (VI) adsorption

The Box-Behnken design of the experiments carried out in this study is presented in Table 7-8. Regression analysis was performed to fit the response functions, i.e., percentage adsorption of Cr (VI) by FAC. The empirical relationship (with coded values) between the response and input variables such as FAC dose (A), initial concentration of Cr (VI) (B), and

pH (C) are presented by the quadratic model shown in Equation 7-7. The insignificant terms were not considered in this model development.

$$\% R_{Cr(VI)} = +55.51+51.30 * A^{-0.069} * B^{-12.203} * C +0.045 * A * B+0.377 * A * C+0.018 B * C-13.800 *A^2+3.32E-4 * B^2+0.500 * C^2 \quad (7\text{-}7)$$

Table 7-8 Adsorption experiments scheme

Standard order	**Run**	**FAC dose (g)**	**Initial concentration (mg/L)**	**pH**	**% removed (experiment)**	**% removed (predicted)**
1	15	0.5	25	5.5	28.35	28.39
2	9	2	25	5.5	58.59	58.41
3	8	0.5	150	5.5	42.46	42.75
4	1	2	150	5.5	81.48	81.33
5	14	0.5	100	2	59.08	58.07
6	12	2	100	2	91.51	91.25
7	11	0.5	100	9	25.02	25.70
8	10	2	100	9	62.26	62.84
9	2	1	25	2	71.32	71.90
10	6	1	150	2	80.16	80.85
11	7	1	25	9	31.38	30.94
12	4	1	150	9	57.25	56.42
13	13	1	100	5.5	50.24	54.38
14	3	1	100	5.5	55.24	54.38
15	5	1	100	5.5	53.74	54.38
16	17	1	100	5.5	54.88	54.38
17	16	1	100	5.5	57.78	54.38

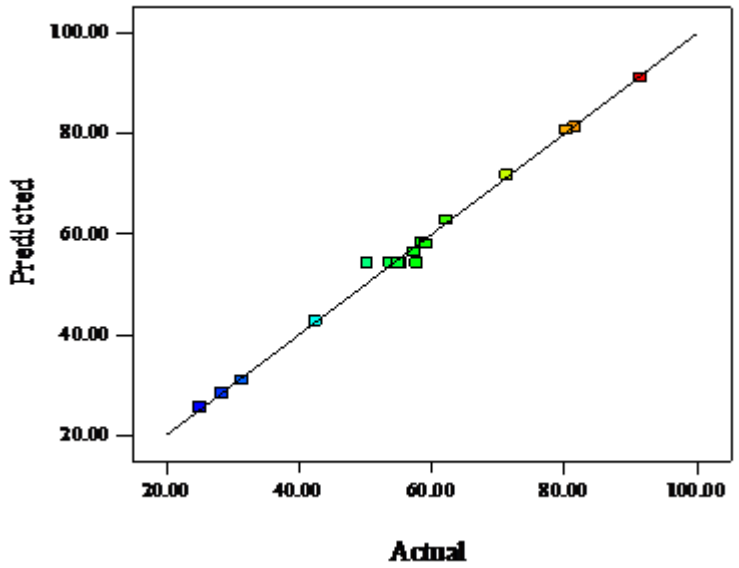

Figure 7-11 Actual and predicted values of % removal of Cr (VI)

The significance of the model terms included in the regression analysis (Equation 7-7) was evaluated by the F-test. Analysis of variance (ANOVA) for the responses (% removal Cr (VI)) is shown in Table 7-9.

Prob > F value less than 0.05 and F-value of 122.01, respectively, indicated that the model terms and the model are statistically significant. In this case A, B, C, BC, A^2, and C^2 are significant model terms. A lack of fit F-value of 0.17 implies that the lack of fit is not significant relative to pure error. A non-significant lack of fit is good and represents the model's robustness. The actual and predicted values of Cr (VI) adsorption are shown in Figure 7-11. Actual values were measured for a particular experiment, whereas predicted values were generated by using an approximating function (e.g., Equation 7-7). The values of pred R^2 of 0.9802 is in reasonable agreement with the Adj R^2 of 0.9855, which advocates a high correlation between actual and predicted values.

The perturbation plot (Figure 7-12) was developed to analyze the individual effect of a factor in coded form such as FAC dose (A), initial Cr (VI) concentration (B), and pH (C). This plot helps to compare the effects at a particular point in the design space. In a perturbation plot, a downward curvature of factor C indicates that the responses increased with decreased pH values. Similarly, responses increased with an increased FAC dose and initial concentration.

In order to determine the optimum values of each independent variable, 3D response surface plots (Figure 7-13) were developed. These plots help in understanding both the main and interaction effects of the factors involved. The contour plots projecting the response surfaces in the x–y plane (bottom of 3D surface diagram), provided the effects of different variables on Cr (VI) adsorption.

Table 7-9 Analysis of variance (ANOVA) for response surface analysis

Source	**Sum of squares**	**DF**	**Mean square**	**F value**	**Prob > F**
Model	5304.24	9	589.36	122.01	< 0.0001significant
A-Dose	2310.60	1	2310.60	478.36	< 0.0001
B-initial concentration	660.88	1	660.88	136.82	< 0.0001
C- pH	1910.44	1	1910.44	395.52	< 0.0001
AB	19.69	1	19.69	4.08	0.0832
AC	4.13	1	4.13	0.86	0.3858
BC	69.59	1	69.59	14.41	0.0068
A^2	189.40	1	189.40	39.21	0.0004
B^2	6.39	1	6.39	1.32	0.2878
C^2	157.97	1	157.97	32.70	0.0007
Residual	33.81	7	4.83		
Lack of Fit	3.74	3	1.25	0.17	0.9143 not significant
Pure Error	30.08	4	7.52		
R-Squared	0.9937				
Adj R-Squared	0.9855				
Pred R-Squared	0.9802				
Adeq Precision	38.883				

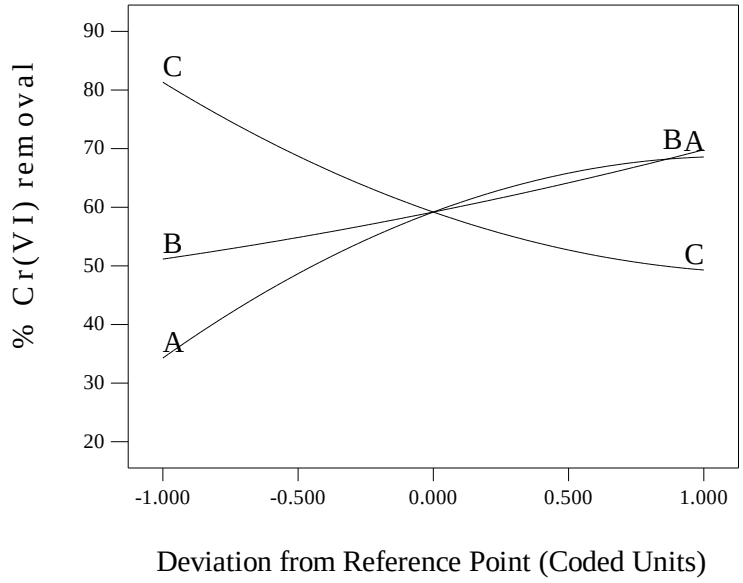

Figure 7-12 Perturbation plots for Cr (VI) removal by FAC

The maximum predicted values are indicated by the smallest ellipse in the contour diagram. A perfect interaction between independent variables formed an elliptical contour shape (Montgomery, 1997). Figure 7-13a shows that initial concentration and FAC dose have a positive effect on Cr (VI) removal. At a maximum set condition, the FAC dose has more influence than the initial concentration. Significant interaction effects were observed for pH and FAC dose. Figure 7-13b shows that the highest removal happened at a maximum FAC dose with a minimum pH. Similarly, the highest Cr (VI) adsorption was observed at a maximum initial concentration with a minimum pH (Figure 7-13c).

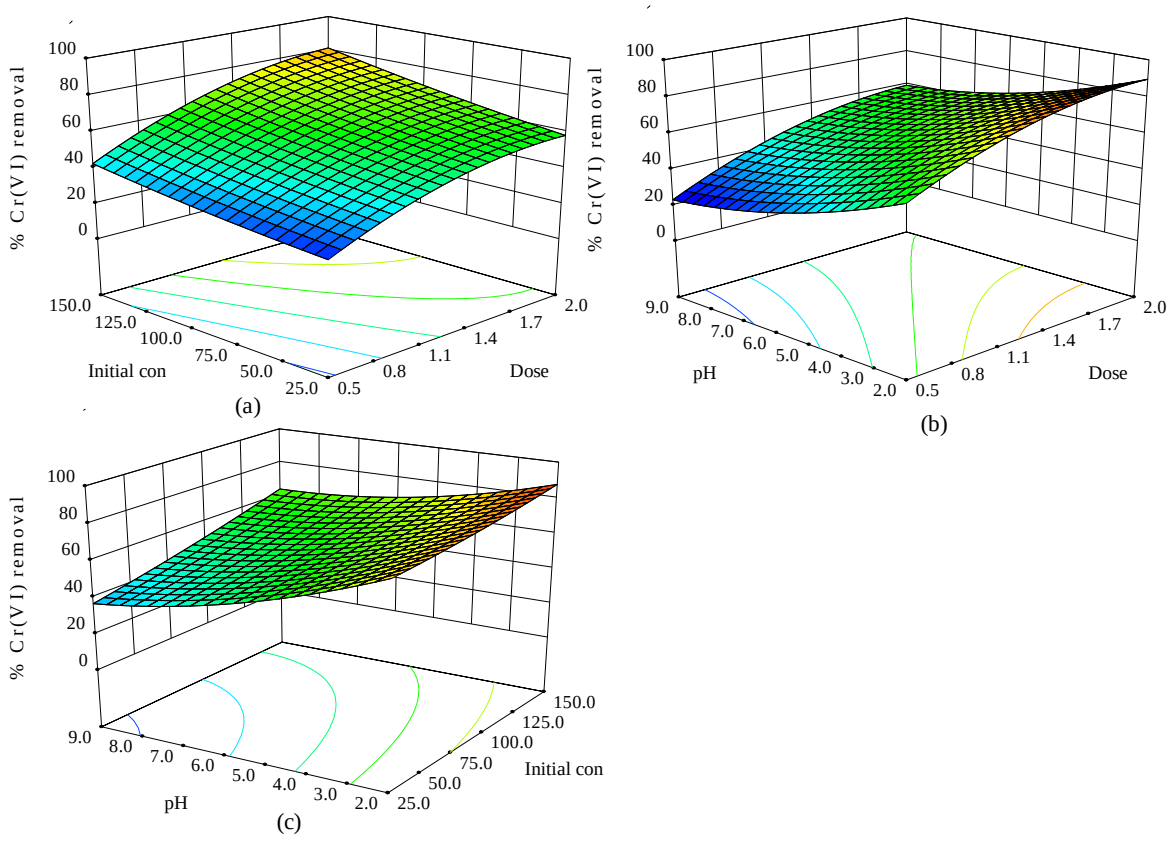

Figure 7-13 Effect of Cr (VI) removal by FAC (a) initial concentration and FAC dose (b) pH and FAC dose (c) initial concentration and pH

By analyzing the 3D response surface plots, it is easy to evaluate the optimum values of the variables. In this case the optimal Cr (VI) adsorption was predicted to be 91.25% at pH 2 with an initial concentration of 100 mg/L.

7.4 Adsorption of Methylene Blue by FAC

To conduct a methylene blue (MB) adsorption experiment, two types of adsorbent, FAC-P03 and HOFA-01, were used. Adsorbent FAC-P03 was prepared by physical activation (Chapter 6) and HOFA-01 as clean unburned carbon generated from the washing process (Chapter 6). The aim of this experiment was to evaluate the MB adsorption capacity of clean HOFA (i.e.,

HOFA-01) and FAC generated from HOFA (i.e., FAC-P03). The characteristics analysis of FAC-P03 and HOFA-01 were reported in Chapter 6 of this thesis.

7.4.1 Preparation of MB stock solution

A stock solution of 1000 mg/L was prepared by dissolving the required quantity (i.e., 1.0 g) of MB powder in 1000 ml distilled water (methylene blue, $C_{16}H_{18}N_3SCl.3H_2O$; molecular weight 373.9 g/mol). The initial pH of the stock solution was 9.5. The experimental solution was prepared by diluting the stock solution with distilled water as necessary.

7.4.2 Experiments for MB adsorption

Batch experiments were conducted to investigate the effects of FAC dose, initial MB concentration, and pH. The experiments were performed in a series of Erlenmeyer flasks of 250 ml capacity, where 50 ml of MB solutions with known initial concentrations (i.e., 20, 40, 50, 60, 80, and 100 mg/L) were agitated at a constant 120 rpm by 0.1-0.3 g of FAC at different temperatures and pH levels. The original pH of the dye solution was adjusted to the desired value by adding quantities of 0.5 N NaOH or 0.5 N HCl solutions. An equilibrium contact time was selected based on the series of batch experiments. In this case, 50 ml of an MB solution of known concentration (i.e., 20, 40, 50, 60, 80, and 100 mg/L) was kept in 250 ml Erlenmeyer flasks. At room temperature (21ºC±1), 0.2 grams of FAC was added to each flask and agitated by magnetic bars at a rate of 120 rpm on a Fisher stirrer model 11-500-7SH. At given time intervals, the solution was filtered on Whatman No. 42 filter paper. The residual dye concentration in each solution was measured by a UV-visible spectrometer (Hewlett-Packard Model 8453) at a wavelength of 665 nm. In order to eliminate errors due to the adsorption of MB on filter paper, a parallel control set (without fly ash) experiment was run in an identical manner. Individual experiments were conducted to evaluate the effects of

temperature and pH. Equations 7-1 and 7-2 were used to calculate the adsorption of MB (mg/g) and the removal efficiency, respectively.

7.4.3 Effect of contact time on MB removal

To determine the equilibrium time, the adsorption experiments were carried out at different time intervals (e.g., 10-140 minutes); the results are plotted in Figure 7-14. The effect of contact time was studied at a pH of 8.5. This test revealed that MB uptake was rapid in the initial stage of the experiment (e.g., 10-30 minutes) but slowed near the equilibrium. The reason for the higher adsorption rate initially is probably due to the large number of surface sites available for adsorption. Both adsorption isotherms (i.e., HOFA-01 and FAC-P03) followed the same pattern. However, the higher surface area of FAC-P03 adsorbed more MB than HOFA-01. Based on the isotherm study, the equilibrium time for MB adsorption was selected as 120 minutes; this time was used for all other experiments.

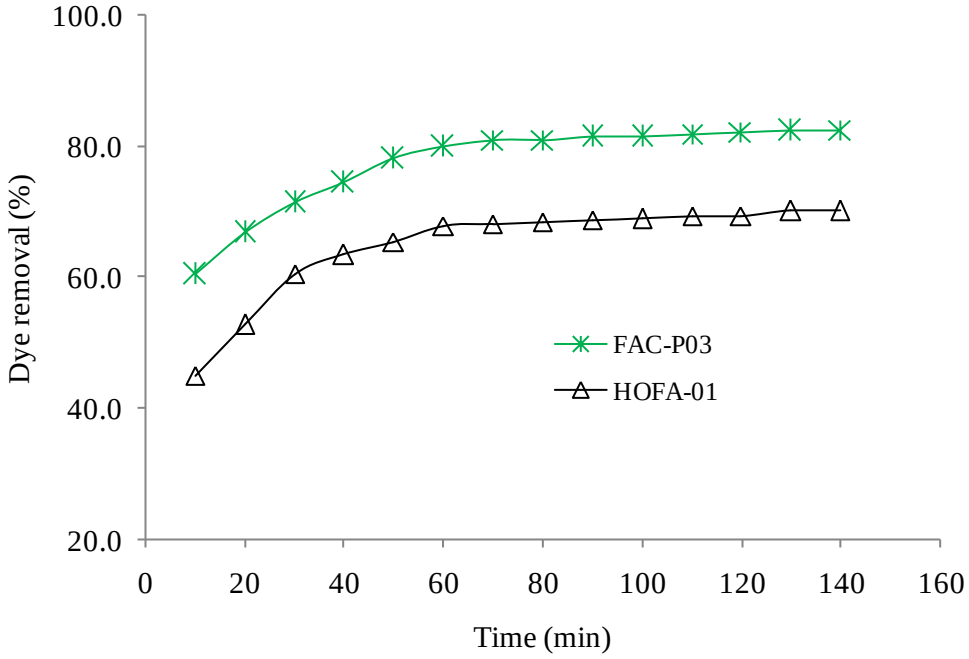

Figure 7-14 Effect of contact time on the removal of MB

(Amount of adsorbent 0.2 g/50 ml of MB solution and concentration 150 mg/L)

7.4.4 Effect of pH on MB adsorption

The effect of pH on MB adsorption was analyzed by 0.2 g/50 ml of MB solution with a concentration of 150 mg/L and a contact time of 120 minutes. When the initial pH of the dye solution was increased from 4.5 to 11.5, the adsorption increased from 75% to 90% (Figure 7-15). This study revealed that pH has a significant influence on MB adsorption, in this case around 30% more adsorption occurs at pH 10.5 compared to pH 4.5.

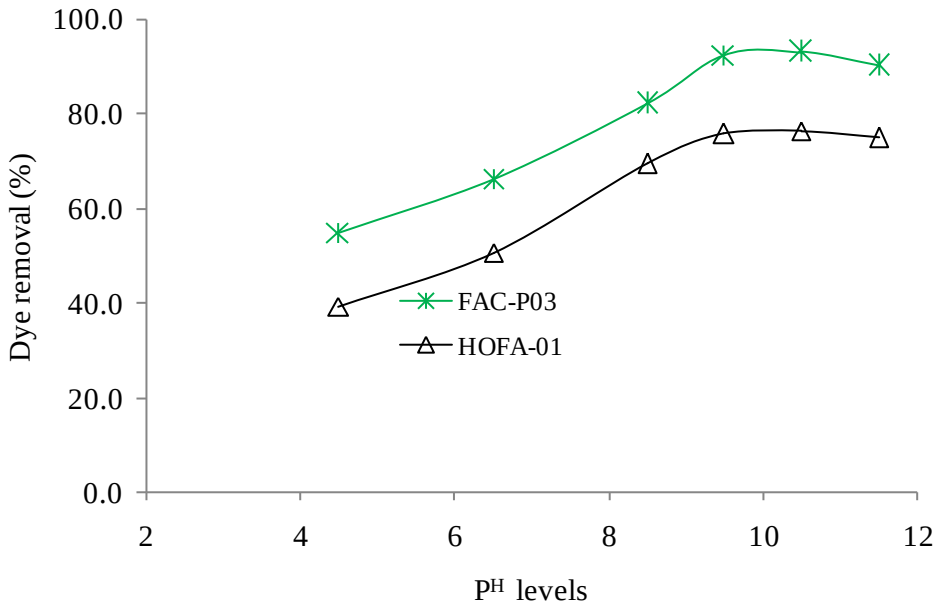

Figure 7-15 Effect of pH on MB removal

(Amount of adsorbent 0.2 g/50 ml of MB solution and contact time 120 minutes)

7.4.5 Effect of temperature on MB removal

The effect of temperature on MB adsorption was studied by varying the temperature during batch experiments. The isotherm at different temperatures (22, 25, 40, and 50°C) is shown in

Figure 7-16. The experiment was conducted on 0.2 g/50 ml of MB solution with a concentration of 150 mg/L at pH 8.5 and a contact time of 120 minutes. The results indicate that the effect of temperature on MB adsorption is negligible (Figure 7-16). For this reason, a room temperature of 22±1°C was used throughout this work.

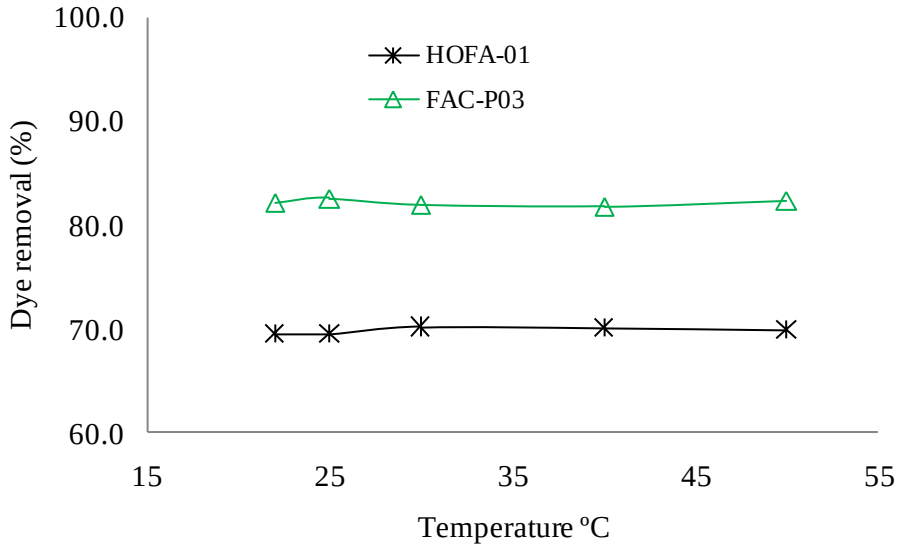

Figure 7-16 Effect of temperature on MB adsorption

(pH 8.5 and contact time 120 minutes)

7.4.6 Effect of FAC dose on MB adsorption

The effect of adsorbent dose on the removal of MB was studied by five different doses: 0.10, 0.15, 0.20, 0.25, and 0.3 g/50 ml. The results proved that the adsorbent dose has a significant influence on MB adsorption (Figure 7-17). The dye adsorbed increased from 77% to 94% as the adsorbent dose was increased from 0.1 g/50 ml to 0.3 g/50 ml. The initial concentration of the MB solution was 150 mg/L and the pH 8.5. At higher doses more surface area is available for adsorption, which may lead to higher adsorption.

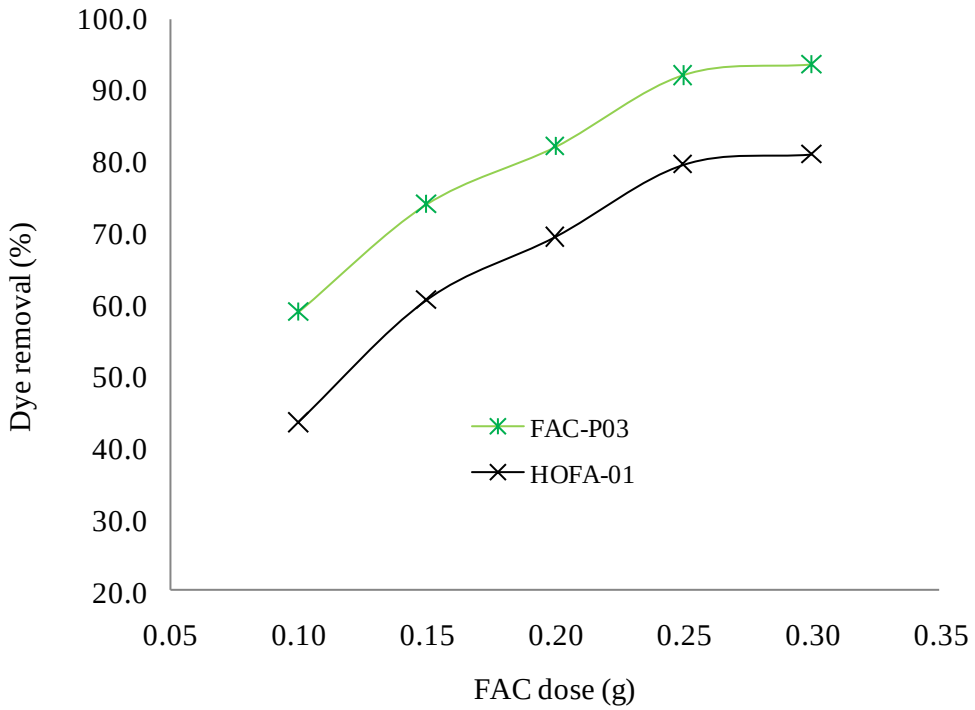

Figure 7-17 Effect of adsorbent dose on MB adsorption

7.4.7 Effect of initial concentration on MB adsorption

The effect of the initial concentration on MB adsorption was evaluated by varying the initial concentrations (i.e., 20, 40, 50, 60, 80, and 100 mg/L). In this case, an adsorbent dose (e.g., 0.2 g) and pH (e.g., 8.5) remained constant. Results show that removal efficiency decreased with an increase in initial concentration (Figure 7-18). For HOFA-01 about 81% and 60% of MB was removed at initial concentrations of 20 mg/L and 100 mg/L, respectively. Similar results were observed for FAC-P03. In this case, about 85% and 71% of MB was removed at initial concentrations of 20 mg/L and 100 mg/L, respectively.

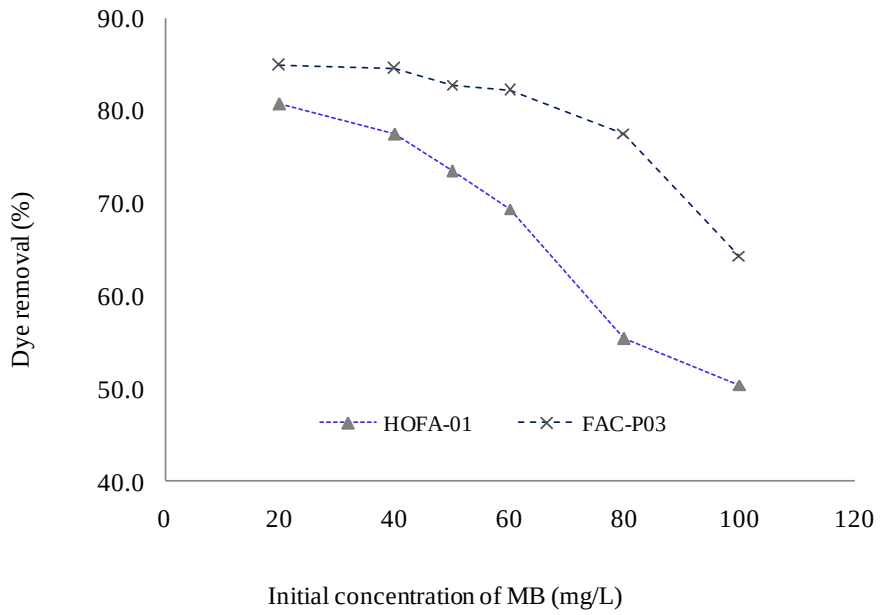

Figure 7-18 Effect of initial concentration on MB adsorption

7.4.8 Analysis of MB adsorption isotherm

Adsorption isotherms were used to determine the equilibrium between the concentration of MB in aqueous solution (*Ce*) and the amount of MB adsorbed on the adsorbent (*qe*) (i.e., mass of MB per unit mass of adsorbent). The adsorption isotherm (Figure 7-19) was developed by varying the initial concentration of MB solution from 20 mg/L to 100 mg/L and maintaining an adsorbent dose of 0.2 g/50 ml at pH 8.5. Figure 7-19 shows that the adsorption capacity (mg/g) increased from 4.25 mg/g to 15.50 mg/g with an increase in MB equilibrium concentration of 3.01 mg/L to 17.97 mg/L (e.g., FAC-P03). With a further increase in equilibrium concentration, the adsorption capacity eventually attained a constant value. Langmuir and Freundlich isotherm models were used to model the adsorption behaviour of MB.

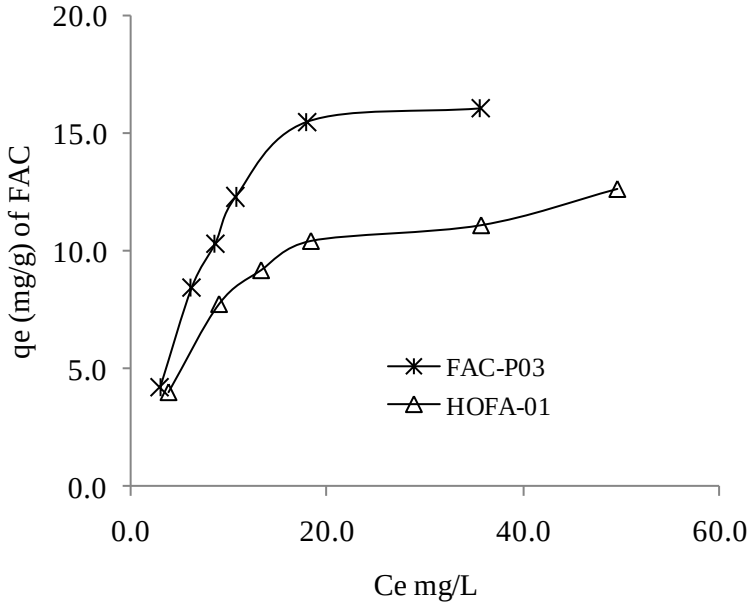

Figure 7-19 Adsorption isotherms for MB adsorption

Table 7-10 Isotherm constants for adsorption of MB on FAC

Langmuir Isotherm		**HOFA-01**	**FAC-P03**
	α	0.117	0.109
	β	14.493	21.277
	R^2	0.991	0.971
Freundlich Isotherm	*K*F	1.557	1.589
	1/n	0.412	0.541
	R^2	0.883	0.874

The isotherm data was linearized using the Langmuir-1 equation shown in Table 7-1. A high correlation coefficient (R^2 = 0.97 to 0.99) indicated a good agreement between the parameters (Figure 7-20). The constant β, which is a measure of the adsorption capacity of a monolayer, was found to be 21.277 mg/g for FAC-P03 and 14.493 mg/g for HOFA-01 at a pH of 8.5. The constant α, which denotes adsorption energy, was determined to be equal to 0.109 and 0.117 L/mg, respectively, for HOFA-01 and FAC-P03. The regression constants of the Langmuir model parameters are tabulated in Table 7-10. The Langmuir model parameter

(Δ) found to be in the range of 0.078-0.314 confirmed that the adsorption process was favourable.

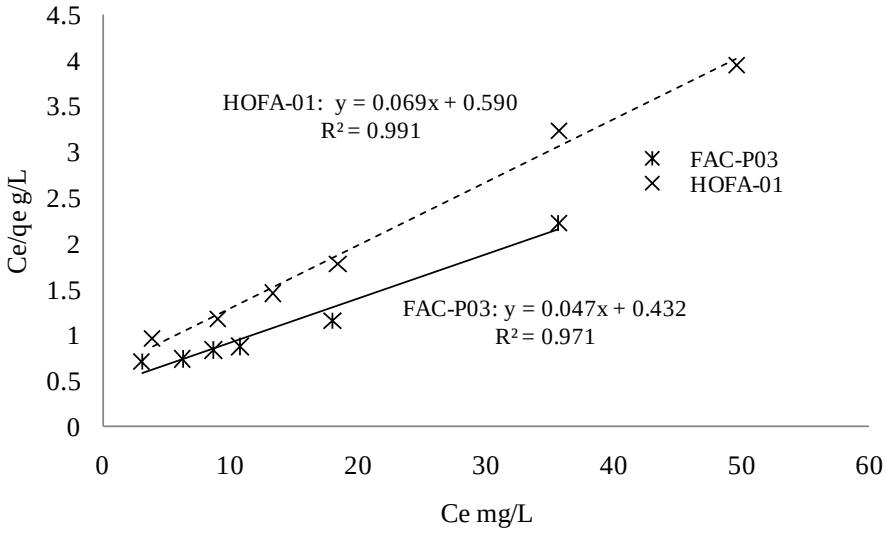

Figure 7-20 Langmuir isotherms for adsorption of MB

(Dose 0.2 g/50 ml, p^H 8.5, and contact time 120 minutes)

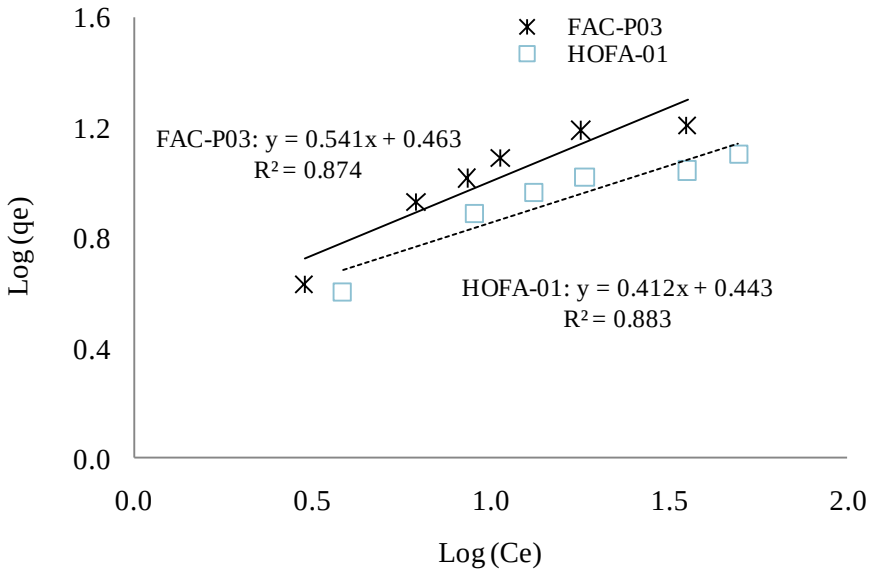

Figure 7-21 Freundlich isotherm for MB adsorption

(Dose 0.2 g/50 ml, pH 8.5, and contact time 120 minutes)

The data also fit the Freundlich equation (Table 7-1) and is represented in Figure 7-21. The Freundlich regression constants are listed in Table 7-10. A high correlation coefficient confirmed that the Freundlich equation fits MB adsorption process. The constant values of *1/n <1* indicated that favourable adsorption occurred during the batch experiments.

When compared with other non-conventional adsorbents (Table 7-11), the present study's results indicate that adsorbent prepared from HOFA has the very good capacity to adsorb MB.

Table 7-11 Summary of MB adsorption capacity of various adsorbents

Adsorbent	**Maximum MB adsorption capacity (mg/g)**	**Reference**
Activated carbon (olive stones)	303	Voudrias et al., 2002
Cotton waste	240	Weber and Chackravorti, 1974
Date pits	80.3	Suteu and Bilba, 2005
Perlite	162.3	Stephenson and Sheldon, 1996
Zeolite	53.1	Stephenson and Sheldon, 1996
FAC-P03	21.277	Present study
HOFA-01	14.493	Present study
Fly ash	53.84	Ozcan et al., 2004
Neem leaf powder	8.76	Bhattacharyya and Sarma, 2004
Wheat shells	16.56	Bulut and Aydin, 2006
Rice husk	40.58	Vadivelan and Kumar, 2005
Teak tree bark powder	333.33	Patil et al., 2011
Bamboo based activated carbon	454.20	Kannan and Sundaram, 2001
Bamboo dust activated carbon	143.20	Kannan and Sundaram, 2001
Coconut shell activated carbon	277.90	Kannan and Sundaram. 2001
Groundnut shell activated carbon	164.90	Kannan and Sundaram, 2001
Rice husk activated carbon	343.50	Kannan and Sundaram, 2001

7.4.9 Regeneration of MB saturated FAC

The FAC saturated by MB was washed with hot water at 100^{o}C for 90 minutes at a dosage of 1.0 g/10 ml water. The washing process was repeated until clean water was observed (e.g., 3

to 4 times repetition). Finally, filtrated FAC was dried at 105ºC for 12 hr. Subsequently, the MB adsorption experiments were carried out. The regeneration of FAC was repeated three times. At equilibrium, the amount of MB adsorbed on regenerated FAC was estimated. Figure 7-22 shows that regeneration processes reduced the adsorption efficiency of FAC. According to experimental conditions, the MB adsorptions were reduced about 10%, 14.5%, and 25.5% respectively for first-, second-, and third-cycle regeneration.

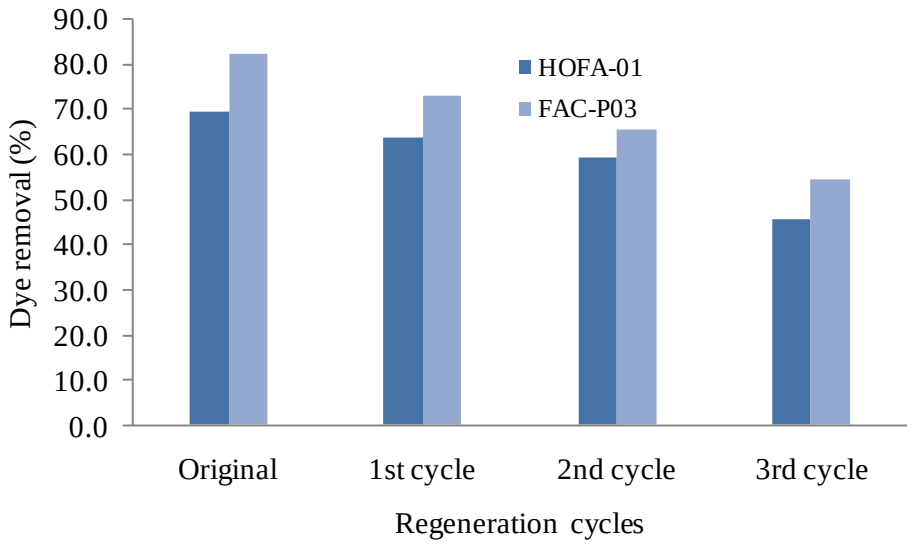

Figure 7-22 Regeneration effects on MB removal

(Co = 50 mg/L, adsorbent dosage = 0.2 g/50 ml, pH = 8.5 at room temperature)

7.5 Summary

In this chapter the adsorption efficiency of produced FAC was investigated. Different batch adsorption experiments confirmed that produced FAC has a notable adsorption capacity, for example, 85% naphthalene, 91.0% Cr (VI), and 82% MB. In conclusion, the present study showed that HOFA can be used effectively as a raw material in the development of AC. The

produced AC can be used to treat wastewater. It is well known that the production costs of AC depend on the cost of raw materials. Since HOFA is very cheap (almost zero cost) at the generation point, the production of AC from HOFA is expected to be inexpensive. Finally, the results of this study advocated that HOFA can be used as an effective and economically feasible raw material for AC, which can be used to treat various wastewater pollutants.

Chapter 8

Conclusions and Recommendations

8.1 Conclusions

During this research HOFA samples were collected directly from an electrostatic precipitator (ESP) at two different power plants: the first HOFA sample (e.g., FA-SA) was collected from a power plant in Saudi Arabia; the second (e.g., FA-NB) was collected from a power plant in New Brunswick. Various management and reuse options of HOFA such as a natural adsorbent, fill/stabilized material for construction use, and a colour ingredient for ornamental concrete were investigated.

A detailed HOFA characteristics study was conducted and reported in Chapter 3. The physical, chemical, and mineralogical properties of two HOFA samples were examined. Standard batch leaching tests were conducted to identify the mobility of potential hazardous elements within HOFA. The results showed that most of the toxic elements in HOFA can easily leach into the environment, which could result in toxicity to ecosystems and humans through the contamination of surface and underground water.

In order to quantify the health risk associated with airborne metals released from an FA dumping site, a probabilistic risk assessment (PRA) study was conducted in Chapter 4. An ISC3 air dispersion model was used to predict the possible risk agent to the nearest receptor point. Inhalation pathways for selected airborne metals were considered in order to estimate the cancer and non-cancer risk at receptor points. The results demonstrated that FA dust released from a landfill could be a potential risk source to the neighbouring population.

Although the calculated 95th percentile values of the cancer and non-cancer risks of selected metals is likely to be within the regulatory acceptable ranges, possible long-term effects of toxic metals are expected from an FA dumping site.

The possible utilization of HOFA as a stabilizer or fill material for various construction activities was examined and reported in Chapter 5. In order to recycle HOFA as fill material, it was mixed with Portland cement at different ratios. Laboratory batch and column experiments were performed for HOFA and fill materials to investigate the leaching behaviour and possible environmental impacts of toxic metals within the HOFA.

The metal Leachate Concentration (LC) from raw HOFA exhibited potential environmental threats; on the other hand, metals leach from the stabilized ash was within permissible limits. The leaching tests confirmed that HOFA mixed with 40% cement is environmentally safe and can be used for construction purposes.

Another possible use of HOFA, as a black pigment in concrete material, was investigated (Chapter 5). The environmental risk that may be posed by concrete made with HOFA was studied by a laboratory batch leaching test (BLT). The results show that the addition of 2% to 5% HOFA with concrete is safe for the environment; as well, this ratio does not pose any significant change in the concrete's compressive strength. Based on a comparative analysis, this study concluded that HOFA can be used as a black pigment in ornamental concrete. However, further experiments on the quality and permanence of concrete colour are recommended.

Based on the characteristics study (Chapter 3), the Saudi Arabian HOFA was selected as a raw material for FAC production and to treat wastewater. FAC was prepared by two activation methods: physical and chemical activation. For physical activation, FAC was

prepared at different temperatures and activation times. On the other hand, KOH, NaOH, and H_3PO_4 were used as chemical agents in the chemical activation process.. All activation was conducted under a N_2 environment. The FAC was characterized according to the BET surface area, porosity, and adsorption capacity of methylene blue and iodine. The production and characteristics study of the produced FAC was conducted and reported in Chapter 6.

The adsorption capacity of FAC generated in this study was investigated for the adsorption of Cr (IV), naphthalene, and MB. The initial concentration of the pollutants in simulated wastewater and the FAC dose, temperature, and pH range of the solutions were investigated in the experimental conditions described in Chapter 7. Kinetic experiments were also carried out and the data from kinetic adsorption onto FAC were modeled using the Lagergren pseudo-first-order/second-order approach (Chapter 7). The relevance of this study is the fact that HOFA can be used as an effective and inexpensive raw material for the removal of selected pollutants from industrial or municipal wastewater. Although the study found that the lower adsorption capacity of FAC compared with that indicated in selected published data, further investigation will improve the adsorption capacity of FAC. There are significant long-term environmental and economic benefits to reusing HOFA, including a clean environment (e.g., reduced environmental pollution), a low adsorbent cost and the possibility of the regeneration of spent FAC should also be considered.

The general conclusions from this research include:

a. Fly ash from heavy fuel oil burning is recyclable and can be used as construction material such as a soil stabilizer or a colour ingredient in ornamental concrete.
b. HOFA can be used as an effective and inexpensive raw material for AC production.

c. Adsorption experiments show that produced AC from HOFA has the potential to remove organic and inorganic pollutants (e.g., dyes, naphthalene, and Cr) from wastewater.

d. FAC regeneration and its reuse in wastewater treatment shows potential..

8.3 Recommendations for future work

In the present work several methods and techniques were applied to develop the reuse and management options of HOFA. However, further work is required in this direction to find feasible HOFA reuse options. The general recommendations for future work can be summarized as:

Recovery of valuable metals

HOFA contains a high percentage of heavy metals, especially vanadium and nickel. The recovery of such valuable metals could be feasible. Procedures should be developed to recover valuable metals and to produce clean unburned carbon from HOFA. In this way, the production cost of FAC would be reduced significantly and minimize the environmental impact due to wastewater generated in the HOFA cleaning process.

Adsorption capability and surface area improvement of FAC

Particle size distribution is an important property of FA; smaller particles produce a greater surface area. This property is also important during the interaction of the ash with various solutions: it affects the mobilization of trace elements on the particle surface. Generally, the particle size ranging from 1 µm to 10 µm provides a high surface area of AC. The particle size of Saudi Arabia fly ash is is large enough to produce AC with a high surface area like commercial AC (e.g., 300-2500 m^2/g). A process should be developed to segregate HOFA

from finer to larger particles. Different types of ESP may be used in a series to collect larger to finer particles from the power plant site.

FAC produced from chemical activation were found to have a better BET surface area compared to those from physical activation. However, the BET surface area of produced FAC (i.e., 4-143 m^2/g) was found to be lower than the commercially available AC (i.e., 300-2500 m^2/g). Methods to improve the BET surface area need to be explored. Different chemicals or combinations of chemicals could be used.

It is recommended that more work be carried out on how to improve the pollutant adsorption capability of FAC. Different physical or chemical treatments of HOFA or FAC may used in this case. In addition, a pilot scale experiment using the operating conditions described in this thesis (Chapter 7) should be conducted with FAC prior to commercial design.

Development of a HOFA management system

To mitigate future environmental challenges linked to HOFA, a Decision Support System (DSS) needs to be developed by integrating environmental, economical, cultural, and social aspects of HOFA management. Multi-criteria decision-making (MCDM) methodology would be capable of integrating various social and environmental parameters. Fuzzy based mathematical modeling may be applied to handle uncertainties associated with the environmental and social criteria.

Development of risk management and mitigation plan

The human health risk assessment methodology presented in this study was developed based on the direct inhalation of FA dust released from a dumping area. The deposition of dust is another factor that may cause nearby soil and water pollution. A detailed risk assessment is recommended and should consider other exposure scenarios such as the ingestion of

contaminated soil and home-grown food and skin contact via contaminated soil. The development of risk management and mitigation plans are also recommended.

Regeneration of spent activated carbon

As contaminants are adsorbed, the carbon's adsorptive capacity is gradually exhausted. When the carbon's adsorptive capacity is reached in saturation, it must be regenerated or discarded. The regeneration of AC usually involves removing the adsorbed contaminants from it without destroying its surface structure. Through this study, two kinds of regeneration techniques were tested. A preliminary investigation on regeneration (Chapter 7) determined that FAC could be regenerated for further use. However, further studies are necessary in order to explore the possible feasible techniques to regenerate spent FAC.

The effective use of HOFA generated in power plants can have environmental and economic benefits. However, reuse methodology may change depending on the chemical composition of the fly ash. Each case should be treated independently for possible application of this by-product.

References

ADG (Adsorption design guide), (2001). Department of the Army, U.S. Army Corps of Engineers, DG 1110-1-2.

Ahalya, N., Ramachandra, T. V., Kanamadi, R. D., (2003). Biosorption of heavy metals. Res. J. Chem. Environ. vol. 7 (4), pp. 71-78.

Ahmad, A. L., Loh, M. M., Aziz, J. A., (2007). Preparation and characterization of activated carbon from oil palm wood and its evaluation on methylene blue adsorption. Dyes Pigments, vol. 75, pp. 263–272.

Ahmadpour, A., DO, D.D., (1996). The preparation of active carbons from coal by chemical and physical activation. Carbon, vol. 27 (4), pp. 471-479.

Ahmadpour, A., DO, D.D., (1997). The preparation of activated carbon from macadamia nutshell by chemical activation. Carbon, vol. 35 (12), pp. 1723-1732.

Ahmaruzzaman, M., Sharma, D. K., (2005). Adsorption of phenols from wastewater. Journal of Colloid and Interface Science, vol. 287, pp. 14-24.

Ahmed, M. J., Dhedan, S. K., (2012). Equilibrium isotherms and kinetics modeling of methylene blue adsorption on agricultural wastes-based activated carbons. Fluid Phase Equilibria, vol. 317, pp. 9-14.

Ahmedna, M., Johnson, M., Clarke, S. J., Marshall, W. E., Reo, R. M., (1997). Potential of Agricultural By-Products Based Activated Carbon for use in raw surge decolorization. Journal of the Science of Food and Agriculture, vol. 75 (1), pp. 117-124.

Ahn, D. H., Chang, W. S., Yoon, T., (1999). Dyestuff wastewater treatment using chemical oxidation, physical adsorption and fixed bed biofilm process. Process Biochemistry, vol. 34 (5), pp. 429-439.

Akgerman, A., Zardkoohi, M., (1996). Adsorption of phenol from wastewater by peat, fly ash and bentonite. Journal of Chemical Engineering, vol. 41, pp. 185-187.

Akita, S., Maeda, T., Takeuchi, H., (1995). Recovery of vanadium and nickel in fly-ash from heavy oil. Journal of Chemical Technology and Biotechnology, vol. 62, pp. 345-350.

Alade, A. O., Amuda,O. S., Afolabi, T. J., Okoya, A. A., (2012). Adsorption of naphthalene onto activated carbons derived from milk bush kernel shell and flamboyant pod. Journal of Environmental Chemistry and Ecotoxicology, vol. 4 (7), pp. 124-132.

Alina, C., Ion, I., Alina, C., (2011). Adsorption of naphthalene onto carbonic Nanomaterial graphitic nanoplatelets in Aqueous solutions, U.P.B. Sci. Bull., Series B, vol. 73 (2).

Allen, S. J., Koumanova, B., (2005). Decolourisation of water/wastewater using adsorption. Journal of the University of Chemical Technology and Metallurgy, vol. 40, pp. 175-192.

Andrew J., Ghio, Silbajoris, R., Johnny, L. C., James M. S., (2002). Biologic Effects of Oil Fly Ash. Environmental Health Perspectives, vol. 110 Supplement 1.

Ania, C. O., Cabal, B., Parra, J. B., Pis, J. J., (2007). Importance of the hydrophobic character of activated carbons on the removal of naphthalene from the aqueous phase. Adsorption Science and Technology, vol. 25 (3-4), pp. 155-167.

Ardizzone, S., Gabrielli, G., and Lazzari, P., (1993). Adsorption of methylene blue at solid/liquid and water/air interfaces. Colloids Surfaces, vol. 76, pp. 149-157.

ASTM D854-00, (2006). Standard Test for Specific Gravity of Soil Solids by Water Pycnometer ASTM International.

ASTM 1112-01, (2006). Standard Test Method, Iodine Value, Test Procedure, October 16.

ASTM D2866-94, (2000). Standard Test Method for Total Ash Content of Activated Carbon, Designation.

ASTM D4607-94, (2011) Standard Test Method for Determination of Iodine Number of Activated Carbon.

AWWA (American Water Works Association), (1997). Standard for Granulated Activated Carbon, ANSI/AWWA B604-96. AWWA, 6666 W. Quincy Ave., Denver, CO 80235.

AWWA, (1991). Standards for granular activated carbons American Water Works Association, ANSI/AWWAB604-90 Denver Co.

Baçaoui, A., Yaacoubi, A., Dahbi, A., Bennouna, C., Luu, R. P. T., Maldonado-Hodar, F. J., Rivera-Utrilla, J., Moreno-Castilla, C., (2001). Optimization of conditions for the preparation of activated carbons from olive-waste cakes. Carbon, vol. 39, pp. 425-432.

Baek, J. I, Yoon, J. H, Lee S. H., Ryu, C. K, (2007). Removal of Vapor-Phase Elemental Mercury by Oil-Fired Fly Ashes. Ind. Eng. Chem. Res., vol. 46, pp. 1390-1395.

Banarjee, S. S., Joshi, M. V., Jayaram, R. V., (2004). Removal of Cr (VI) and Hg (II) from aqueous solutions using fly ash and impregnated fly ash. Sep. Sci. Technol, vol. 39 (7), pp. 1611-1629.

Bansal R. C., Goyal, M., (2005). Activated Carbon Adsorption, CRC Press, New York, NY, USA.

Bayat, B., (2002). Comparative study of adsorption properties of Turkish fly ashes. The case of chromium (VI) and cadmium (II). J. Hazard. Mater, vol. 95 (3), pp. 275-290.

Belen, C., Budinova, T., Ania,C.O., Tsyntsarski,B., Parra, J.B., Petrov, B., (2009). Adsorption of naphthalene from aqueous solution on activated carbons obtained from bean pods. Journal of Hazardous Materials, vol. 161, pp. 1150-1156.

Benekos, I. D., Shoemaker, C. A., Stedinger, J. R., (2007). Probabilistic risk and uncertainty analysis for bioremediation of four chlorinated ethenes in groundwater. Stoch Environ Res Ris Assess, vol. 21, pp. 375-390.

Bergmann, K., O'Konski, C. T., (1963). A spectroscopic study of methylene blue monomer, dimer and montmorillonite. J. Phys. Chem. vol. 67, pp. 2169-2177.

Bhattacharyya, K. G., Sarma, A., 2004. Kinetics and thermodynamics of methylene blue adsorption on neem (Azadirachta indica) leaf powder. Dyes and Pigments, vol. 65, pp. 51-59.

Blanco, C. J., Bonelli, P. R., Cerella, E. G., Cukierman, A. L., (2000). Phosphoric Acid Activation of Agricultural Residues and Bagasse from Sugar Cane: Influence of the Experimental Conditions on Adsorption Characteristics of Activated Carbons. Industrial and Engineering Chemistry Research, vol. 39, pp. 4166-4172.

Break-bulk online news (2010-07-20).

Brunauer, S., Deming, L., Deming, W., Teller, E., (1940). On a Theory of the van der Waals Adsorption of Gases. J. Am. Chem. Soc, vol. 62 (7), pp. 1723-1732.

Bulut, Y., Aydin, H., (2006). A kinetic and thermodynamic study of methylene blue adsorption on wheat shells. Desalination, vol. 194, pp. 259-267.

Cabal, B., Ania, C.O.,Parra, J.B., Pis, J.J., (2009). Kinetics of naphthalene adsorption on an activated carbon: Comparison between aqueous and organic media, Chemosphere, vol. 76, pp. 433–438

Caramuscio, P., De Stefano, L., Seggiani, M., Vitolo, S., Narducci, P., (2003). Preparation of activated carbons from heavy-oil fly ashes. Waste Management, vol. 23, pp. 345-351.

CEC (Council of the European Communities), (1991). Proposal for a Council Directive on the landfill. Council of the European Communities 34 (C 190).

Chang, C-Y., Chen, K-H., Tsai, W.T., Shie, J-L., Chen, Y.H., (2004). Adsorption of naphthalene on zeolite from aqueous solution. Journal of Colloid and Interface Science, vol. 277, pp. 29-34.

Chengtang, L., Hui, X., Huaming, L., Ling, L., Li, X., Zhixiang, Y., (2011). Efficient degradation of methylene blue dye by catalytic oxidation using the $Na_8Nb_6O_{19}\cdot 13H_2O/H_2O_2$ system. Korean J. Chem. Eng., vol. 28 (4), pp. 1126-1132.

Choi, S.K., Lee, S., Song, Y.K., Moon, H.S., (2002). Leaching characteristics of selected Korean fly ashes and its implication for the groundwater composition near the ash disposal mound. Fuel, vol. 81, pp. 1083-1090.

Christopher M., Raquel, D. D., Bernard F., Betty, N., David, W., Ping, J. S., Martin, I., Drew, G., Pollard, S., (2006). Modeling human exposures to air pollution control (APC) residues released from landfills in England and Wales. Environment International, vol. 32, pp. 500-509.

Cimorelli, A. J., Perry, S. G., Venkatram, A., Weil, J. C., Paine, R. J., Lee, R. S., Peters, W. D., (1998). AERMOD Description of model formulation. Version 98315 (AEMOD and AERMET), USEPA document.

Clausnitzer, H., (1996). Respirable-dust Production from Agricultural Operations in the Sacramento Valley. Journal of Environmental Quality, vol. 25, pp. 877-884.

Cohrssen, J. J., Covello, V. T., (1989). Risk Anaysis: a guide to principles and methods for analyzing health and environmental risks. The National Technical Information Service, U.S. Department of Commerce.

Collin, J. G., Yii, F., (2008). Textural and chemical characterization of activated carbons prepared from rice husk (Oryza sativa) using a two-stage activation process. Journal of Engineering Science and Technology, vol. 3 (3), pp. 234-240.

Comba, P., Bianchi, F., Fazzo, L., Martina, L., Menegozzo, M., Minichilli, F., Mitis, F., Musmeci, L., Pizzuti, R., Santoro, M., Trinca, S., Martuzzi, M., (2006). Cancer Mortality in an Area of Campania (Italy) Characterized by Multiple Toxic Dumping Sites. Annals of the New York Academy of Sciences, vol. 1076, pp. 449-461.

Cooney, D. O., (1999). Adsorption design for wastewater treatment, Lewis publication, New York, Washington, D.C. ISBN 1-56670-333-6.

Cuhadaroglu, D., Uygun, O. A., (2008). Production and characterization of activated carbon from a bituminous coal by chemical activation. African Journal of Biotechnology, vol. 7 (20), pp. 3703-3710.

Dakiky, M., Khami, A., Manassra, A., Mer'eb, M. (2002). Selective adsorption of chromium (VI) in industrial wastewater using low cost abundantly available adsorbents. Advances in Environmental Research, vol. 6 (4), pp. 533-540.

Davini P., (2002). Flue gas treatment by activated carbon obtained from oil-fired fly ash. Carbon, vol. 40, pp. 1973-1979.

Diaz-Teran, J., Nevskaia, D. M., Lopez-Peinado, A. J., Jerez, A., (2001). Porosity and absorption properties of an activated charcoal, Colloids and Surfaces. Physiochemical and Engineering Aspects, vol. 187-188, pp. 167-175.

Doan, T., Morlot, C., Meisner, J., Serrano, M., Henriques, A.O., (2009). Novel Secretion Apparatus Maintains Spore Integrity and Developmental Gene Expression in Bacillus subtilis. Plos Genet 5(7).

DWT, (2001). Drinking Water Threshold Values in U.K., Properties and use of coal fly ash: a valuable industrial by-product. (Derived from Guidance Note, CI RCI Note 59/83). In: Sears LKA (ed), Thomas Telford Publishing, Thomas Telford Ltd., London.

ECAEC (Environmental Canada and Alberta Environmental Centre), (1986). Test methods for Solidified Waste Characterization.

ECRA (Electricity & Cogeneration Regulatory Authority), (2009). Annual report Electricity & Cogeneration Regulatory Authority, Saudi Arabia.

Edil, T., Acosta, H., Benson, C., (2006). Stabilizing Soft Fine-Grained Soils with Fly Ash. J. Mater. Civ. Eng., vol. 18, special issue, pp, 283-294.

Etyemeziana, V., Kuhnsb, H., Gilliesb, J., Chowb, J., Hendricksonc, K., McGownc, M., Pitchfordd, M., (2003). Vehicle-based Road Dust Emission Measurement (III): Effect of Speed, Traffic Volume, Location, and Season on PM 10 Road Dust Emissions in the Treasure Valley. Atmospheric Environment, vol. 37, pp. 4583-4593.

Fatimah, I., Wang, S., Wulandari, D., (2011). ZnO/montmorillonite for photocatalytic and photochemical degradation of methylene blue. Appl. Clay Sci., vol. 53 (4), pp. 553-560.

Faust, G. T., Hathaway J. C., Millot, G., (1959). A restudy of stevensite and allied minerals. Am. Miner., vol. 44, pp. 342-370.

Fernandez, A., Wendt, J. O. L., Wolski, N., Hein, K. R. G., Wang, S., Witten, M. L., (2003). Inhalation health effects of fine particles from the co-combustion of coal and refuse derived fuel. Chemosphere, vol. 51, pp. 1129-1137.

Francis, C. W., White, G. H., (1987). Leaching of toxic metals from incinerator ashes. J Water Pollut Control Fed, vol. 59 (11) , pp. 979-986.

Freundlich, H. M. F, (1906). Uber die adsorption in losungen, Zeitschrift fur Physikalische Chemie (Leipzig). vol. 57A, pp. 385-470.

Fytianos, K., Tsaniklidi, B., Voudrias, E., (1998). Leachability of heavy metals in Greek fly ash from coal combustion. Environ Int., vol. 24, pp. 477-486.

Gergova, K., Petrov, N., Eser, S., (1994). Adsorption properties and microstructure of activated carbons from agricultural by-products by stream pyrolysis. Carbon, vol. 32 (4), pp. 693-702.

Gernjak, W., Krutzler, T., Malato, A. G. S., Caceres, J., Bauer, R., Fernández-Alba, A. R., (2003). Photo-Fenton treatment of water containing natural phenolic pollutants. Chemosphere, vol. 50(1), pp. 71-78.

Ghosh, D., Bhattacharyya, K. G., (2002). Adsorption of methylene blue on kaolinite. Appl. Clay Sci., vol. 20, pp. 295-300.

Gilcreas, F. W., Tarars, M. J., Ingols, R. S., (1965). Standard methods for the examination of water and wastewater, American Public Health Association, New York.

Gode, F., Pehlivan, E., (2006). Chromium (VI) adsorption by brown coals. Energy Sources, vol. 28 (5), pp. 447-457.

Gong, Z., Alef, K., Wilke, B., Li, P., (2007). Activated carbon adsorption of PAHs from vegetable oil used in soil remediation, J. Hazard. Mater., vol. 143, pp. 372-378.

Gregg, S. J., and Sing, K. S. W., (1982). Adsorption, Surface Area and Porosity; London, Academic Press.

Guibal, E., Guzman, J., Navarro, R., Revilla, J., (2003). Vanadium extraction from fly ash – preliminary study of leaching, solvent extraction, and sorption on chitosan. Separation Science and Technology, vol. 38, pp. 2881-2899.

Guo, J., Lua, A. C., (1998). Characterization of chars pyrolyzed from oil palm stone for the preparation of activated carbons. Journal of Analytical and Applied Pyrolysis, vol. 46, pp. 113-125.

Gupta, C. K., Krishnamurthy, N., (1992). Extractive Metallurgy of Vanadium. Elsevier, Amsterdam.

Gupta, V. K., and Ali, I., (2004). Removal of lead and chromium from wastewater using bagasse fly ash a sugar industry waste. J. Colloid Interface Sci., vol. 271 (2), pp. 321-328.

Hayashi, J., Kazehaya, A., Muroyama, K., Watkinson, A. P., (2000). Preparation of activated carbon from lignin by chemical activation. Carbon, vol. 38, pp. 1873–1878

Health Canada, (2007) (draft). Federal Contaminated Site Risk Assessment in Canada. Part II: Health Canada Toxicological Reference Values (TRVs). Version 2.0.

Hiltz, R. H., (1988). Design and construction of mobile activated carbon regeneration system, Journal of Hazardous Materials, vol. 18, pp. 207-210.

Ho, K. F., Lee, S. C., Chow, J. C., Watson, J. G., (2003). Characterization of PM10 and PM2.5 Source Profiles for Fugitive Dust in Hong Kong. Atmospheric Environment, vol. 37, pp. 1023-1032.

Ho, Y. S., Mckay, G., (1999). Pseudo-second order model for sorption processes. Process Biochem, vol. 34, pp. 451-465.

Holoubeki, I., Kocan, A., Holoubkova, I., Hilscherova, K., Kohoulek, J., Falandys, Z. J., Roots, O., (2000). Persistent, Bioaccumulations and Toxic Compounds in Central and Eastern European Countries – State of the Art Report. TOCOEN Report No 150a.

Howell, S., Pszenny, A. A. P., Quinn, P., Huebert, B., (1998). A Field Intercomparison of Three Cascade Impactors. Aerosol Science and Technology, vol. 29, pp. 475-492.

Hsieh, Y. M., Tsai, M. S., (2003). Physical and chemical analyses of unburned carbon from oil-fired fly ash. Carbon, vol. 41, pp. 2317-2324.

Huang, C. P., Wu, M. H., (1977). The removal of chromium (VI) from dilute aqueous solution by activated carbon, Water Research, vol. 11, pp. 673-679.

Hwang, S. K., Park, J. H., Hong, S. U., Jung, J. H., Jung, M. Y., Son, Y. U., Cho, K. J., (1996). Engineering Development and Operation for Heavy Oil Fly Ash Incineration Plant. Korea Electric Power Research Institute, report no KEPRI-93C-T04.

IARC, (1973). Some Inorganic and Organometallic Compounds. IARC Monographs on the Evaluation of Carcinogenic Risk of Chemicals to Humans, vol. 2. Lyon, France: International Agency for Research on Cancer.

IARC, (1980). Some Metals and Metallic Compounds. IARC Monographs on the Evaluation of Carcinogenic Risk of Chemicals to Humans, vol. 23. Lyon, France: International Agency for Research on Cancer.

Industrial Source Complex (ISC) Dispersion Model User's Guide – Second Edition (Revised), Vol. 1., EPA-450/4-88-002a. U.S.EPA, December 1987.

IRIS., (1995). Integrated risk information system. USEPA. October 1995.

Itskos, G., Itskos, S., Koukouzas, N., (2009). The effect of the particle size differentiation of lignite fly ash on cement industry applications, 3rd World of Coal Ash, WOCA Conference – Proceedings.

Jankowaka, H., Swiatkowski, A., Choma, J., (1991). In Active Carbon; Ed.; Kemp, T. J., Translation. Ellis Horwood Ltd.: West Sussex, England.

Jarup, L., Briggs, D., Hoogh, C., Morris, S., Hurt, C., Lewin, A., Maitland, I., Richardson, S., Wakefield, J., Elliott, P., (2002). Cancer risks in populations living near landfill sites in Great Britain. British Journal of Cancer, vol. 86, pp. 1732-1736.

Jiang, N., Dreher, K. L., Dye, J. A., Li, Y., Richards, J. H., Martin, L. D., Adler, K. B., (2000). Residual oil fly ash induces cytotoxicity and mucin secretion by guinea pig tracheal epithelial cells via an oxidant-mediated mechanism. Toxicol Appl Pharmacol, vol. 163, pp. 221-230.

Jones, D. R., (1995). The leaching of major and trace elements from coal ash, In: Swaine, D. J., Goodarzi, F. (Eds.), Environmental aspects of trace elements in coal. Kluwer Academic Publishing, Dordrecht, pp. 221-262.

Jorkevic, D., Vukmirovic, Z., Tosic, I., Miroslava, U., (2004). Contribution of Dust Transport and Resuspension to Particulate Matter Levels in the Mediterranean Atmosphere. Atmospheric Environment, vol. 38, pp. 3637-3645.

Junjie, G, Naim, M., Faqir, Hans-Jörg, B., (1999). Drying of an Activated Carbon Column after Steam Regeneration. Chem. Eng. Technol., vol. 22 (10), pp. 859-864.

Kannan, N., Sundaram, M. M., (2001). Kinetics and mechanism of removal of methylene blue by adsorption on various carbons- a comparative study. Dyes Pigments, vol. 51, pp. 25-40.

Kentel, E., Aral, M., (2004). Probabilistic-fuzzy health risk modeling. Stoch Envir Res and Risk Ass, vol. 18, pp. 324-338.

Khadija, Q., Inamullah, B., Rafique, K., Abdul, K. A., (2008). Physical chemical analysis of activated carbon prepared from sugarcane bagasse and use for sugar decolorisatoin. International Journal of Chemical and Biomolecular Engeneering, vol. 1 (3), pp. 145-149.

Kiliç,M., Apaydın-Varol, E., Eren Pütün, A., (2012). Preparation and surface characterization of activated carbons from Euphorbia rigida by chemical activation with $ZnCl_2$, K_2CO_3, NaOH and H_3PO_4. Applied Surface Science, vol. 261 (15), pp. 247-254.

Kinniburgh D. G., (1986). General purpose adsorption isotherms. Environ. Sci. Technol., vol. 20, pp. 895-896.

Kruk, M., Jaroniec, M., (2001). Gas Adsorption Characterization of Ordered Organic-Inorganic Nanocomposite Materials. Chem. Mater., vol. 13 (10), pp. 3169–3183.

Kumpiene, J., Lagerkvist, A., Maurice, C., (2007). Stabilization of Pb and Cu contaminated soil using coal fly ash and peat, Environmental Pollution, vol. 145, pp. 365-373.

Kurniawan, T. A., Chan, G. Y. S., Lo, W., Babel, S., (2006). Comparisons of low-cost adsorbents for treating wastewaters laden with heavy metals. Science of the Total Environment, vol. 366, pp. 409-426.

Kwon, W. T., Kim, D. H., Kim, Y. P., (2005). Characterization of Heavy Oil Fly Ash Generated from a Power Plant. Journal of Materials Online, vol. 1, pp 1-8.

Lagergren, S., (1898). Zur theorie der sogenannten adsorption geloster stoffe. Kungliga Svenska Vetenskapsakademiens. Handlingar, vol. 24 (4), pp. 1-39.

Langmuir I., (1916). The constitution and fundamental properties of solids and liquids. Am. J. Chem. Soc., vol. 38, pp. 2221-2295.

Lillo-Rodenas, M. A., Cazorla-Amoros, D., Linares-Solono, A., (2005). Behaviour of Activated Carbons with Different Pore Size Distributions and Surface Oxygen Groups for Benzene and Toluene Adsorption at Low Concentrations. Carbon, vol. 43, pp. 1758-1767.

Lillo-Rodenas, M. A., Juan, J., Cazorla-Amoros, D., Linares-Solano, A., (2004). About reactions occurring during chemical activation with hydroxides. Carbon, vol. 42, pp. 1371-1375.

Lillo-Rodenas, M. A., Marco-Lozar, J. P., Cazorla-Amoros, D., Linares-Solano, A., (2007). Activated carbons prepared by pyrolysis of mixtures of carbon precursor/alkaline hydroxide. J. Anal. Appl. Pyrolysis, vol. 80, pp. 166-174.

Lin, S. H., Juang, R. S., (2009). Adsorption of phenol and its derivatives from water using synthetic resins and low-cost natural adsorbents: a review. J Environ Manage, vol. 90, pp. 1336-1349

Liu, J. J., Wang, X. C., Fan, B., (2011). Characteristics of PAHs adsorption on inorganic particles and activated sludge in domestic wastewater treatment. Bioresource Technology, vol. 102 (9), pp. 5305-5311.

Lowell, S., Shields, J. E., Thomas, M.A, Thommes, M., (2004), Charecterization of porous, solids and powders: surface area, pore size and density. Kluwer Academic Publications, Boston.

Lozano, L.J., Juan, D., (2001). Solvent extraction of polyvanadates from sulphate solutions by primene 81R. Its application to the recovery of vanadium from spent sulphuric acid catalysts leaching solutions, Solvent Extr. Ion Exch., vol. 19, pp. 659-676.

Lua, A. C., Guo, J., (2000). Activated carbon prepared from oil palm stone by one-step CO2 activation for gaseous pollutant removal. Carbon, vol. 38, pp. 1089-1097.

Mahvi, A. H., Dariush, N., Forughand, V., Nazmara, S., (2005). Tea waste as an adsorbent for heavy metal removal from Industrial wastewaters. Am. J. Appl. Sci., vol. 2, pp. 372-375.

Manoli, E., Samara, C., (1999). Polycyclic aromatic hydrocarbons in natural waters: sources, occurrence and analysis. Trends Anal. Chem., vol. 18, pp. 417-442.

Massot, A., Estève, K., Noilet , P., Méoule, C., Poupot, C., Mietton-Peuchot, M., (2012). Biodegradation of phytosanitary products in biological wastewater treatment. Water Research, vol. 46 (15), pp. 1785-1792.

Mattson, J. S., Mark Jr., H. B., (1971). Activated Carbon. New York: Dekker.

Maxwell, R. M., Kastenberg, W. E, (1999). Stochastic environmental risk analysis: an integrated methodology for predicting cancer risk from contaminated groundwater. Stochastic Environ Res Risk Assess, vol. 13, pp. 27-47.

Melih, D. M., Aydilek, A., Seagren, E., Hower, J., (2011). Naphthalene and o-Xylene Adsorption onto High Carbon Fly Ash. J. Environ. Eng., vol. 137 (5), pp. 377-387.

Menendez, D. J. A., Martin, G. I., (2006). Type of carbon adsorbents and there production, Interface science and technology, Edt., Bandosz, T.J., Activated carbon surfaces in environmental remediation, Vol. 7, Academic Press New York, pp. 1-45.

Miura, K., Nozaki, K., Isomura, H., Hashimoto, K., Toda, Y., (2001). Recycling process of fly ash generated from oil burning. Materials Transactions, vol. 42, pp. 2465-2471.

Mofarrah, A., Husain, T., (2011). Fuzzy Based Health Risk Assessment of Heavy Metals Introduced into the Marine Environment. Water Qual Expo Health, vol. 3 (1), pp. 25-36.

Mofarrah, A., Husain, T., (2013). Evaluation of Environmental Pollution and Possible Management Options of Heavy Oil Fly Ash. Journal of Material Cycles and Waste Management. vol. 15 (1), pp. 73-81.

Mofarrah, A., Husain, T., Ekram, Y. D., (2012). Investigation of the Potential Use of Heavy Oil Fly Ash as Stabilized Fill Material for Construction. Journal of Materials in Civil Engineering, vol. 24 (6), pp. 684-690.

Mofarrah, A., Husain, T., (2010). A Holistic Approach for optimal design of Air Quality Monitoring Network Expansion in an Urban Area. Atmospheric Environment, vol. 44 (3), pp. 432-440.

Mohan, D., Pittman Jr., C. U., (2006). Review: activated carbons and low cost adsorbents for remediation of tri- and hexavalent chromium from water. J. Hazard. Mater., vol. 137, pp. 762-811.

Mohan, D., Singh, K. P., Singh, V. K., (2005). Using low-cost activated carbons derived from agricultural waste materials and activated carbon fabric cloth. Ind. Eng. Chem. Res., vol. 44, pp.1027-1042.

Mohapatra, R., Rao, J.R., (2001). Some aspects of characterisation, utilisation and environmental effects of fly ash. Journal of Chemical Technology and Biotechnology, vol. 76, pp. 9-26.

Montgomery, D. C., (1997). Design and Analysis of Experiments, 4th edition, John Wiley and Sons Editions, New York.

Mor, S., Ravindra, K., Bishnoi, N. R., (2007). Adsorption of chromium from aqueous solution by activated alumina and activated charcoal. Bioresour. Technol., vol. 98, pp. 954-957.

Mõtlep, R., Sild, T., Puura, E., Kirsimäe, K., (2010). Composition, diagenetic transformation and alkalinity potential of oil shale ash sediments. J. Hazard. Mater., vol. 184 (1-3), pp. 567-573.

Mukherjee, S., Kumar, S., Misra, A. K., Fan, M., (2007). Removal of phenols from water environment by activated carbon, bagasse ash and wood charcoal. Chemical Engineering Journal, vol. 129, pp. 133-142.

Nagpal, N. K., (1993). Ambient Water Quality Criteria For Polycyclic Aromatic Hydrocarbons (PAHs), Water Quality Branch Water Management Division Ministry of Environment, Lands and Parks Province of British Columbia no. 5-6, pp. 569-571.

Navarro, R., Guzman, J., Saucedo, I., Revilla, J., Guibal, E., (2007). Vanadium recovery from oil fly ash by leaching, precipitation and solvent extraction processes. Waste Management, vol. 27, pp. 425-438.

Neopaney, M., Wangchuk, U. K., Tenzin, S., Chamberlin, K. S., (2012). Stabilization of Soil by Using Plastic Wastes, International Journal of Emerging trends in Engineering and Development. vol. 2 (2), pp. 461-466.

Okiemmen, F., Okiemen, C., Wuana, A., (2007). Preparation and characterization of activated carbon from rice husk. Journal of Chemical Society of Nigeria, vol. 32, pp. 126-136.

Owabor, C. N., Ono, U. M., Isuekevbo, A., (2012). Enhanced Sorption of Naphthalene onto a Modified Clay Adsorbent: Effect of Acid, Base and Salt Modifications of Clay on Sorption Kinetics, Advances in Chemical Engineering and Science, vol. 2, pp. 330-335

Ozcan, A. S., Erdem, B., Ozcan, A., (2004). Adsorption of Acid Blue from aqueous solutions onto Na-bentonite and DTMA-bentonite. J Coll. Inter. Sci., vol. 280, pp. 44-54.

Pala A, Tokat E., (2002). Colour removal from cotton textile industry wastewater in an activated sludge system with various additives. Water Res., vol. 36, pp. 2920-2925.

Patil, S., Renukdas, S., Patel, N., (2011). Removal of methylene blue, a basic dye from aqueous solutions by adsorption using teak tree (Tectona grandis) bark powder. International Journal of Environmental Sciences, vol.1 (5), pp. 711-726.

Patterson, J. W., (1985). Industrial Wastewater Treatment Technology, Second Ed., Butterworth-Heinemann, London.

Paul, M., Caouette, A., (2007). Heavy Fuel Oil Consumption in Canada, Analytical Paper, Statistics Canada.

Pitt, R., Roberson, B., Barron, P., Ayyoubi, A., Clark, S., (1999). Storm water treatment at critical areas: The multi-chambered treatment train (MCTT). U.S. Environmental Protection Agency, Water Supply and Water Resource Division. National Risk Management Research Laboratory. EPA 600/R-99/017. Cincinnati, OH.

Praharaj, T., Powell, M. A., Hart, B. R., Tripathy, S., (2002). Leachability of elements from sub-bituminous coal fly ash from India. Environ Int., vol. 27, pp. 609-615.

Purnomo, C. W., Salim, C., Hinode, H., (2011). Preparation and characterization of activated carbon from bagasse fly ash. Journal of Analytical and Applied Pyrolysis, vol. 91 (1), pp. 257-262.

Qianqian, S., Aimin. L., Zhaolian, Z., Bing, L., (2012). Adsorption of naphthalene onto a high-surface-area carbon from waste ion exchange resin, Journal of Environmental Science, DOI: 10.1016/S1001-0742(12)60017-5.

Querol, X., Juan, R., Lopez-Soler, A., Fernandez-Turiel, J. L., Ruiz, C. R., (1996). Mobility of trace elements from coal and combustion wastes. Fuel, vol. 75, pp. 821-838.

Qureshi, K., Bhatti, I., Kazi, R., Ansari, A. K., (2007). Physical and Chemical Analysis of Activated Carbon Prepared from Sugarcane Bagasse and Use for Sugar Decolorisation, World Academy of Science, Engineering and Technology 10.

Rachakornkij, M., Ruangchuaya, S., Teachakulwiroj, S., (2004). Removal of reactive dyes from aqueous solution using bagasse fly ash. J. Sci. Technol., vol. 26, pp. 13-24.

Rahman, M. A., Asadullah, M., Haque, M. M., Motin, M. A., Sultan, M. B., Azad, M. A. K., (2006). Preparation and characterization of activated charcoal as an adsorbent. J. Surface Sci. Technol., vol. 22 (3-4), pp. 133-140.

Raposo, F., De La Rubia, M. A., Borja, R., (2009). Methylene blue number as useful indicator to evaluate the adsorptive capacity of granular activated carbon in batch mode: influence of adsorbate/adsorbent mass ratio and particle size. J. Hazard. Mater., vol. 165 (1-3), pp. 291-299.

Rapporto Ambientale, 2000ENEL, Italy (cited from Caramuscio et al., 2003).

Readfearn, A., Roberts, D., (2002). Health Effects and Lanfill Sites. Hester, R.E., Harrison, R.M., (Eds.), Environmental and Health Impact of Solid Waste Management Activities Royal Society of Chemistry, pp. 103-140.

Reemtsma, T., Mehrtens, J., (1997). Determination of polycyclic aromatic hydrocarbon (PAH) leaching from contaminated soil by a column test with on-line solid phase extraction. Chemosphere, vol. 35, pp. 2491-2501.

Rodriguez-Reinoso, F., (1997). Introduction to carbon technologies. Eds., Marsh, H., Heintz, E.A., Rodriguez-Reinoso, F., Publicaciones Universidad de Alicante.

Rouquerol, F., Rouquerol, J., Sing, K., (1999). Adsorption by Powders and Porous Solids; Academic Press: San Diego.

Sakai, T., Sugiyama, S., (1970). Residual carbon particles yielded by combustion of atomized heavy-fuel-oil droplets. J. Inst. Fuel., vol. 43 (8), pp. 295-300.

Sari, A., Tuzen, M., Soylak, M., (2007). Adsorption of Pb (II) and Cr (III) from aqueous solution on Celtek clay. J. Hazard. Mater., vol. 144 , pp. 41-46.

Sarkar, M., Acharya, K. P., (2006). Use of fly ash for the removal of phenol and its analogues from contaminated water. Waste Management, vol. 26, pp. 559-570.

Sawyer, C. N., McCarty, P. L., Parkin, G. F., (2004). Chemistry for Environmental Engineering and Science, fifth ed. McGraw-Hill, Boston.

Schuliger, W. G., Riley, G. N., Wagner, N. J. (1988). Thermal Reactivation of GAC: A Proven Technology, Water World News, vol. 4 (1).

Schwarzenbach, R. P., Gschwend, P. M., Imboden, D. M., (2003). Environmental Organic Chemistry. 2nd edition, John Wiley, New York, USA.

Scire, S. J., Strimaitis, D. G., Yamartino, R. J., (2000). A user's guide for the CALPUFF dispersion model (version 5). Earth Tech Inc., 196 Baker Avenue, Concord, MA 01742.

Scott, J., Beydown, D., Amal, R., Low, G., Cattle, J., (1990). Landfill Management, leachate generation and leach testing of solid wastes in Australia and overseas. Critical Reviews in Environmental Science. USEPA.

SEC (Saudi Electric Company) Rabigh stage (vi) Plant extension emissions study June 2007, Document No. 62859/PBP/000009, http://www.coface.fr, web access January 16, 2013.

Sharma, D. C., Forster, C. F., (1994). A Preliminary examination into the adsorption of hexavalent chromium using Low-cost adsorbents. Bioresource Technology, vol. 47, pp. 257-264.

Sing, K. S. W., Everett, D. H., Haul, R. A. W., Moscou, L., Pierotti, R. A., Rouquerol, J., Siemieniewska, T., (1985). Reporting physisorption data for gas/solid systems with special reference to the determination of surface area and porosity. Pure Appl. Chem., vol. 57 (4), pp. 603-619.

Singh, B. P., Besra, L., Bhattacharjee, S., (2002). Factorial design of experiments on the effect of surface charges on stability of aqueous colloidal ceramic suspension. Colloid. Surface., vol. 204 (1-3), pp. 175-181.

Smisek, M., Cerny, S., (1970). Active carbon: manufacture, properties and applications. Elsevier, New York.

Snell, F., Hilton, C., Ettre, L., (1974). Encyclopedia of industrial chemical analysis, Vol. 8. New York, N.Y: Inter Science.

Sponza, D. T., Oztekin, R., (2010). Removal of PAHs and acute toxicity via sonication in a petrochemical industry wastewater. Chemical Engineering Journal, vol. 162 (1), pp. 142-150.

Stephenson, R. J., Sheldon, J. B., (1996). Coagulation and Precipitation of a Mechanical Pulping Effluent: 1. Removal of Carbon and Turbidity. Water Res., vol. 30, pp. 781-792.

Suteu, D., Bilba, D., (2005). Equilibrium and Kinetic Study of Reactive Dye Brilliant Red HE-3B Adsorption by Activated Charcoal. Acta Chim. Slov., vol. 52, pp. 73-79.

Tan, W. T., Ooi, S. T., Lee, C. K., (1993). Removal of chromium (V1) from solution by coconut husk and palm pressed fibres. Environmental Technology, vol. 14, pp. 277-282.

Tryba, B., Morawski, A. W., Kaleńczuk, R. J., Inagaki, M., (2003). Exfoliated Graphite as a New Sorbent for Removal of Engine Oils from Wastewater. Spill Science and Technology Bulletin, vol. 8 (5), pp. 569-571.

Tsai, S. L., Tsai, M. S., (1997). Study on the physical and chemical characteristics, yield and TCLP test of oil-fired fly ash. Mining Metall., vol. 41 (2), pp. 57-68.

Tsai, S.-L., Tsai, M.-S., (1998). A study of the extraction of vanadium and nickel in oil-fired fly ash. Resources, Conservation and Recycling, vol. 22, pp. 163-176.

Tseng, R. L., (2006). Mesopore control of high surface area NaOH-activated carbon. Journal of Colloid and Interface Science, vol. 303 (2), pp. 494-502.

Tseng, R.L., (2007). Physical and chemical properties and adsorption type of activated carbon from plum kernels by NaOH activation. J. Hazardous Mater., vol. 147, pp. 1020-1027.

USEPA, (1989). Physical tests, chemical testing procedures, technology screening, and field activities, stabilization/solidification of CERCLA and RCRA wastes, Center for Environmental Research Information and Risk Reduction Engineering Laboratory Office of Research and Development, USEPA, OH 45268.

USEPA, (1989a). Air/Superfund National Technical Guidance Study Series; Volume III – Estimation of Air Emissions from Cleanup Activities at Superfund Sites, Interim final report EPA-450/1-89-003, January.

USEPA, (1991). Risk Assessment Guidance for Superfund: Volume 1 Human Health Evaluation Manual (Part B, Development of Risk-based Preliminary Remediation Goals). Publication 9285.7-01B. Office of Emergency and Remedial Response, US EPA, Washington, DC.

USEPA, (1993). Secondary maximum contamination levels for trace contaminants in drinking water. USEPA, Office of Water, Washington, DC.

USEPA, (1994). Compilation of Air Pollution Emission Factors (AP-42), USEPA Research Triangle Park, N.C.

USEPA, (1995). User's Guide for The Industrial Source Complex (ISC3) Dispersion Models Office of Air Quality Planning and Standards Emissions. Monitoring, and Analysis Division Research Triangle Park, North Carolina 27711.

USEPA, (1996). Summary Report for the Workshop on Monte Carlo Analysis, Risk Assessment Forum. USEPA, Washington, DC. EPA-630-R-96-010.

USEPA, (1999). Technical background document for the report to Congress on remaining wastes from fossil fuel combustion: waste characterization. March 15.

USEPA, (2001). Risk assessment guidance for superfund (RAGS), Vol. III – Part A, Process for conducting probabilistic risk assessment, EPA 540-R-02-002, Office of emergency and remedial response, Washington, DC.

USEPA, (2002). Compendium of Reports from the peer review process for AERMOD U.S. Environmental Protection Agency, RTP, NC.

USEPA, (2006). Drinking Water Standards and Health Advisories, Summer Edition, EPA 822-R-06-013.

Vadivelan, V., Kumar, K. V. (2005). Equilibrium, Kinetics, Mechanism, and Process Design for the Sorption of Methylene Blue onto Rice Husk. Journal of Colloid and Interface Science, vol. 286, pp. 90-100.

Van der Sloot, H. A., (2002). Characterization of the leaching behaviour of concrete mortars and of cement-stabilized wastes with different waste loading for long term environmental assessment. Waste Management, vol. 22 (2), pp. 181-186.

Vargas, A. M. M., Cazetta, A. L., Kunita, M. H., Silva, T. L., Almeida, V. C., (2011). Adsorption of methylene blue on activated carbon produced from flamboyant pods (Delonix regia): Study of adsorption isotherms and kinetic models. Chemical Engineering Journal, vol. 168, pp. 722-730.

Vitolo, S., Seggiani, M., Falaschi, F., (2001). Recovery of vanadium from a previously burned heavy oil fly ash. Hydrometallurgy, vol. 62, pp. 145-150.

Voudrias, E., Fytianos, K., Bozani, E., (2002). Sorption-desorption isotherms of dyes from aqueous solutions and wastewaters with different sorbent materials. Global Nest, the Int. J., vol. 4, pp. 75-83.

Wang, Y. Q., Song, D., Wang, K., (2008). Caching of coal and its combustion residues. Shizuishan, China, Int. J. Coal Geol., vol. 75, pp. 81-87.

Wayne C. T., Steve Doty, Energy Management Handbook, 7th edition, Fairmont Press, Inc., Lilburn, Georgia, 2009.

Weber, T. W., Chackravorti, R. K., (1974). Pore and solid diffusion models for fixed bed adsorbers. Amer. Inst. Chem. Eng. J., vol. 20, pp. 228-238.

Weng, C. H., Shama, Y. C., Chu, S. H., (2000). Adsorption of Cr (VI) from aqueous solutions by spent activated clay. J. Hazard. Mater., vol. 155, pp. 65-75.

Wesche, K., Alonso, I. L., Bijen, I., Schubert, P., Vom Berg, W., Rankers, R., (1989). Test methods for determining the properties of fly ash and of fly ash for use in building materials. Materials and Structures / Matdriaux et Constructions, vol. 22, pp. 299-308.

WHO (World Health Organization), (2007). Population Health and Waste Management: Scientific Data and Policy Options, a report of WHO workshop, Regional Office for Europe, Copenhgen, Denmark.

WHO, (2003). Chromium in drinking-water: Background document for preparation of WHO Guidelines for drinking-water quality. WHO, Geneva, WHO/SDE/WSH/03.04/4.

Xia, X. H., Yu, H., Yang, Z. F., Huang, G. H., (2006). Biodegradation of polycyclic aromatic hydrocarbons in the natural waters of the Yellow River: Effects of high sediment content on biodegradation. Chemosphere, vol. 65 (3), pp. 457-466.

Xue, Y., Hou, H., Zhu, S., (2009). Adsorption removal of reactive dyes from aqueous solution by modified basic oxygen furnace slag: isotherm and kinetic study. Chem Eng J, vol. 147, pp. 272-279.

Yao, Y., Xu, F., Chen, M., Xu, Z., Zhu, Z., (2010). Adsorption behavior of methylene blue on nanotubes. Bioresource Technology, vol. 101 (9), pp 3040-3046.

Yaumi, A. L., Hussien, I. A., Reyad, A., Shawabkeh, R. A., (2013). Surface modification of oil fly ash and its application in selective capturing of carbon dioxide. Applied Surface Science, vol. 266, pp. 118-125.

Yuan, M., Tong, S., Zhao, S. and Jia, C. Q., (2010). Adsorption of polycyclic aromatic hydrocarbons from water using petroleum coke-derived porous carbon. Journal of Hazardous Materials, vol. 181, pp. 1115-1120.

Zanitsch, R. H., Lynch, R. T., (1997). Selecting a Thermal Regeneration System for Activated Carbon, Carbon Adsorption Handbook, Calgon Carbon Corporation.

Zhang, P., Inoue, K., Tsuyama, H., (1995). Recovery of metal values from spent hydrodesulfurization catalysts by liquid–liquid extraction. Energy Fuels, vol. 9, pp. 231-239.

Appendix A

Experimental Data

Table A-1 Chemical composition of Saudi Arabian heavy oil fly ash (ICPMS study)

Elements (ppm = mg/kg)	**Sample 1**	**Sample 2**	
	FA- SA -1	**FA- SA -2**	**Maximum**
Arsenic (As)	2.239	2.17	2.239
Bromide (Br)	339	370.9	370.9
Cadmium (Cd)	0.415	3.275	3.275
Cobalt (Co)	*Not detectable*	*Not detectable*	*Not detectable*
Chromium (Cr)	1.286	4.056	4.056
Copper (Cu)	12.4	170.4	170.4
Iron (Fe)	981	521	981.0
Mercury (Hg)	0.177	0.245	0.245
Manganese (Mn)	9.343	20.675	20.675
Molybdenum (Mo)	18.368	26.047	26.047
Nickel (Ni)	1052.78	1762.22	1762.22
Lead (Pb)	3.996	10.995	10.995
Selenium (Se)	11.592	9.764	11.592
Tin (Sn)	0.568	17.274	17.274
Vanadium (V)	2957.701	1753.889	2957.701
Zinc (Zn)	63.645	130.84	130.84
Carbon	85.56%	-	-
%S	6.24		

Table A-2 Chemical composition of NB fly ash (ICPMS study)

Elements (ppm = mg/kg)	FA-NB
Arsenic (As)	68.281
Bromide (Br)	124.5
Cadmium (Cd)	1.588
Cobalt (Co)	247.79
Chromium (Cr)	107.60
Copper(Cu)	120.30
Iron (Fe)	22633
Mercury (Hg)	*Not detectable*
Manganese (Mn)	135.385
Molybdenum (Mo)	398.387
Nickel (Ni)	11852.93
Lead (Pb)	116.095
Selenium (Se)	13.186
Tin (Sn)	9.556
Vanadium (V)	34487.12
Zinc (Zn)	592.131
Carbon	51.86%

Table A-3 Characteristics of FAC produced by different activation process

Activated Carbon	**BET surface area (m^2/g)**	**Total pore volume, (cm^3/g)**	**Micropore volume (cm^3/g)**	**Meanpore diameter (nm)**	**Iodine number**	**Methylene blue number**
AC1	75.38	0.1219	0.05364	0.0683	80.50	19.75
AC2	82.674	0.1329	0.05489	0.0780	95.50	21.48
AC3	91.22	0.1440	0.058815	0.0852	110.20	23.58
AC4	123.19	0.2215	0.097609	0.1239	130.25	31.45
AC5	79.48	0.1285	0.061587	0.0669	90.75	20.71
AC6	130.06	0.1662	0.057476	0.1087	140.45	33.10
AC7	102.778	0.2105	0.086994	0.1235	120.50	33.10
AC8	143.888	0.2326	0.109519	0.1231	160.85	36.36
FAC-P01	4.1266	0.0182	0.0019	17.631	6.52	1.85
FAC-P02	12.69	0.0239	0.0074	7.541	15.23	3.82
FAC-P03	14.038	0.0221	0.0054	6.306	16.25	4.58
FAC-P04	10.737	0.0248	0.0039	9.25	13.3	3.05

Appendix B

Calibration curve for Cr (VI) adsorption process

A calibration curve (Figure B-1) was obtained by using standard Cr (VI) solutions of known concentrations at pH 5.5. The unknown concentration was estimated by using Beer's law, as shown in Equation B-1.

$$A = \varepsilon.c.l \qquad \text{(B-1)}$$

where, A is the absorbance, ε is the the molar extinction coefficient, c is the concentration of dye (mg/L), l is the path length of the absorbing solution (in cm), the cells used are 1 cm^2 in cross-section, so l is considered 1 cm.

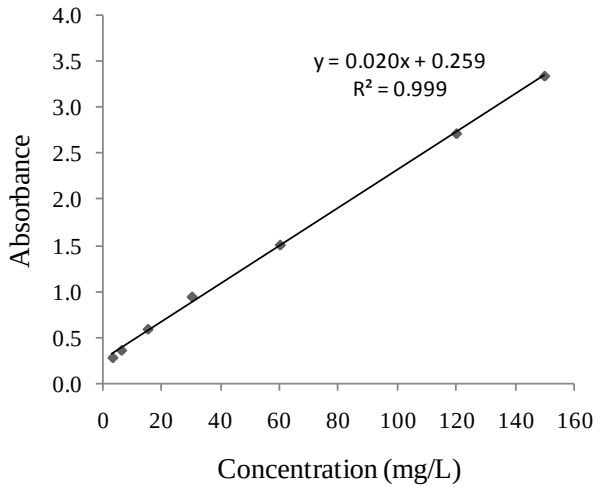

Figure B-1 Cr (VI) adsorption calibration curve

A calibration curve (Figure B-1) with a high determination coefficient (R^2 = 99.9) allows us to consider that the molar extinction coefficient is constant over the concentration range being investigated.

Calibration curve for naphthalene adsorption process

A calibration curve (Figure B-2) was obtained by using standard naphthalene solutions of known concentrations at pH 6.5. The naphthalene concentration in each solution was measured by a UV-visible spectrometer (Hewlett-Packard Model 8453) at a wavelength of 276 nm (Belen et al., 2009). The unknown concentration was estimated by using Beer's law, as shown in Equation B-1.

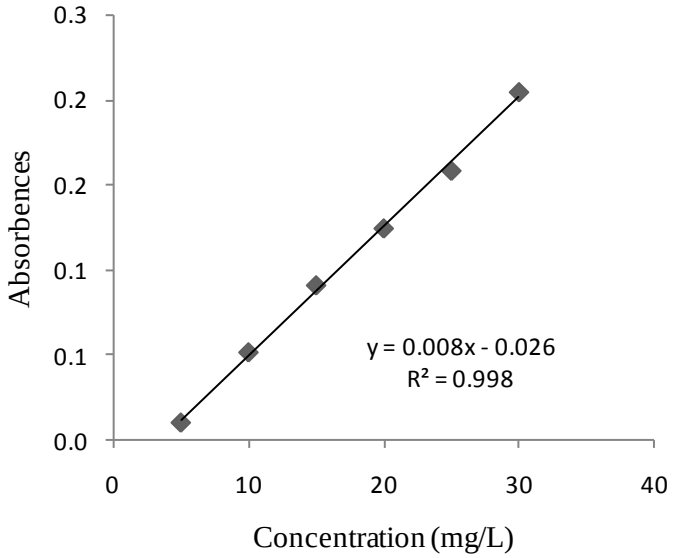

Figure B-2 naphthalene adsorption calibration curve

A calibration curve (Figure B-2) with a high determination coefficient (R^2 = 99.8) allows us to consider that the molar extinction coefficient is constant over the concentration range being investigated.

Control Experiments for naphthalene adsorption process

To eliminate error due to the adsorption of naphthalene onto the filter paper, a parallel control set (without FAC) was run in an identical manner. In this case, the solutions with known initial concentration were filtered on Whatman No. 42 filter paper. After filtration the

naphthalene concentration in each solution was measured by a UV-visible spectrometer (Hewlett-Packard Model 8453) at a wavelength of 276 nm (Belen et al., 2009). Finally, the naphthalene adsorbed by the filter paper were calculated by the difference of initial and final naphthalene concentration in the solution. Table B-1 shows the control experiments results found from naphthalene adsorption process.

Table B-1 Control experiments results for naphthalene adsorption process

Sample #	Initial concentration (mg/L)	Final concentration (mg/L)
#1	25	24.50
#2	30	29.50
#3	40	39.55
#4	50	49.63
#5	60	59.25
#6	80	79.50
Equilibrium contact time = 12 hrs, pH = 6.5		

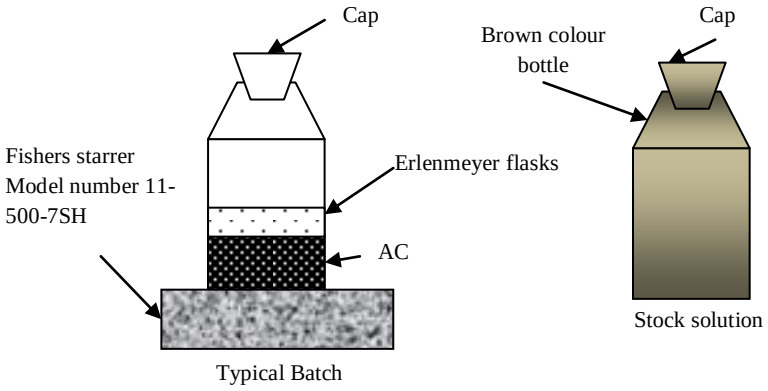

Figure B-3 Typical batch experiment for naphthalene adsorption process

Appendix C

Experiment Photos

Figure C-1 Sample cement mortar blocks prepared by mixing HOFA at different ratios

Figure C-2 Sample laboratory setup used to prepare FAC in this research

Figure C-3 Sample laboratory setup used to clean HOFA

Figure C-4 Leach from HOFA (a) before and (b) after cleaning